1D single-cell migration on microlanes and at interfaces

Christoph Schreiber

München 2019

1D Einzelzellmigration auf Bahnen und an Grenzflächen

Christoph Schreiber

München 2019

1D single-cell migration on microlanes and at interfaces

Christoph Schreiber

Dissertation
an der Fakultät für Physik
der Ludwig-Maximilians-Universität
München

vorgelegt von
Christoph Schreiber
aus Weilheim

München, den 30.09.2019

Erstgutachter: Prof. Dr. Joachim O. Rädler
Zweitgutachter: Prof. Dr. Chase P. Broedersz
Tag der mündlichen Prüfung: 20.11.2019

Zusammenfassung

Zellmigration ist essentiell um die Funktionalität des menschlichen Körpers aufrecht zu erhalten, zum Beispiel für das Immunsystem. Aber auch bei Krankheiten, wie bei der Metastasierung von Krebs, spielt die Fähigkeit von Zellen sich im Körper Fortzubewegen eine große Rolle. Um das Verhalten von Zellen in Abhängigkeit von Umwelteinflüssen vorhersagen zu können und um Medikamente zu entwickeln, die eine Kontrolle der Zellmigration erlauben, brauchen wir ein besseres Verständnis des Prozesses und Methoden um dies quantitativ untersuchen zu können. In ihrer natürlichen Umgebung sind Zellen vielen Reizen aus ihrer Umgebung ausgesetzt. Um Zellmigration unabhängig davon untersuchen zu können oder um gezielt bestimmte Einflüsse zu studieren, benötigt man definierte Umgebungen in denen die Zellbewegung analysiert werden kann. Mit Hilfe von mikrostrukturierten Oberflächen ist es durch die Kontrolle der Oberflächenbeschichtung möglich definierte Modellsysteme zu schaffen. Durch die Verwendung von verschiedenen Beschichtungen, die es Zellen entweder erlauben daran zu haften oder zellabweisend sind, ist es möglich die Bewegung der Zellen auf eindimensionale Bahnen zu beschränken. Mittels Abrastern durch Zeitraffermikroskopie lässt sich so die Bewegung von hunderten einzelnen Zellen parallel beobachten.

In dieser Arbeit wurde festgestellt, dass sich die Bewegung von Brustkrebszellen auf Bahnen näherungsweise mit einem Zweizustandsmodell beschreiben lässt. Dabei wechseln sich Phasen mit gerichteter und zufälliger Bewegung ab. Zusätzlich kann durch den Einbau von Barrieren, bestehend aus zellabweisender Oberflächenbeschichtung, die Fähigkeit der Zellen auf Änderungen im Substrat zu reagieren untersucht werden. Daraus resultieren charakteristische Messgrößen, die das Zellverhalten auf den Bahnen genau beschreiben und somit eine Multiparameterquantifizierung der Zellbewegung ermöglichen.

Die Adhäsionspunkte der Zellen zum Substrat spielen eine große Rolle für die Kraftübertragung und damit für das Vorwärtskommen der Zellen. Um diesen Einflussfaktor genauer zu untersuchen, wurde eine neue Mikrostrukturierungsmethode entwickelt, die es erlaubt Bahnen mit sich stufenweise verändernder Adhäsivität herzustellen. Auf diesen Bahnen kann ein und dieselbe Zelle in Umgebungen mit unterschiedlicher Adhäsivität untersucht werden. Damit konnte die Existenz eines Maximums der Zellgeschwindigkeit für mittlere Adhäsivität auf Einzelzellebene reproduziert werden. Es zeigt sich, dass sich die Geschwindigkeit der Zellen an den Stufenübergängen sowohl beim Übergang der Zellvorder- als auch der Rückseite ändert. Dies, und das Maximum der Geschwindigkeit kann mit einem einfachen phänomenologischen Modell erklärt werden, bei dem die Zelle nur an zwei Punkten – hinten und vorne – mit dem Substrat interagiert, wobei Vorder- und Rückseite gekoppelt sind. Weiterhin zeigt sich, dass Zellen an den Übergängen relative Messungen der Adhäsivität durchführen und vor allem auf eine Verringerung der Adhäsivität reagieren. Diese Erkenntnisse sind von

Bedeutung für die Steuerung von Zellen durch Umgebungseinflüsse und deren Einfluss auf die Zellgeschwindigkeit, aber sie werfen auch neue Fragen auf, etwa über die Funktionsweise der Kopplung von Zellvorder- und Rückseite auf molekularer Ebene.

Darüber hinaus findet die Multiparameterquantifizierung der Zellbewegung auf Bahnen Anwendung bei der Unterscheidung von verschiedenen Zelltypen und bei der Untersuchung der Wirkung von möglichen migrationshemmenden Medikamenten, die in der Krebstherapie eingesetzt werden könnten. Auch für die Untersuchung der Wirkungsweise von micro RNA 200c auf die Zellbewegung, eines Kandidaten für neuartige Formen der Gentherapie, erwies sich diese Methode als nützlich. Insbesondere ermöglicht sie Änderungen des Migrationsverhaltens auf den Bahnen zeitaufgelöst zu erfassen. Somit können bestimmte Zeitpunkte identifiziert werden, zu denen man Änderungen in der Expression beteiligter Proteine erwartet. Entsprechende Korrelationsstudien, zwischen Genexpression und Änderung des Phänotyps, könnten dabei helfen komplizierte regulatorische Netzwerke aufzuklären und so neue wirkungsvolle Ansätze für die Krebstherapie zu finden.

Summary

Cell migration is essential to maintaining the functionality of the human body, for example in immune response. Nonetheless, the ability of cells to move in the body also plays a major role in diseases, such as cancer metastasis. In order to be able to predict how cell migration is affected by environmental cues and to find drugs that allow controlling cell migration, we need a better understanding of the process and methods to quantitatively investigate this. In their natural environment, cells are exposed to many influences from their surrounding. In order to study cell migration independently of those cues or to specifically study certain effects, defined conditions are required in which cell movement can be analysed. With the help of microstructured surfaces, it is possible to get defined environments by controlling surface coatings. By the use of different coatings, which are cell adhesive or cell repellent, it is possible to confine the movement of cells to one-dimensional lanes. Applying scanning time-lapse microscopy, the movement of hundreds of individual cells can be observed in parallel.

In this work, we find that the movement of breast cancer cells on lanes can be approximately described with a two-state model where phases of directed and random motion alternate. In addition, the ability of the cells to react to changes in the substrate can be investigated by incorporating barriers consisting of cell-repellent surface coatings. This results in characteristic measures that provide a detailed description of the cell behaviour on lanes and thus enables a multiparameter quantification of cell movement.

The adhesion points of the cells to the substrate play an important role for transmission of forces and thus for the locomotion of cells. In order to investigate this factor in more detail, a new micropatterning method was developed that allows producing lanes with steps of changing adhesiveness. On these lanes, one and the same cell can be examined in environments with different adhesiveness. This made it possible to reproduce the existence of a maximum cell velocity for medium adhesiveness at the single-cell level. We show that the velocity of the cells changes twice at the steps–when the front and when back traverses. This, and the maximum in the velocity, can be explained by a simple phenomenological model in which the cell interacts with the substrate at only two points–at the front and the back–and with a coupling between front and back. Furthermore, we show that cells perform relative measurements of adhesiveness at the transitions and strikingly react almost exclusively to a reduction of adhesiveness. These findings are important for guiding cells by environmental cues and for their effects on cell velocity, but they also raise new questions, for instance about how the coupling of the front and back of the cell works at the molecular level.

In addition, the multiparameter quantification of cell motility is applied to differentiate cell types and to study the effect of possible anti-migration drugs that could be used in cancer therapy. This method also proved useful for the investigation of the mode

of action of micro RNA 200c on cell migration, a candidate for novel forms of gene therapy. In particular, the assay allows recording changes in migration behaviour in a time-resolved manner. Thus, certain points in time can be identified at which changes in the expression of involved proteins are expected. Corresponding correlation studies between gene expression and changes of the phenotype could help to elucidate complex regulatory networks and thus contribute to finding new effective approaches in cancer therapy.

Contents

Zusammenfassung vii

Summary ix

List of publications 1

1. Introduction 3

2. Fundamental concepts 7
- 2.1. Cell migration . . . 7
  - 2.1.1. The cell migration mechanism . . . 7
  - 2.1.2. Mechanistical models of cell migration . . . 9
- 2.2. Microstructures for confining cell migration . . . 10
- 2.3. Mathematical description of cell trajectories . . . 12
  - 2.3.1. Persistent random motion . . . 12
  - 2.3.2. Two state motion . . . 13
  - 2.3.3. Generalized Langevin equation and models with memory . . . 15
  - 2.3.4. Cells confined to dumbbell micropatterns . . . 16
- 2.4. Micro RNA . . . 18

3. Single cell migration and interaction with chemical barriers 21
- 3.1. Cell migration on 2D surfaces . . . 21
- 3.2. 1D cell migration on ring-shaped microlanes . . . 22
- 3.3. Two-state motion . . . 23
- 3.4. Barrier crossing . . . 27
- 3.5. The migratory fingerprint . . . 30

4. Controlling cell migration with micro RNA 200c 33
- 4.1. Inducible expression of micro RNA 200c . . . 33
- 4.2. Micro RNA 200c decreases cell motility . . . 35
- 4.3. Micro RNA 200c affects morphology and regulates filamin A . . . 39
- 4.4. Time resolved switching of cell motility . . . 41

5. Cell migration depending on substrate adhesiveness 47
- 5.1. A two protein patterning technique . . . 47
- 5.2. Maximal velocity for intermediate fibronectin concentrations . . . 50
- 5.3. Velocity changes during traversals . . . 53
- 5.4. A two-point model of a migrating cell . . . 55
- 5.5. A mechanical approach to describe the velocity relation . . . 57
- 5.6. A phenomenological model explains the velocity relation . . . 60

5.7. Dynamics of the rear . . . 62
5.8. Stochastic reversals at the interface . . . 65

6. Conclusion and outlook **69**

A. Methods and experimental details **75**
A.1. Micropatterning . . . 75
A.1.1. Stamp production . . . 75
A.1.2. Protein labelling . . . 75
A.1.3. Microcontactprinting . . . 76
A.1.4. Two protein patterning . . . 76
A.2. Cell culture . . . 77
A.3. Microscopy . . . 77
A.4. Determination of fibronectin surface concentrations . . . 78

B. Image and data analysis **81**
B.1. Semi-automated tracking of nuclei . . . 81
B.2. Change point analysis . . . 82
B.3. Pattern detection and automated cell tracking . . . 85
B.3.1. Line detection . . . 85
B.3.2. Evaluation of pattern homogeneity . . . 86
B.3.3. Cell tracking . . . 88
B.4. Kymographs . . . 90

Bibliography **95**

List of publications and manuscripts

Publication 1: Ring-Shaped Microlanes and Chemical Barriers as a Platform for Probing Single-Cell Migration
Christoph Schreiber*, Felix J. Segerer*, Ernst Wagner, Andreas Roidl, and Joachim O. Rädler, *Scientific Reports* 6:26858. 2016 [1]

Publication 2: Stochastic nonlinear dynamics of confined cell migration in two-state systems
David B. Brückner*, Alexandra Fink*, Christoph Schreiber, Peter J. F. Röttgermann, Joachim O. Rädler, and Chase P. Broedersz, *Nature Physics* 15(6):595-601. 2019 [2]

Publication 3: Contractility as a global regulator of cellular morphology, velocity, and directionality in low-adhesive fibrillary micro-environments
Simon L. Schuster, Felix J. Segerer, Florian A. Gegenfurtner, Kerstin Kick, Christoph Schreiber, Max Albert, Angelika M. Vollmar, Joachim O. Rädler, Stefan Zahler, *Biomaterials* 102:137-147. 2016 [3]

Publication 4: Inducible microRNA-200c decreases motility of breast cancer cells and reduces filamin A
Bojan Ljepoja, Christoph Schreiber, Florian A. Gegenfurtner, Jonathan García-Roman, Stefan Zahler, Joachim O. Rädler, Ernst Wagner, Andreas Roidl, *PLoS One* 14, e0224314. 2019 [4]

Publication 5: Area and Geometry Dependence of Cell Migration in Asymmetric Two-State Micropatterns
Alexandra Fink, David B. Brückner, Christoph Schreiber, Peter J. F. Röttgermann, Chase P. Broedersz, and Joachim O. Rädler, *Biophysical Journal* in press [5]

Publication 6: Quasi-Periodic Migration of Single Cells on Short Microlanes
Fang Zhou, Sophia A. Schaffer, Christoph Schreiber, Felix J. Segerer, Andriy Goychuk, Erwin Frey, and Joachim O. Rädler *bioRxiv* 809939. 2019 [6]

Manuscript 1: Cell velocity and reversal kinetics studied on micropatterned lanes with steps of different adhesiveness
Christoph Schreiber, Behnam Amiri, Martin Falcke, and Joachim O. Rädler

Manuscript 2: Non-Markovian data-driven modeling of single-cell motility
Bernhard Mitterwallner, Christoph Schreiber, Jan Daldrop, Joachim Rädler, and Roland R. Netz, accepted in Physical Review E

* authors contributed equally

1. Introduction

We, as human beings would not be able to survive without many small cells that are able to migrate in our body, because cell migration is crucial for essential processes like immune response, wound healing and homeostasis. Furthermore, cell migration is important in embryogenesis, but it can also give rise to diseases like arthritis or the formation of cancer metastasis [7–12].
Cells are capable to move forward by a complex mechanism that is based on treadmilling of their actin cytoskeleton. By polymerization of actin at the cell front, the leading edge is pushed forward, and contractile forces are generated by myosin motor proteins that pull on the back of the cell. To transmit these forces to the substrate, cells need to form adhesions that link the cytoskeleton to their surrounding. These processes are controlled by a complex regulation network with hundreds of proteins being involved [13, 14].
Although the main players of the migration mechanism have been identified, there is still no fundamental understanding of the process. For example, it is not clear how external influences like the adhesiveness of the substrate define the emerging migration patterns, or how internal processes in the cell are coordinated. A more comprehensive understanding of this process is needed to be able to predict cell behaviour in a specific environment and to finally control cell migration in therapeutic applications.
In order to detect and to characterize changes in the migration behaviour, a framework is needed that quantifies cell motility. However, this quantification of motility is not straight forward as cells can behave very heterogeneously. Additionally, the migration patterns of cells have been described by many different mathematical models such as the persistent random walk or by extensions of it. Therefore, it is not clear which parameters should be used to quantify the cell motion [15, 16].
An investigation of cell motility in the natural 3D environment is very challenging and in this case the influences of the environment are difficult to control. Furthermore, due to the heterogeneity of the cells, it is important to develop classification methods that allow to perform measurements with high throughput, to obtain meaningful statistics. Consequently, there is a need for *in vitro* experiments that allow studying the motility of cells in a defined environment in high number. In the last decades, micropatterning techniques have been developed that are well suited to fulfil this task [17–19]. Using these techniques cell adhesive patterns of defined geometry can be created which provide a defined environment for migration experiments. The surface can be coated with cell adhesive substances such as the extra-cellular matrix protein fibronectin surrounded by cell repellent coatings that lead to a confinement of the cells.
Especially, the restriction of cells to lanes have been proved useful since this simplifies the analysis of the cell motion to a 1D problem [20]. By using scanning time-lapse microscopy, this allows tracking hundreds of cells in parallel over several days and therefore a detailed investigation of the cell migration behaviour.
In addition to studying migration on a homogenous lane, it is also possible to introduce

obstacles into the micropatterns. Cells migrating in the body, often have to squeeze through small pores or are faced to areas with varying adhesiveness. By studying cell behaviour at artificial barriers or restrictions, possible connections to the migration patterns *in vivo* can be investigated and the mechanism of overcoming barriers can be studied.
Micropatterns do not only provide a defined confining geometry, but also allow controlling the number of available binding sites. Previous studies showed that the average velocity of cells shows a maximum for intermediate adhesiveness of the substrate and cells are slower on substrates with low or high adhesiveness [21–24]. This biphasic behaviour is believed to be caused by the fact that, on the one hand adhesions are necessary to transmit forces that are needed for protrusion formation. On the other hand, adhesions have to be broken when the rear of the cell is moving forward. However, there is still no comprehensive biophysical model that can explain to what extend these processes influence the cell behaviour as it is difficult to measure these two factors independently. Therefore, new assays like micropatterns with areas of different adhesiveness are needed, that are able to disentangle these processes with purposive single-cell experiments.
The adhesiveness of the substrate also plays a role in cell guidance. On gradients of surface bound adhesion ligands cells have been found to move preferentially towards higher ligand density [25]. Cell guidance by surface bound cues is a process called haptotaxis and plays an important role in immune response and cancer metastasis. For cells migrating on a smooth gradient of adhesiveness it is usually difficult to discriminate between the random walk behaviour of a single cell and actual effects of the gradient. How cells react on stepwise changes of ligand density is mostly unexplored and this could give further insights on this cell guidance mechanism.
A multiparameter quantification of the cell migration behaviour on micropatterns could be applied for drug screening and can lead to a better understanding of the effects of potential drug candidates. For example, many anti cancer drugs aim to decrease cell motility to prevent cells from invading other tissues.
As cancer is usually caused by modifications of the genome, there was a great hope that gene therapy could be successful in fighting cancer. However, there is also a great risk in therapies that try to permanently modify the DNA of cells. Therefore, new therapy concepts that transiently change the gene expression of certain cells could be more promising. One class of potential candidates for therapeutic applications are micro RNAs (miRNA) – small parts of RNA, that are involved in transcriptional regulation of gene expression. Many cancer types show abnormal levels of certain miRNAs, which could play an important role in cancer progression.
In order to identify cancer repressing miRNAs, a proper understanding of the gene regulatory networks is needed. miRNAs often regulate several genes, thus it is difficult to connect changes in the phenotype to an altered expression level of certain proteins. In order to extend our knowledge of such a network, it is possible to perform time resolved studies that detect changes of protein expression caused by a miRNA. In combination with time resolved studies of the cell phenotype this could help to identify causal relations between cell behaviour and gene expression.
For usual cell migration experiments, often a time average is applied and long time intervals are needed to even obtain meaningful parameters. Thus, there is a need to develop assays that allow to calculate motility parameters without averaging over time,

which can be used to detect changes in the cell behaviour.

The aim of this thesis is to establish micropatterned lanes as an assay to quantify 1D single-cell migration that provides a multiparameter characterization of cell motility. Moreover, to gain a better mechanistic understanding of the cell migration process and its dependence on adhesions, we introduce steps of different adhesiveness and non-adhesive barriers into the lanes. Furthermore, to prove the utility of the assay for studying effects of potential drug candidates and to investigate their mode of action, we quantify changes of cell motility caused by salinomycin or by miRNA 200c.

The thesis is structured as follows:
In **Chapter 2** the fundamental concepts of cell migration and its analysis, micropatterns, and miRNA are described.
Chapter 3 introduces ring shaped microlanes as a platform to quantify cell motility. The quasi 1D motion on these lanes can be approximately described by a two state process. Additionally, the ability of cells to overcome non-adhesive barriers is studied. The resulting parameters provide a characteristic fingerprint of the cell migration behaviour that can be used to discriminate cell lines and to quantify drug effects.
In **Chapter 4** the effect of miRNA 200c on cell migration is studied in detail. By studying induced changes in the protein expression of cells, candidates are identified that are involved in the regulation network. In order to reduce the number of candidates, time points when changes in the motility occur are identified that can be correlated with changes in gene expression.
In **Chapter 5** the dependence of cell motility on the adhesiveness of the substrate is studied. We reproduce the existence of a maximal velocity for intermediate adhesiveness on single-cell level by using microlanes with steps of fibronectin concentrations. At transitions, the velocity of the cell front changes when the front traverses and also when the rear traverses. This allows us to formulate a simple phenomenological two point model of a cell coupling to the substrate only at front and back. This model can describe the velocity changes at the interface and the maximum of the velocity. Further, the stochastic reversal behaviour at the interface is studied, which shows that cells perform relative measurements of the adhesiveness.
Chapter 6 gives an outlook and discusses implications and further experiments. In the supplementary **Chapter A** more experimental details are given and protocols of the utilized methods are provided. In **Chapter B** the algorithms used for automated image analysis are described. Furthermore the analysis of the cell trajectories with the classification into the two states is presented.

2. Fundamental concepts

2.1. Cell migration

Cell migration plays an important role in many processes in biology. It is essential in the development of structures in embryos [8], wound healing [9] and immune response [10]. But it can also be part of diseases like in rheumatoid arthritis [12] and cancer metastasis [7, 11]. On the molecular scale, cell migration is a highly complex process that involves the coordination of hundreds of different proteins [13]. After decades of research on cell migration, much is known about the key players in the cell migration machinery, but there is still no fundamental understanding of this intricate process.

There are also several modes of cell migration. Cells can either migrate as single cells or collectively [14, 26]. Single cells may perform amoeboid cell migration, which does not depend on adhesions to the substrate but is mainly driven by deformations of the cell membrane in a 3D environment. Alternatively, cells can move in the mesenchymal mode of migration that relies on strong adhesions to the substrate [27] and cells can also switch between modes in response to the environment [28]. In this thesis, we focus on cancer cells that exhibit mesenchymal cell migration. The basic mechanism of how mesenchymal cells move forward is described in the following section.

2.1.1. The cell migration mechanism

Cells move forward in a cyclic process that can be separated into five key steps (see also Fig. 2.1). The first requirement for a cell to perform directed motion is to polarize, which means that the symmetry has to be broken to define the front and the rear of the cell. At the front, actin is polymerized which pushes the membrane forward. As a next step, new adhesions are formed that connect the newly formed protrusion to the substrate. Furthermore, a mechanism for contraction is needed that is mediated by myosin II motor-proteins which condense the actin meshwork. In the last step adhesions at the rear end are released, which leads to a forward motion of the cell body [14].

At the front, cells can form several different types of protrusions: Filopodia are thin rod-like protrusions that contain straight actin fibres. In mesenchymal cells, lamellipodia are the most important protrusions to generate forward motion. The lamellipodium consists of a branched actin network where fibres are interconnected by actin binding proteins like the Arp 2/3 complex. The actin network is connected to the substrate by focal adhesions that consist of integrins which are transmembrane proteins that can bind specifically to certain extra cellular matrix proteins. The integrins form clusters

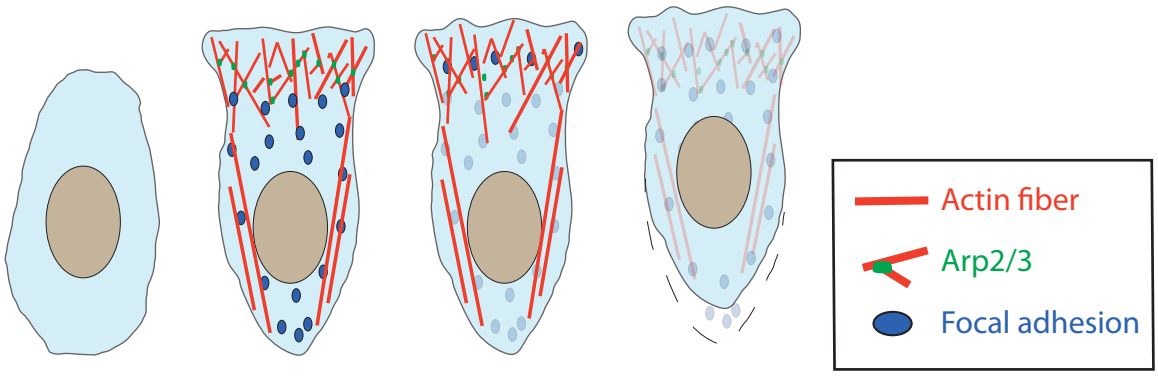

Figure 2.1.: Key processes of cell migration. First, cells polarize and develop a lamellipodium at the front that includes a branched actin network. By polymerisation of actin the leading edge is pushed forward. In the next step new focal adhesions are formed at the front and the actin network is contracted by myosin motor proteins. Finally, adhesions are released at the back, which leads to a forward sliding of the cell rear.

by binding to several different proteins in the cytoplasm, which in turn bind to the actin cytoskeleton. By these linkages forces are transmitted from the cytoskeleton to the substrate.

Actin monomers can polymerize and form polar actin fibres with so called pointed and barbed ends. The barbed ends are pointing to the front of the cell and new actin monomers can bind here which leads to an elongation of the fibres. Further to the back, actin fibres disassemble and monomers get free to move to the front, which means that there is actin tread-milling [13, 14, 29, 30].
On top of that, the actin network is constantly contracted by non-muscle myosin II motor proteins that bind to the actin fibres and build up contractile force. Usually, the speed of polymerisation of new filamentous actin at the leading edge is higher than the speed of the leading edge. This means that the whole actin network is moving backwards inside the lamellipodium which gives rise to a retrograde actin flow [30, 31].
The formation of new adhesion is a process that starts with very small clusters of intergrins that are forming at the front, which are called nascent adhesions. They grow over time until they form mature focal adhesions located usually a few μm behind the leading edge. The maturation of adhesion is a mechano-sensitive process that only takes place if pulling forces act on the adhesions. The protein clusters at the focal adhesions take also an important role in signalling as they, for example, give positive feedback on actin polymerization. [32, 33]

When taking a closer look at the process at the front of the cell it becomes evident that the cell front is not moving forward continuously but shows an oscillatory behaviour. After phases of actin polymerization, where the front moves forward, there are phases where the front is retracted [34]. When newly formed protrusions are not connected perfectly to the substrate the leading edge gets pulled backward by the contracting actin network until the next pulse of actin polymerization pushes the front forward again. In the regulation of these process, hundreds of different proteins are involved. However, it is known that so-called small GTPases play a key role. In particular, Rac1,

RhoA, and Cdc42 are main regulators of cell polarity, actin polymerization and myosin activity. [35–38] These master regulators of cell migration have been shown to have oscillating activity in the cells, probably defining the timing of the retraction protrusion cycles [39].
To retract the cell rear, adhesions at the back have to be dissembled. RhoA plays an important role in this process by activating myosin II motors that can produce contractile forces that may be strong enough to break adhesions. In addition to mechanical forces, there are also other signalling molecules that play an active role in disassembling adhesions at the rear and also Calcium levels are assumed to be involved. [14, 33]

2.1.2. Mechanistical models of cell migration

As the main molecular players in the process of cell migration have bee identified, there have been extensive efforts to create models that explain this mechanism. However, due to the complexity of the process it is often needed to do great simplifications. In order to tackle this problem, many models focus on subprocesses like protrusion formation, actin tread-milling, adhesion, or contractility.

The pushing of the membrane at the front by actin polymerization was first explained by ratchet models, where thermal fluctuations give room for growth of actin filaments [40, 41]. Further, more complex models were introduced, which model whole actin networks that include branching and capping of filaments [42]. Another approach is to model the actin network as an elastic gel actively generating stress at the surface [43–45]. Experiments showed that the protrusion velocity does not change also in response to small forces acting against the protrusion. Only if a certain force threshold is exceeded protrusion velocity decreases abruptly [46]. Those models or extensions that include for example excluded volume effects can successfully explain the protrusion force–velocity relationship [47, 48] and give a good understanding of the protrusion formation.
Compared to the many models that exist on protrusion formation, there are only few models that explicitly study the contraction of actin networks by myosin motors. It has been shown that actin and myosin filaments can self-organize and form ordered contracting structures [49, 50].
Adhesions consist of very complex clusters with many molecules, thus it is very difficult to model them on a molecular level, similar to polymerization of actin networks. often they are approximated by elastic springs that connect the actin cytoskeleton and the substrate which can bind unbind or slip along the surface [51]. This leads to an effective drag of the actin network [52]. In conclusion, when the friction is high actin polymerization can be converted into protrusion. However, for low coupling to the substrate the actin network tread-mills without being able to push the front forward [53]. In addition to this, adhesions also respond to mechanical cues from their surrounding and get strengthened in response to forces [32] which needs to be incorporated in more detailed models.

In order to incorporate all of this into a model of a whole cell is very difficult and there is still some work needed to get a good understanding of how all the processes are connected. Often, great simplifications are made, by for example formulating a 1D model [22]. Nevertheless, for complete model of the cell also signalling mechanisms that define the polarity of cells have to be included [54]. Another way to simplify models is to use so called potts models where cells consist of a set of pixels and cytoskeletal processes are translated into discrete rules that define propagation of cell [55, 56]. For the description of cell migration in 2D also cell shape gets important which enters into the models [57, 58]. Furthermore, influences of the environment such as micropatterns can be considered [59, 60]. There have been also approaches to actually build a 3D model [61] which is the next step to a realistic model of cell migration.

There are many more studies available in this large field of modelling cell migration. An excellent introduction that explains the most important modelling approaches is the review by Danuser et al. [48] and there are more reviews that give a detailed overview of possible models [62–65].

2.2. Microstructures for confining cell migration

Many cell types do not survive without adhering to their surrounding, thus cell adhesive substrates are needed to culture those cells *in vitro*. With the development of so called soft lithography techniques that were described in the 1990ies by Whitesides and co-workers [17, 66–69] it got possible to easily produce cell adhesive micro-environments with defined geometries. This allows addressing specific biological questions that are connected to a spacial confinement of cells.

The methods for creating those micropatterns summarized as soft lithography are based on a polymer stamp with a relief pattern, consisting usually of PDMS. These stamps can be produced from a master engraved with the inverse structure which, in turn, can be created by classical photo-lithography. Using these stamps, it is possible to create surfaces which are selectively modified to obtain cell adhesive and cell repellent areas. One of the methods is called microcontactprinting, which means that the stamp is inked with a layer of, for example, cell adhesive molecules that is subsequently transferred to the substrate of interest [66, 70–72]. Alternatively, the stamp can also be used to protect some areas to achieve a selective coating, cleaning or other surface modification of some parts of the substrate, for example by plasma treatment [17, 73, 74]. With increasing control of photochemistry that involves the controlled binding of biomolecules there are now also many techniques available that create micropatterns using photolitographic approaches [19, 75–78].

The most common class of molecules to create cell adhesive surfaces are ECM proteins, as they are the natural environment for cells. Out of those, fibronectin is most abundantly used, but also other ECM proteins like collagens or laminin can be utilized. To create cell repellent surfaces, the adsorption of proteins has to be prevented. Usually, polyethylen glycol (PEG) coatings are used for this purpose. For example, using PLL-

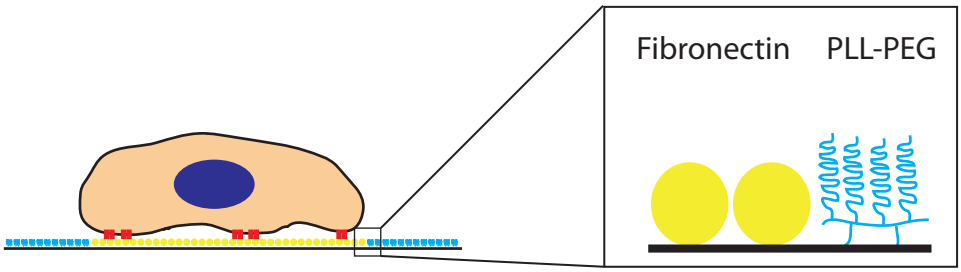

Figure 2.2.: Schematic drawing of a cell on a micropattern. On cell-adhesive areas (for example coated with fibronectin, yellow) cells can form adhesions (red). Cell-repellent surfaces can be created by coating with PLL-PEG (blue). The PLL backbone binds to the surface and the PEG chains prevent protein binding. (Molecule sizes not drawn to scale.)

PEG block-copolymers (poly-L-lysine grafted with PEG chains), whose binding to the surface is mediated by the PLL backbone, results in a coverage of the surface with PEG chains. The PEG chains form a brush, thus sterically hindering proteins, and subsequently also cells, from binding to the surface (see also Fig. 2.2).
For cells to be able to bind to the surface coatings, integrins have to be able to bind. For example for fibronectin cells can bind to the RGD sequence (Amino-acids Arginine, Glycine, and Aspartate) that is abundant in fibronectin. For some proteins it is important that the structure is intact so that they can provide a binding site for cells. When proteins are unspecifically bound to the surface it is possible that proteins get degenerated. To prevent this, proteins can be bound to certain linker proteins which can attach to the substrate [79]. In addition to this also the conformation of the proteins can be important. For example for fibrous fibronectin it is known that additional binding sites can get accessible when domains are unfolded in response to forces that are exceeded by the cells [80, 81].

Typically micropatterns consist of two different coatings. However, more sophisticated methods have also been developed that allow creating more complicated microenvironments for cells, consisting of several areas with different surface coatings. This is realized by combining some of the techniques mentioned above, by subsequent patterning steps or by removing surface coatings from defined areas [70, 74, 78, 82–84].

Micropatternes are applied for investigating many different biological questions. Patterns of the size of a single cell have been used to prevent cell migration and study dynamics of cell death [85–88] and gene expression [89] or the arrangement of and changes in the cytoskeleton [65, 90–93]. Micropatterns have often been used to study cell migration. In particular, they are handy to confine cell migration to a quasi 1D motion by using long stripes. On these stripes, Maiuri et al. [20] performed *"the first world cell race"* and compared the motility of many different cell types. Thus, micropatterned lanes have been utilised to quantify motility and also the effects of the confinement to 1D [3, 54, 94–98]. Interestingly, on 1D tracks the cell morphology is closer to the morphology of cells in the natural 3D environment than on 2D [94]. On the isotropic stripes, cells do not have a preferential direction of motion. By introducing micropatterns with

anisotropic shapes it is possible to bias cell migration to one direction, for example by using ratchets or tear drop shapes [99–102]. Furthermore, micropatterns have been used to study collective cell migration in defined geometries and also the interaction of small groups of cells [74, 103–105].

Another class of micropatterns goes beyond different surface modifications and also includes a 3D structuring of the environment. For example, it is possible to create small channels consisting of polymers, substructures in the nm regime, or to tune the rigidity of the substrate. Methods to create those micropatterns and their application are reviewed here: [18, 106, 107].

2.3. Mathematical description of cell trajectories

The study of random motion of particles goes back to the famous observation of the botanist Robert Brown who found that pollen particles move irregularly on a water film [108]. This so-called "Brownian motion" was explained by theory, for example by Enstein [109, 110], and predicted that the Mean-Square-Displacement (MSD) of the particles is proportional to the observation time. When studying cell migration, on the first glimpse, it looks quite similar to the thermally driven Brownian motion. But cells or other living organisms are self-propelled and therefore it is not clear whether the movement can be captured with a similarly simple formula.

2.3.1. Persistent random motion

The first studies on the motion of small organisms were conducted in the 1920ies [111, 112], where Fürth found that the motion is not purely random but shows some persistence. This can be described mathematically by the Ornstein Uhlenbeck process

$$\frac{\partial v}{\partial t} = -\beta v + \sigma \overrightarrow{\eta} \tag{2.1}$$

where $\overrightarrow{\eta}$ is Gaussian white noise, thus a random vector without correlations in time drawn from a Gaussian distribution with standard deviation 1 and σ gives the noise strength. By introducing the effective friction term $-\beta v$ this leads to a persistence time of $\tau = \frac{1}{\beta}$ [113].
For persistent random motion the MSD is proportional to t^2 for timescales shorter than τ and proportional to t on long timescales:

$$MSD(t) = \langle (x(t) - x(0))^2 \rangle = \frac{n\sigma^2}{\beta^3}(e^{-\beta t} + \beta t - 1) \tag{2.2}$$

where n is the the number of dimensions. The MSD of the small organisms seemed to be well described by Formula 2.2 which is called Fürth's Formula. Also, for the

first studies with cells crawling on a 2D surface the behaviour matched the Ornstein Uhlenbeck process [15, 114], thus Fürth's Formula became the standard formalism for analysing cell migration [115, 116]. In this sense, the motility of a cell migrating on a 2D surface is characterized by two parameters. Namely, by the persistence time τ and by σ^2 which is basically a measure for the magnitude of the cell velocity.

The first experiments were performed by marking the positions of the observed organisms by hand while looking through the microscope, which limited the amount and quality of the data. With the development of automatized microscopes and digital image analysis the data acquisition and analysis became much easier. This allowed a more detailed analysis and showed many deviations from the persistent random walk (PRW) [16, 117–120].
Thus, other models are needed to describe cell motion. In principle there are many possible models that can also get very complicated. The most common ones are introduced here.
In general, there are different possibilities to formulate such a model. One option is to write down a stochastic differential equation as for the Ornstein Uhlenbeck process. However, the data acquisition is always in discrete time steps, thus for data analysis and for modelling often a discrete version of the model is needed. Alternatively, it is possible to define discrete rule-based models.

A corresponding simple discrete model of a PRW would be a walker making steps to the left and right on a 1D lattice. To incorporate persistence, the walker has a higher probability $p > 0.5$ to make a step in the same direction than in the opposite direction (with probability 1-p). In this case, the probability to make n subsequent steps in one direction would be $P_n = p^n \cdot (1 - p)$. Thus, for this simple example it is easy to to see that for a PRW the probability to make n consecutive steps is exponentially distributed.

2.3.2. Two state motion

One class of possible models to describe cell migration is two state motion. By definition, this means that the walker has two different modes that could both be described by all possible migration models. However, for two state models the following assumptions are usually made: One state is described by ballistic motion, meaning a straight motion in one direction. The other state is diffusive random motion. In the simplest case, there is a constant probability to switch from one state to the other, and back. Thus, the switching behaviour is a Poisson process and rates do not depend on the behaviour in the past, as, for example, is found for the decay of a radioactive isotope. One important property of such a process is that the probability distribution of the duration of the states follows an exponential distribution.

There are many examples in biological systems for two state processes. Most prominent is maybe the motion of E-Coli bacteria that perform a run and tumble motion by either clockwise or counter clockwise rotation of their flagella. [121, 122]
Also, the motion of eukaryotic cells on 2D surfaces has been described as two state motion [123–125]. An explanation why two state motion is commonly found in nature,

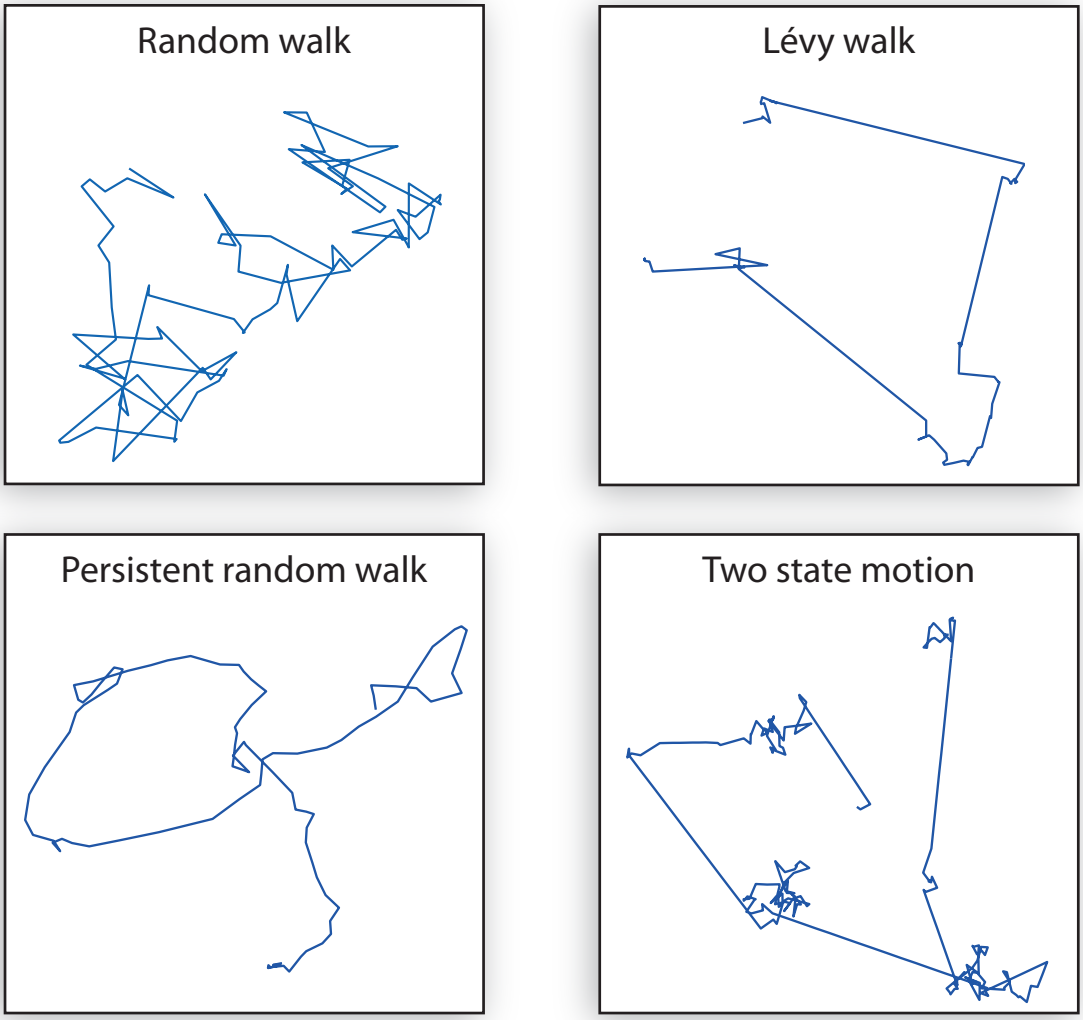

Figure 2.3.: Comparison of trajectories for different random walk models. Exemplary trajectories were generated using discrete versions of random walk, Lévi walk, persistent random walk and two-state motion.

could be that it is much more efficient in search processes compared to simple random walks [126]. Thus, for example, when animals are looking for food it makes sense to switch between phases of exploring the surrounding area in detail and of moving to another spot. Without the phases of ballistic motion this would give rise to oversampling in some areas and thus decreasing the efficiency of the search process.

A Lévi walk is also a simple random walk model that produces similar trajectories as the two-state motion. Lévi walks are characterized by random steps and a heavy tailed step length distribution. Thus, very long steps are possible, which also reduces the effect of oversampling in search processes. Consequently, Lévi walks also have been found to describe the motion of animals or also single cells [119, 126, 127].
On the first glimpse, it is often not easy to tell whether one trajectory resembles persistent random motion, two-state motion, or a Lévy walk (Fig. 2.3). All of these models

have in common that on long time scales the motion is random but on short time scales there are signs of ballistic behaviour. In 1D it is quite easy to evaluate the probability distribution of consecutive steps. Here, there are differences in the models. A PRW gives rise to an exponential distribution, whereas for two state motion we would get a sum of two exponentials. In contrast, Lévy walks have by definition a heavy tailed distribution of step lengths.

When describing the motion of cells by a two state process it is also interesting to know the underlying molecular mechanism that gives rise to the two states. In general, cells can be polarized or unpolarized, naturally giving two states. However, it is not clear whether those states are clearly separated or merge continuously. In a model by Maiuri et al. [54], the unpolarized state is stable due to equalization of concentrations by diffusion. By adding a self-reinforcing mechanism that amplifies changes of concentrations of a regulator binding to the actin network that increases the differences through retrograde actin flow, it is possible to get a bistable system. Thus, this could be a possible mechanism giving rise to two-state motion in cells.

2.3.3. Generalized Langevin equation and models with memory

Although it is possible that cells or other organisms follow a simple random walk model, it is mostly just a matter of how precise the measurements are to find some deviations. To account for possible deviations it makes sense to use a more general approach. Therefore, often a generalized Langevin equation is used:

$$\dot{v}(t) = F(v(t)) + \sigma \vec{\eta}(t) \tag{2.3}$$

Here, $F(v(t))$ can be any kind of function that depends on v and $\vec{\eta}(t)$ represents the noise in the system. In the case of cell migration the velocity is very small, thus inertia does not play a role in these systems. Thus, F(v) can be interpreted as effective force, rather than an actual friction force or similar as known from a classical mechanical system. In a complex system, like a cell, it is possible that there are memory effects. Thus, it is possible that changes in the velocity do not solely depend on the present velocity as in the Ornstein Uhlenbeck process (Equation 2.1), but could also depend on the velocity in the past. This memory could be stored in the cytoskeletal organization where, in a polarized cell, clearly some information about the present orientation is preserved. Mathematically, the memory can be expressed by a memory kernel Γ:

$$F(v(t)) = -\int_{-\infty}^{t} \Gamma(t-s)v(s)ds \tag{2.4}$$

The value for $\Gamma(0)$, thus without time delay, would be a simple friction term like in the Ornstein Uhlenbeck process. The other values for $\Gamma(t)$ weight the influence of the velocity in the past. Those kind of models have been successfully used to describe the motion of cells [118, 128].
Mostly, it is assumed that the noise $\vec{\eta}(t)$ is uncorrelated.

$$\langle \vec{\eta}(t) \cdot \vec{\eta}(t') \rangle = 0 \tag{2.5}$$

But this does not necessarily have to be true. The existence of correlated noise, also termed coloured noise, constitutes another possibility of how behaviour in the past can influence changes in the velocity.

In collaboration with the group of Roland Netz we analysed trajectories of MDA-MB-436 cells on ring-shaped microlanes in terms of this formalism including a memory kernel and explicitly considering the possibility of coloured noise. To be able to extract meaningful memory kernels from the trajectories we did experiments with a time resolution of 2.5 min. A further increase of the sampling rate was not achieved as phototoxic effects of the UV illumination become problematic. We found that the cell motion can indeed be described by such an approach. The cell motion is governed by a memory kernel with a positive value for $\Gamma(0)$, which then drops to negative friction and relaxes to zero in about 10 min. More details of the analysis are summarized in Manuscript 2.

2.3.4. Cells confined to dumbbell micropatterns

For now, the mathematical description of cell trajectories focussed mostly on homogeneous environments. However, in the human body cells are faced with a complex structured environment. It is not clear how the equation of motion of a cell would look like in such a confined situation, and features of the environment would have to enter into the mathematical description. As 3D environments are very complicated, we used dumbbell shaped micropatterns as a simplified version of a cell migrating in confinement and analysed how the motion of the cell can be described, which is presented in Publication [2] in greater detail. This work was done in collaboration with Alexandra Fink and with the group of Chase Broedersz.
The dumbbell patterns consist of two quadratic 37x37 μm islands that are connected by a thin bridge. On these patterns, cells perform repeated stochastic transitions from one site to the other (Fig. 2.4a, b). In this artificial two-state system we investigate the dwell times between the transitions and find that they increase with the length of the connecting bridge.
At the first glance, it looks like the effects of a the confinement could mathematically be described by introducing a potential V(x) like proposed also for similar situations [129–132].

$$\dot{v}(t) = F(v) - \partial_x V(x) + \sigma \overrightarrow{\eta}(t) \tag{2.6}$$

The observed dwell times however, could not be explained by such an approach. We found that a second order equation

$$\dot{v}(t) = F(x, v) - \sigma(x, v) \overrightarrow{\eta}(t) \tag{2.7}$$

in which the deterministic force F and the noise strength σ are both dependent on x and v describes the cell migration behaviour on the dumbbell patterns very well. Here, the noise is uncorrelated, thus no memory is needed.
We used a data-driven approach to determine the values of F(x,v) and σ(x,v), which gives rise to characteristic landscapes in x-v space (Fig. 2.4c, d). The landscapes for the deterministic terms reveal that without noise there is a non-linear dynamic that

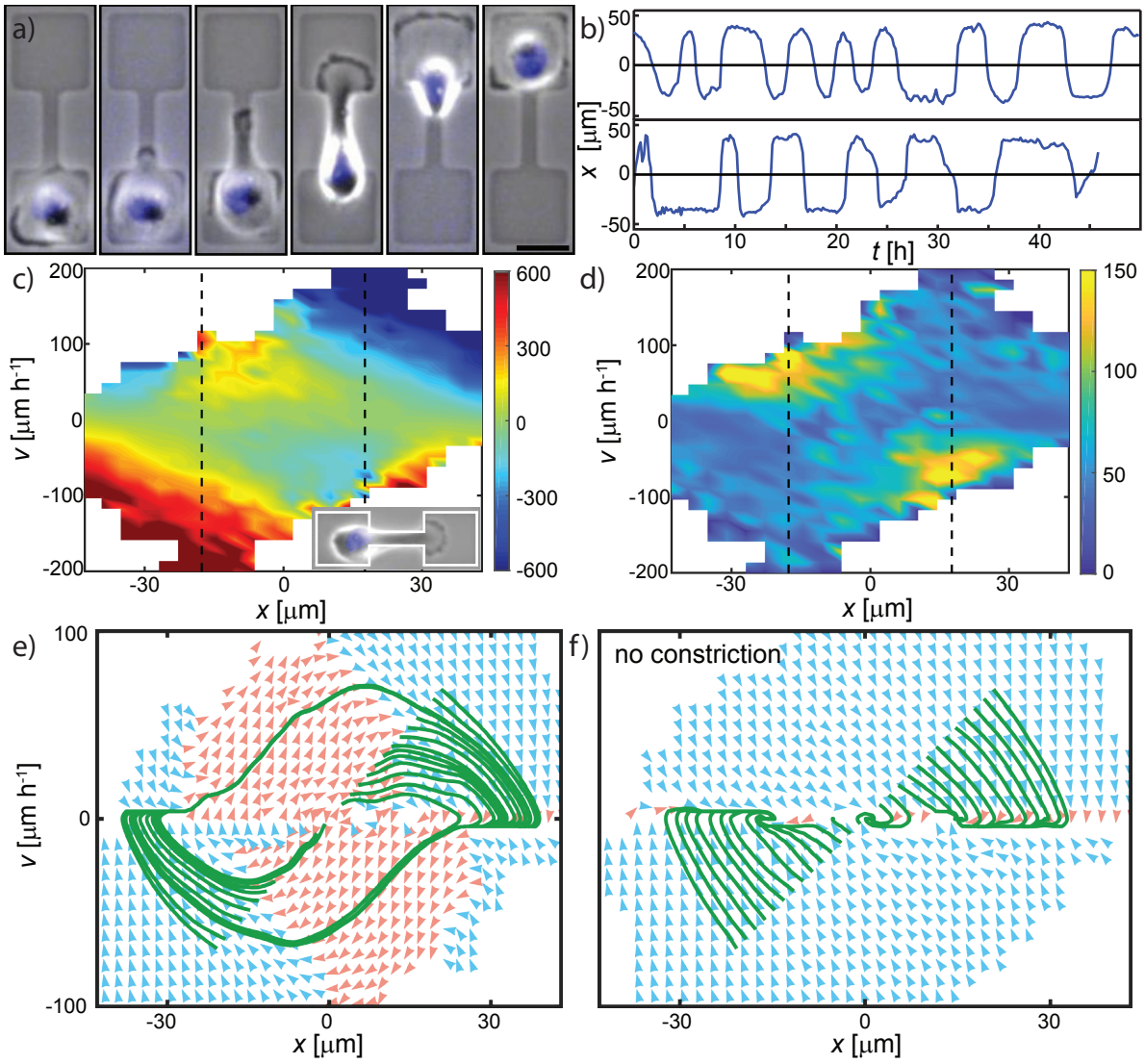

Figure 2.4.: a) Time series of a MDA-MB-231 cell migrating on a dumbbell micropattern. Phase-contrast images and the labelled nucleus (blue) are overlaid (scale bar 25 μm). b) Two exemplary cell tracks on the dumbbells. The position of the nucleus along the long axis of the micropattern (x), is plotted over time. c) F(x,v) and d) σ(x,v) inferred from the cell trajectories. The right and left side of the bridge is marked by the dashed lines. e) Flow fields of the deterministic dynamics of cells on dumbbells and on rectangles (f) (acceleration orange, deceleration blue). In green, simulated trajectories with different initial conditions are shown. Figure adapted from Publication [2] with permission.

underlies the cell motion. For the MDA-MB-231 cells on dumbells we find that cells perform limit cycle oscillations from one side to the other (Fig. 2.4e) around an unstable fix-point at x,v = (0,0). In contrast, on a rectangular pattern without the constriction in the middle this fixpoint becomes stable (Fig. 2.4f). This shows that active particles like cells can show fascinating types of motion when they are in a confining environment.
The dumbbell assay is also a useful setup to let a single cell probe different micro-environments. It turns out that the area and also the geometry of the islands can change the dwell times of cells, which is described in Publication [5].

2.4. Micro RNA

Proteins are the most important building blocks of cells. The production of new proteins is described by the central dogma of molecular biology: The information encoded in the DNA is transferred to a messenger RNA (mRNA) in a process called transcription. The mRNA then has to get from the nucleus to the cytosol where the translation into protein takes place. To gain specific functions and to adapt to changes in the environment, cells have to be able to control the proteins which are expressed. This is done, for example, on the transcriptional level where transcription factors change transcription rates for specific genes by binding to the DNA. But there is also a lot of regulation taking place on the post transcriptional or translational level [133].

One important mechanism of post-transcriptional regulation is by micro RNAs (miRNA), small non-coding pieces of RNA. Those pieces with a length of about 22 nucleotides can bind to complementary regions of mRNAs and block translation or even lead to degradation of the mRNAs. miRNAs have been found to be very widespread in biology. More than 24,000 miRNAs have been found in over 200 species and at least 60% of the human genome is believed to be regulated by miRNAs. To bind to the mRNA, miRNAs need a perfect matching sequence in a certain seed region. Otherwise, a few mismatches can still lead to a down-regulation of the gene. Thus, miRNAs usually come in families with similar sequences that have overlapping targets. miRNAs can often bind more than one mRNA and therefore can regulate several genes that might be involved in different cellular functions.
In many diseases, for example in a lot of cancer types, the expression of miRNAs is changed. Consequently, this makes miRNAs an interesting target for diagnostics and therapeutic approaches. In cancer cells, some miRNAs are up-regulated and others are down-regulated, so that they can act either as oncogene or as tumour repressor [134–136].

One prominent miRNA that plays an important role in many cancer types is micro RNA 200c (miR-200c), which is the most prominent player in the miR-200 family. It mainly acts as a tumour repressor by interfering with many processes such as epithelial-mesenchymal-transition (EMT), chemoresistence, invasion, proliferation, and apoptosis. Therefore, miR-200c is a potential biomarker or could be used in therapeutic applications [134, 137, 138].
Through the regulation of EMT, miR-200c is also connected to cell migration. EMT is one of the hallmarks of cancer and describes the process of epithelial cells transforming to more motile mesenchymal cells. This is a natural process that plays an important role in embryonic development. But in cancer it can lead to invasive cells and the formation of metastasis. During EMT, epithelial cells that are well connected to their neighbours, for example by E-cadherins, lose their cell-to-cell contacts and get the ability to move as single cells [139, 140].

It has been found that miR-200c triggers EMT by down-regulating E-cadherins [134]. However, there is evidence that cell migration is also affected independently of this mechanism [141]. A detailed investigation of how miR-200c affects cell migration is presented in chapter 4.

3. Single cell migration and interaction with chemical barriers

In order to characterize cell motility, which allows to distinguish cell lines and to quantify changes in motility caused for example by drugs, assays have to be developed that allow measuring with high throughput. Additionally, metrics allowing an extraction of meaningful parameters are needed. Therefore, in this chapter, we introduce ring-shaped microlanes with non-adhesive barriers. On these lanes cells are performing a two-state motion quantified by several parameters that lead to a fingerprint like characterisation of cell motility.
Most of the results presented in this chapter are published in Publication [1].

3.1. Cell migration on 2D surfaces

Single cell migration is often studied on homogeneous 2D surfaces, as experiments are easy to perform. Cells on these surfaces can polarize and form a lamellipodium which leads to a seemingly random migration of the cells. During this process cells show a variety of different morphologies (Fig. 3.1a). Sometimes cells are rather round with no clear polarization axis or cells are polarized with a lamellipodium at the front and a tapered tail at the rear. The lamellipodium can get very broad, usually when the cell is shorter or narrower for more elongated cells. Lamellipodia can also split which leads to a cell with two lamellipodia pulling in different directions.
In order to do a more detailed investigation of the migration behaviour, we performed automated cell tracking of the fluorescently labelled nuclei (Fig. 3.1b). By analysing the MSD of 550 tracks we find the characteristic behaviour of random walks with persistence that show super-diffusive or ballistic behaviour at short timescales and random motion on time scales larger than a persistence length that is here on the order of 2 h (Fig. 3.1c).
However, the cell motion can not be described by a simple persistent random walk model like the Ornstein-Uhlenbeck process. It needs actually a more complicated model that includes a memory kernel, which is described in more detail in the supplementary information of Publication [2].
Although it is quite easy to do cell migration experiments on a 2D surface there are some drawbacks. First of all, cells can collide and enter or leave the field of view, which leads to many short trajectories. Additionally, a reduction of the dimensionality reduces the complexity of the analysis. Using a confinement to 1D, processes like the splitting of lamellipodia cannot occur, thus maybe even the inherent complexity is reduced. Furthermore, we run into problems when we introduce changes in substrate adhesiveness

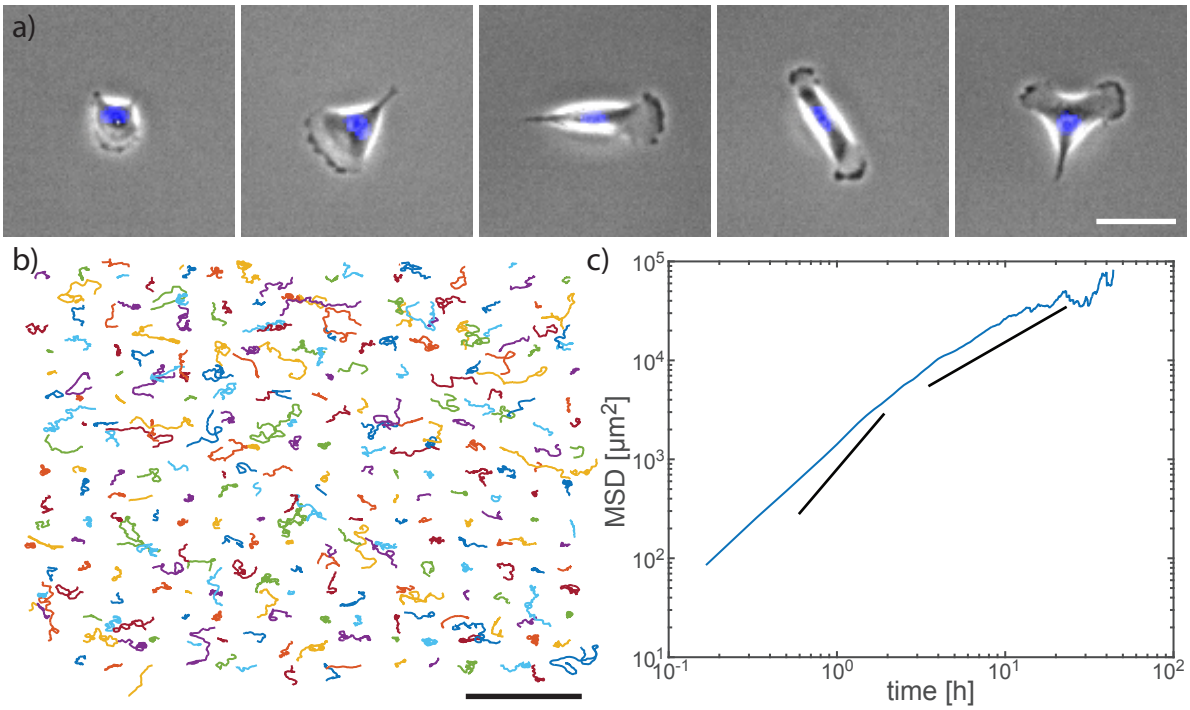

Figure 3.1.: a) Phase-contrast images of a MDA-MB-231 cell on a homogeneously fibronectin coated 2D substrate. The nucleus is shown in blue. The cell shows different morphologies over time. Either no clear polarization axis, one lamellipodia and a tapered tail or two lammellipodia can be observed. Scale bar represents 50 μm. b) Random selection of cell trajectories of the cell nucleus. Scale bar represents 1 mm. c) MSD over time in log-log representation. Black lines have a slope of 2 which represents ballistic motion and a slope of 1 which is typical for random motion.

or obstacles to study the cell behaviour in more complex situations. On 2D substrates cells can be confronted with these obstacles at all possible angles which makes the analysis more difficult.

3.2. 1D cell migration on ring-shaped microlanes

Using micropatterned lanes, the cell movement can be restricted to quasi 1D motion. Therefore, 1D cell migration has been widely used to quantify cell motility [20,54,94,95]. Furthermore, cell on 1D lines show a more elongated morphology, which is closer to the morphology found in 3D [94]. Although this is mainly true for very thin lines. We choose lanes with 20 μm width, which is about the usual width of a cell to have a morphology comparable to 2D, combined with quasi 1D motion.
In order to study the quasi 1D motion of cells, we decided to use ring shaped lanes because they have the advantage over lines that single cells always stay in the field of view. Additionally, if there is only one single cell on a ring the cell cannot interact with other cells, which leads to very long trajectories that are only limited by the time between cell division events, thus up to several days. In contrast, on lines one would get shorter trajectories because cells collide frequently and there is a potential bias to observe slow cells longer as they need more time to reach the image borders or other

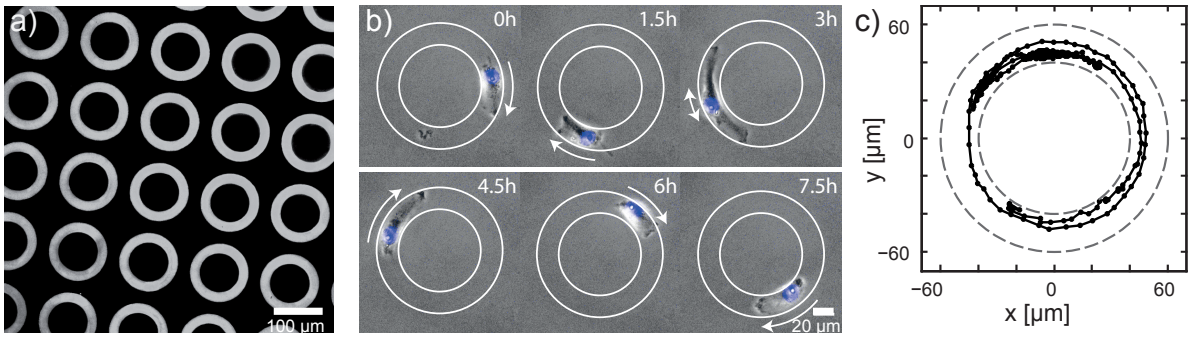

Figure 3.2.: a) Flourescent image of micro lanes coated with labelled fibronectin. Dark regions are coated with PLL-PEG. b) Time series of a single MDA-MB-436 cell migrating on a ring-shaped micropattern (white rings). Phase contrast images overlayed with flourecent images of the nucleus (blue). Arrows indicate the direction of the cell's motion. c) Position of the nucleus over time of an exemplary cell track. Figure adapted from Publication [1] permitted by the creative commons licence.

cells. However, on lines there is the advantage that cells can separate after cell division, which allows to analyse more trajectories.
For the diameter of the ring a compromise between the curvature of the lanes and the number of rings that fit into one field of view has to be made. Smaller rings allow to observe more cells at the same time, because rings need less area and can be placed in a higher density. Larger rings decrease possible effects of the curvature of the lanes on cell migration behaviour [142, 143] and reduce spanning of cells over the middle part. For experiments with MDA-MB-436 cells and HuH7 cells we used a outer diameter of 120 μm and 150 μm for MDA-MB-231 cells because they tend to span over the middle part of smaller rings.
Fibronectin coated ring shaped lanes where created by microcontact printing like described in Section A.1.3 (Fig. 3.2a). On these rings cells are seeded and they adhere to the fibronectin coated lanes. Cells can show a polarized morphology with a clear lamellipodium at the front or a second lamellipodium forms at the back. (Fig. 3.2b) When cells have a polarized morphology they mostly migrate persistently. With two lamellipodia, one at the front and one the back, cells often get elongated and it looks like a tag of war of the two pseudopods that leads to an erratic motion of the cell. In rare cases no lamellipodia can be observed. By tracking the nuclei of single cells (Fig. 3.2c) the motion can be analysed in detail. In the next section we first focus on MDA-MB-436 cells and later compare the data of different cell lines.

3.3. Two-state motion

The cell trajectories can look very different and irregular, thus they are resulting from a stochastic process. The first question when analysing the cell motion is whether it can be described by a simple model such as a persistent random walk, which is often used to describe 2D cell motion [15, 114–116]. Therefore, we look at the MSD of the cells (Fig. 3.3a). On short timescales the MSD has a slope of two in the log-log plot

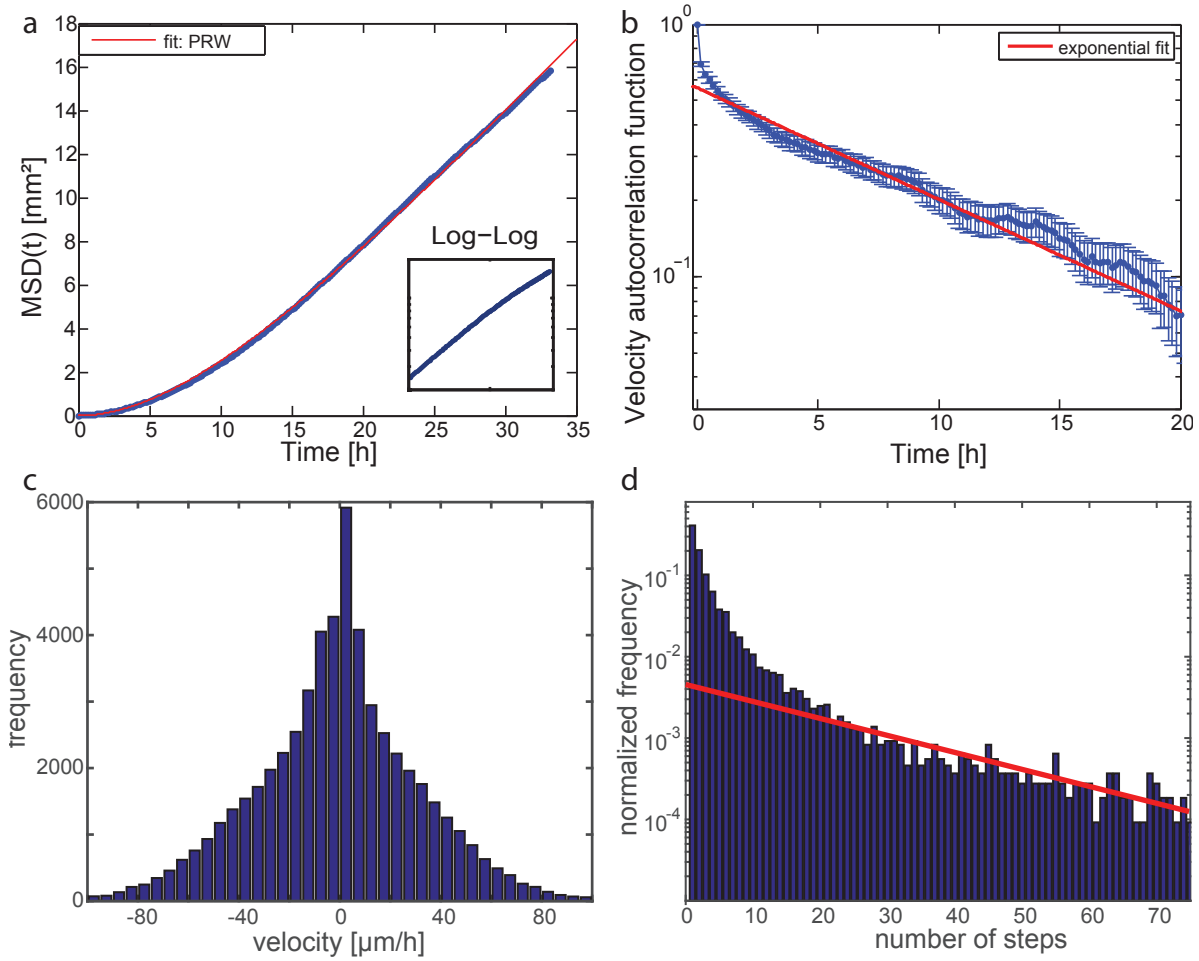

Figure 3.3.: a) MSD of MDA-MB-436 cells migrating on the ring-shaped microlanes. The MSD is fitted with the expression of the PRW model (Equation 2.2). Inlet: MSD(t) in log log scale. b) The log-lin plot of the average velocity autocorrelation function with exponential fit (red). Error bars represent the standard error of the mean. c) The velocity distribution shows a non-Gaussian shape. d) Log-lin plot of the distribution of consecutive steps cells do in one direction. The red line shows that there is an exponential relation for long timescales.

and the slope decreases to one after about 10 h. This is typical for random walks with persistence that show ballistic motion on short timescales and random motion on long timescales [144]. The MSD can be fitted by the PRW model (equation 2.2) reasonably well. However, there are also some deviations from the PRW model. The velocity autocorrelation function shows not just a simple exponential decay (Fig. 3.3b) although the discrepancy is not very large.

The velocity distribution is clearly not a Gaussian distribution (Fig 3.3c). This shows that the PRW model can not explain the data. When looking at the number of consecutive steps cells do in one direction until they turn around we find many short periods but also high numbers of consecutive steps (Fig. 3.3d). For a simple persistent random walker on a lattice one would get an exponential distribution of the number of consecutive steps, which strengthens the finding that the data cannot be explained by the PRW.

When considering single trajectories we find long phases of directional motion and also phases with many directional changes (Fig. 3.4a). This is typical for two-state motion and also for Lévy flights. Lévy flights are random processes that have a heavy tailed probability distribution of step lengths. Therefore, they have a finite probability of very long steps in one direction, which is quite similar to the observed cell behaviour. However, as Fig. 3.3d shows an exponential tail, only a two-state model remains as a possible candidate to explain the cell motion with a simple model.

A two state model would make sense as cells can be either polarized or unpolarized.

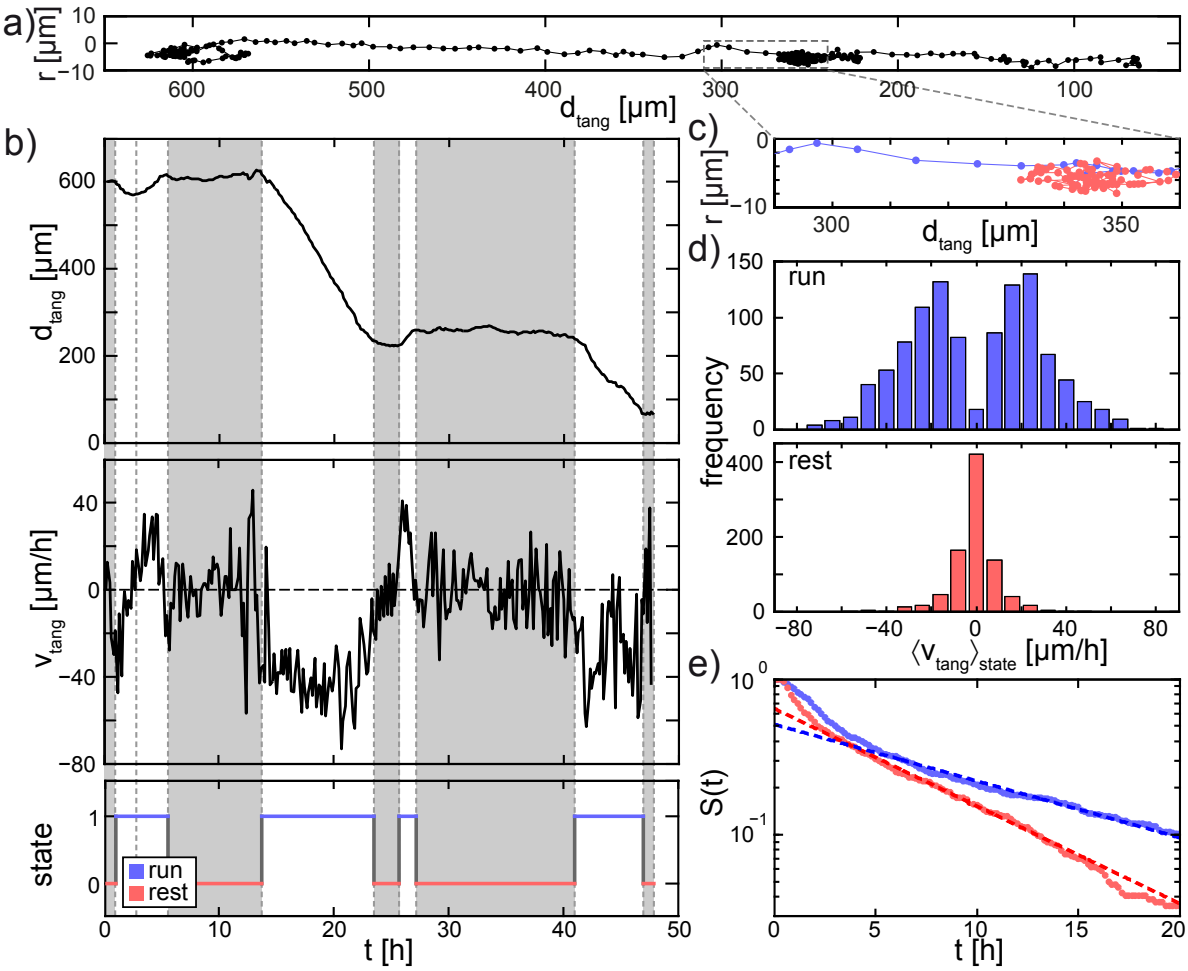

Figure 3.4.: a) Cell trajectory on a ring-shaped lane rolled out. This means that the radial position of the cell is plotted against the angular position d_{tang}. b) Angular position d_{tang} and angular velocity v_{tang} over time. The motion is separated into run and rest states. c) Zoom in of the trajectory shown in a) with classification in run (blue) and rest states (red). d) Velocity distribution for run and rest states. Angular velocity is averaged over each individual state. e) Survival distributions of the duration of run (blue) and rest states (red). Each distribution is fitted with an exponential function that describes the behaviour on long timescales. Figure adapted from Publication [1] permitted by the creative commons licence.

Indeed, the two regimes of the cell motion go along with a varied morphology of the cells. Phases of directional motion is predominantly shown by polarized cells that have only one lamellipodium at the front. During the phases of erratic motion cells often have two competing lamellipodia at the front and the back. For a detailed investigation

of the cell motion we define the angular position as $d_{tang}(t) = R \cdot \phi(t)$ with the mean radius of the micropattern $R = 50\,\mu$m and the angular coordinate ϕ. d_{tang} plotted over time shows clear phases with constant velocity and also plateaus where the cell effectively stays at the same position (Fig. 3.4b). Consequently, it makes sense to separate the motion of cells into run and rest states. Nonetheless, the classification is not trivial. Instantaneous velocities can vary a lot and although they are distributed around zero during rest states they can still be large for single time points (Fig. 3.4b). Therefore, a simple velocity threshold is not suitable to discriminate between the states as it also would not allow to have slow run states that could however still have a high directionality. To get a classification that does not depend on a global velocity threshold but rather depends on the intrinsic noise level of the velocities we implemented a change point analysis based on cumulative sum statistics that is similar to approaches used in climate research or healthcare [145, 146]. The algorithm iteratively detects change points where the trend of the velocity shifts. Phases between two change points are subsequently classified as run states when the MSD grows ballistically or as rest states respectively. The algorithm is explained in further detail in Section B.2.
The separation in the two states allows to evaluate the velocity separately for phases of polarized directional motion and for rest phases with random motion. The velocity of the rest states is distributed around zero. The velocity of the run states shows two peaks representing clockwise and counter clockwise angular motion (Fig. 3.4d). By ignoring the rest phases we can define a meaningful measure for the velocity of migrating cells: $v_{run} = \langle |v_i| \rangle = 30.2 \pm 0.8\,\mu$m/h averaged over the individual run states i. This value is higher than the mean velocity that also includes rest states $v_{mean} = 25.2 \pm 0.8\,\mu$m/h. Further, the duration of the run and rest states can be analysed. Therefore, we calculate the survival function of the run and the rest states. The survival function gives the proportion of states that have a duration T that is lager than t $S(t) = P(T \geq t)$. Thus, it is a monotonically decreasing function starting at one that basically describes a decay process of the investigated state. A simple exponential decay is typical for a Poisson process that has a constant probability that the state is changing over time [147]. We find that S(t) for run and rest states decay exponentially for times larger than 5h (Fig. 3.4e). For shorter times there is a faster decay which means that there are more short run and rest states. The deviations at short time scales can have several reasons. They could be caused by internal movements of the nucleus inside the cell or there is a timescale in which the states are stabilizing. Also falsely detected change-points of the algorithm could have an influence on the survival functions. In conclusion, the cell motion can be approximately described as a two-state motion with a constant probability to switch to the other state. To quantify the dominant behaviour at longer time scales an exponential is fitted to the survial function. The slope in the log lin plot of the exponential function reassembles the typical duration of the respective states: $\tau_{run} = 13.6 \pm 0.5\,$h, and $\tau_{rest} = 6.5 \pm 0.2\,$h. The three measures τ_{run}, τ_{rest}, and v_{run} parametrize the quasi 1D motion of the cells on the ring-shaped microlanes.

3.4. Barrier crossing

In this thesis the approach was used to not only study cell migration in a homogeneous environment, but also to vary the substrate coating to see how cells adapt their behaviour. The reaction on those perturbations can give additional insights and lead to a better understanding of the machinery driving the cell forward. The easiest way to create such a perturbation is to leave a gap in the fibronectin coated ring-shaped lane and coat it with PEG as done also for the surrounding area (Fig. 3.5b). In chapter 5 interfaces between two adhesive areas, namely of different fibronectin concentrations, are studied.
The gaps coated with PLL-PEG have a defined size that is varied from 3 to 19 μm and provide a chemical barrier for the cells as the formation of focal adhesions is suppressed. Cells that interact with the barrier either reverse or, depending on the gap size, traverse the barrier (Fig. 3.5a). During the reversal process, first the cell front interacts with the barrier. The lamellipodium stops protruding, but the cell rear still moves forward for some time. When the nucleus comes closer the lamellipodium at the front disappears and the nucleus comes to halt. Thus, the cell switches from run to rest state. After some time the cell repolarizes in the opposite direction as the PEGylated area suppresses the formation of new protrusions. Usually the cell edge does not stop exactly at the interface but invades into the passivated surface. In some cases, the cell can even reach over to the other side and traverse over the barrier.
By evaluating cell tracks generated by automated tracking of the labelled nuclei (Fig. 3.5c) we investigate reversal and traversal statistics in dependence of the gap width. Therefore, we define an interaction area starting 50 μm in front the barrier. When a cell enters this interaction area we discriminate between the case where the cell nucleus actually crosses the middle of the barrier. This is counted as a traversal event. And between cases where the cells turn around and the nucleus leaves the area at the same side, which we count as an reversal event. Taking together, all interactions with the barrier of many cells we get the traversal probability P_{trans} and the reversal probability $P_{turn} = 1 - P_{trans}$. With increasing gap size d_{gap}, P_{trans} decreases and can be fitted with an exponential decay $P_{trans}(d_{gap}) = (1 - P_{turn}(0)) \cdot exp(-d_{gap}/\mu_{trans})$ (Fig. 3.5d). The exponential relation reminds of tunnelling effects in a potential barrier, but it is not clear how this can be translated to cells confined in a micropattern. Also, the data is not far off a liner relation, thus more data points would be necessary to discriminate between possible models. Attention should be drawn on the fact that P_{trans} is not equal to one for zero gap size. This is caused by cells having a finite probability to turn around even with no barrier present.
In order to study how cells overcome the PEGyalted barrier, we performed experiments of cells migrating on stripe micropatterns. Here, cells reverse at the edge of the stripe, which is basically a blind ally. To investigate how cells reach out into the PEGylated area, we used a time resolution of 5 s, as protrusion dynamics can be on the order of a few seconds. During the reversal, cells reach out of the micropattern (Fig. 3.6a,b). We manually quantify the maximal invasion depth d_{inv} for each observed reversal. In the survival function, $S_{inv}(d) = P(d_{inv} > d)$, we can see that for each reversal all cells reach out of the pattern for a minimum lenght of 2 μm. Subsequently, $S_{inv}(d)$ decays

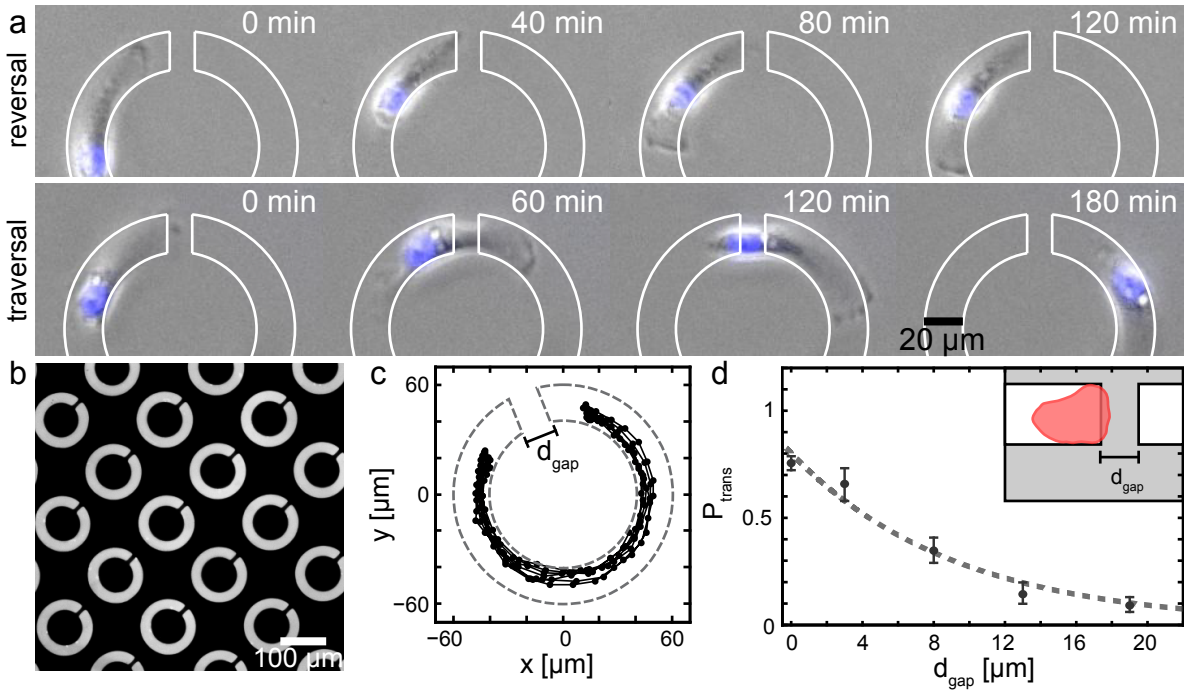

Figure 3.5.: a) Time series of a reversing and a traversing cell. Overlay of the phase contrast images of the cells and the flourescence images of the nucleus (blue). The border of the micropatterns is drawn in white. b) Fluorescent image of a FN coated ring-shaped lane with gap. c) Exemplary trajectory of a single cell migrating on the micropattern for 48h. d) Traversal probability of cells to overcome the PEGylated barrier in dependence of barrier width. Dotted line is an exponential fit. Figure adapted from Publication [1] permitted by the creative commons licence.

and can be fitted with an exponential function $S_{inv}(d) = S_0 \cdot exp(-d/\mu_{inv})$ with a decay length $\mu_{inv} = 11.8 \pm 1.0\mu$m. μ_{inv} is in the same order of magnitude as μ_{trans}, thus we can hypothesize that the traversal probability is mainly determined by the ability of a cell to reach to the other side of the barrier. The PEGylated area functions as a barrier for cells as it mostly prevents the binding of proteins [148]. Thereby the formation of focal adhesions is hampered, which are essential for migration and provide positive feedback for actin polymerization at the front [14]. It is known that the first mature focal adhesions form a few μm behind the leading edge [32, 149]. This is comparable to the length all cells reached out of the blind alley micropatterns and to the difference between μ_{trans} and μ_{inv}. Thus, cell traversal is possibly connected to the formation of mature focal adhesions on the other side of the gap. Analogously, if cells do not succeeded to reach over the gap, the missing positive feedback from the adhesions should lead to a breakdown of the polarization of the cells. The maximal length cells reached out of the pattern was 30 μm. This could set a limit of the gap size where cells cannot overcome the barrier. Studies on similar micropatterns also found such a limit in the distance of individual adhesion points that cells are able to spread [150].

The assumption that the barrier induces a breakdown of the run states is supported by the frequency of rest states that shoots up next to the barrier (Fig. 3.7a). The frequency of run states is constant outside of the interaction area. In the interaction area the probability to find run states decreases mostly in a distance of about 25 μm from the gap. Rest states show the opposite behaviour, but outside of the interaction area the

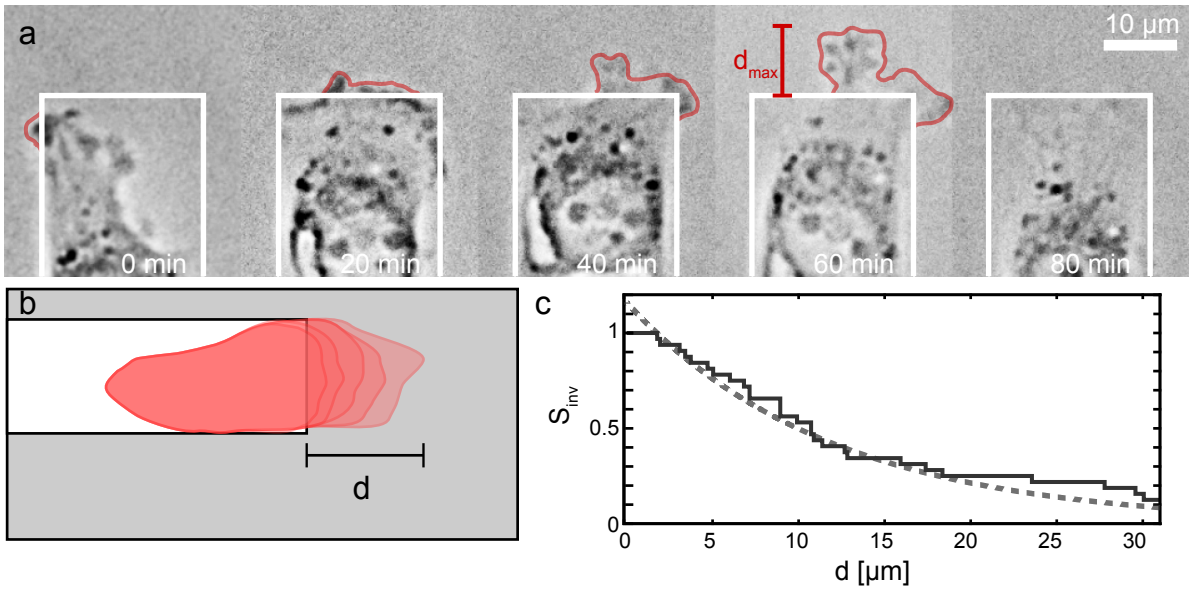

Figure 3.6.: a) Time series of a cell turning around at the end of a micropatterned stripe (white). Bright field images show that the cells edge can reach out into the PEGylated surface (outlines highlighted in red) b) The maximal invasion depth d_{inv} is evaluated for each reversal. c) Survival function S_{inv} of the invasion depth d_{inv}. The dashed line represents an exponential fit. Figure adapted from Publication [1] permitted by the creative commons licence.

probability shows more variation. This is most likely caused by some long rest states in which cells typically do not move much and therefore produce large variations in the rest state statistics. Similar as for the survival times in Figure 3.4e, we can calculate the survival function for the length of the run states. The survival length shows an analogous behaviour as the survival time with an exponential tail and a larger decay rate on short scales (Fig. 3.7b). The first length scale is on the order of 70 μm and therefore on the order of one cell length. This could mean that internal reordering processes inside the cell that take place during polarization play a role in this regime [97].
With introducing gaps of different widths, we observe that the probability of very long runs goes down with increasing d_{gap}. This makes sense because we would expect that a fraction of runs that approach the gap are terminated. Interestingly, mostly the large gaps also reduce the number of very short states in the first regime of short length/time scales. This might be caused by the inherent asymmetry next to the barrier that could help the cells to polarize properly. Furthermore, there is a striking decay of the survival length at a distance when cells start at the one interaction area and travel once around the circle to the interaction area on the other side (dashed lines). This indicates that the start of long runs is not evenly distributed around the circle, but they start predominantly next to the barrier. Additionally to the asymmetry at the gap this could also be caused if there is a memory effect of polarization. Some exceptional cells move repeatedly around the circle and repolarize at the barrier very quickly (Fig. 3.7c). To see whether these cells really do not loose polarization completely but rather reverse it at the interface would need further investigation. Manual tracking of front and back of the cell reveals a very regular behaviour when interacting with the barrier (Fig. 3.7c). First, the cell length shortens when the front stops protruding and the rear still moves

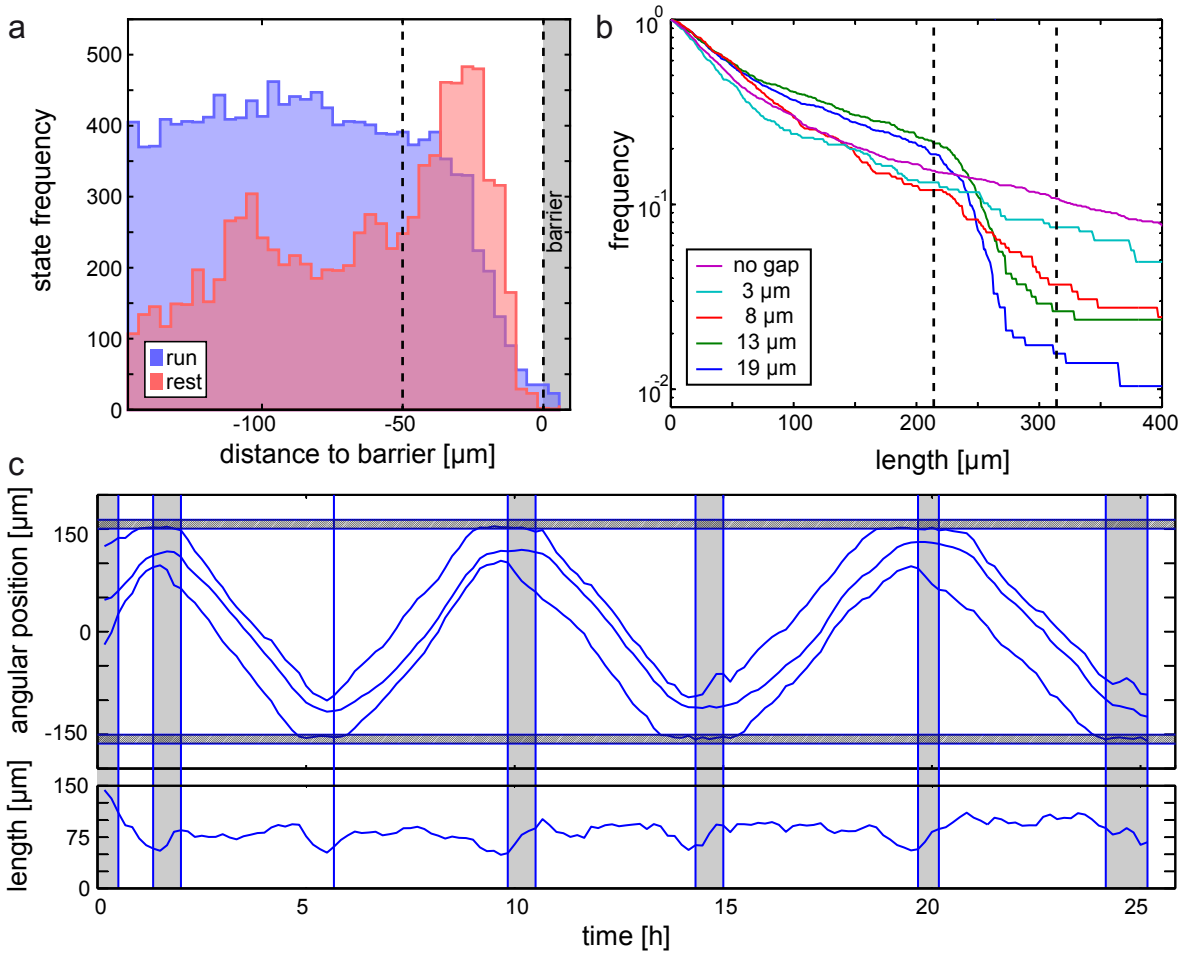

Figure 3.7.: a) Frequency of run and rest states depending on the distance to a 19 μm gap. In the interaction area, 50 μm in front of the barrier (dashed line) cells are mostly in the rest state whereas further away run states are predominant. b) Survival length of run states on patterns with varying gap sizes. The dashed lines mark the interaction area in the case for a run state starting at the other side of the gap. c) Exemplary trajectory of a cell showing periodic reversing at a 13 μm gap and running around the circle. Run (white) and rest phases (grey) are shown. Blue lines mark the manually tracked front and back. The middle line represents the position of the nucleus. The cell length over time is given below. Figure a) adapted from Publication [1] permitted by the creative commons licence

forward. When the rear comes to halt, which we mostly detect as start of a short rest state, immediately at the back a new lamellipodium is formed that spreads and the rear follows when the full cell length is reached again. This shows that analysis of front and rear motion exhibits interesting features. Thus, the motion of the front and the rear of the cell is investigated in Chapter 5 in more detail.

3.5. The migratory fingerprint

In order to quantify the motility of certain cell types and to detect changes in the migration behaviour caused by diseases or drugs, a set of distinctive parameters is needed.

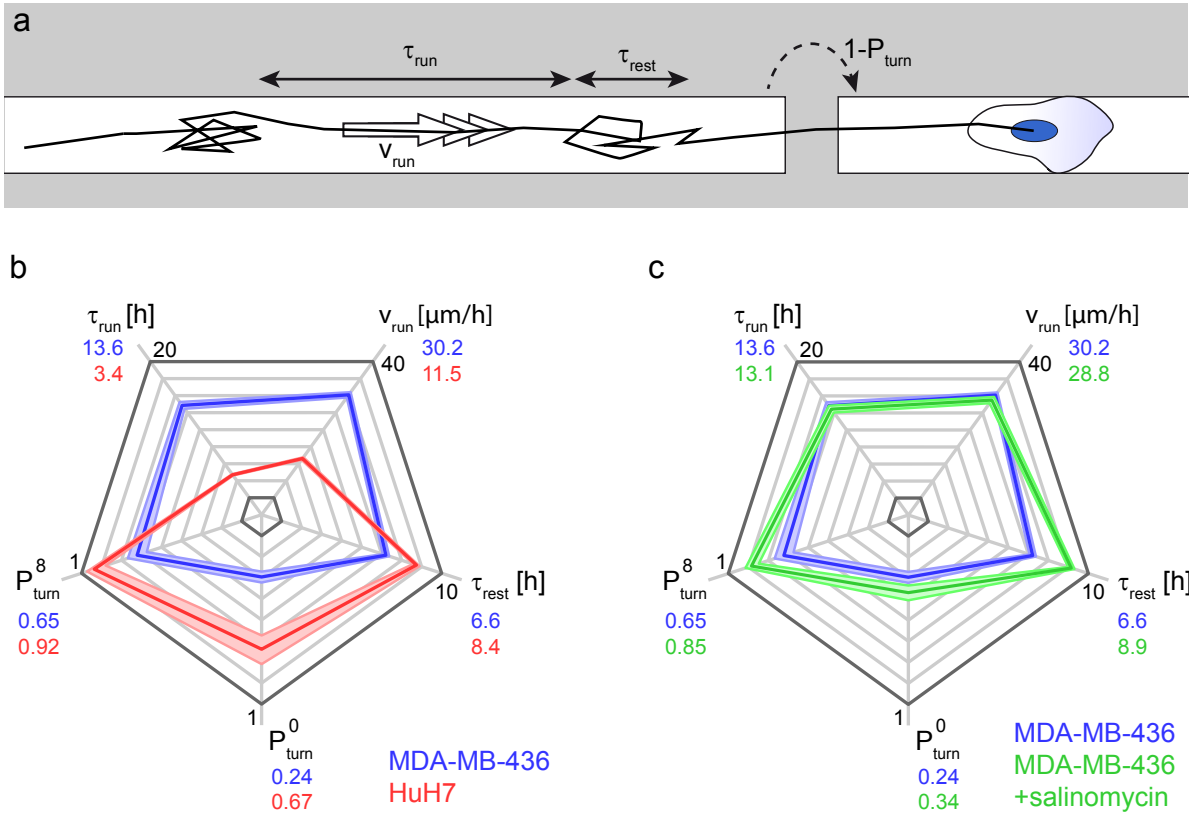

Figure 3.8.: Multiparameter characterzation of cell migration: a) Two state motion and crossing of chemical barriers is characterized by the run velocity v_{run} , the duration of run and rest states τ_{run} and τ_{rest} and the turning probability $P_{turn}^{d_{gap}}$ b,c) Migratory fingerprint: 5 characteristic motility ar plotted to compare MDA-MB-436 cells with HuH7 cells (b) or the effect of Salinomycin (c). The values for each parameter are connected and form a characteristic polygon with shaded areas representing the error range. HuH7 cells are less motile in all parameters, whereas Salinomycin changes only τ_{rest} and the behavior at the gap. Figure adapted from Publication [1] permitted by the creative commons licence.

The motion on the rings without gap is characterized by the three parameters v_{run}, τ_{run} and τ_{rest}. To quantify the ability of cells to overcome PEGylated areas we chose the probability to reverse at a $8\,\mu$m gap P_{turn}^{8}. At this size, reversals and traversals are frequently observed for MDA-MB-436 cells, thus deviations in both directions can be measured. This probability has to be compared to the probability to turn around with no barrier present P_{turn}^{0}. Taken together we get five parameters characterizing the motility of cells and the potential to overcome chemical barriers (Fig. 3.8a).

Radar charts can be used to visualize parameters of cell motility as similarly used for morphological parameters [151]. The resulting polygon gives a fingerprint like characterization of the cell motility. We arraged the parameter in a way, and used P_{turn}^{d} instead of P_{trans}^{d}, so that for more motile cells the fingerprint is shifted to the top and for less motile cells to the bottom. In Figure 3.8b we compare MDA-MB-436 breast cancer cells to HuH7 liver cancer cells. The position of the polygons shows that the HuH7 cells, which are more epithelial, are much less motile than the more mesenchymal MDA-MB-436 cells. Differences can be seen in all measured parameters. HuH7 cells are slower and have shorter run phases and longer rest states. Also for overcoming barriers

HuH7 cells show a very low probability, which is decreased by a factor of four compared to the MDA-MB-436 cells.
Furthermore, the effect of cell motility affecting drugs can be visualized by the fingerprints. In Figure 3.8c the effect of Salinomycin on MDA-MB-436 cells is shown. Previous studies showed that Salinomycin reduces velocity and persistence of cells migration on 2D surfaces [152]. The two state analysis on the ring-shaped lanes shows that run velocity and run time is not affected by Salinomycin. It's only the rest states that get longer and also the ability to overcome chemical barriers is reduced.
These findings are in agreement with the knowledge that MDA-MB-436 cells are more invasive than the HuH7 cells [152–154]. Although we have an artificial system, the different cell types behave according to their invasiveness *in vivo*. Thus, the multiparameter characterization of cell motility can potentially be used to get a meaningful classification of cancer cell types. However, further studies that clarify the correlation of *in vivo* and *in vitro* behaviour are needed to investigate the potential of this assay.
The fact that the parameters describing the behaviour in the run state are not altered by Salinomycin implicate that it does not affect the processes that drive a polarized cell forward. The anti-migratory effect of Salinomycin is rather caused by interfering with the process of establishing polarization of the cell. This is supported by the fact that Salinomycin leads to a calcium influx into to the cell, which can affect the natural calcium gradients or patterns that are important for cell polarization [155, 156].
Consequently, we showed with these examples that the multiparameter quantification of cell migration gives a more precise picture of cell motility compared to classical 2D cell migration assays. The parameters (except for P^0_{turn}, which could be expressed as a combination of v_{run}, τ_{run} and τ_{rest}) are in principle independent of each other. To have these orthogonal parameters is especially useful to link changes in single parameters to the underlying processes. Of course, these parameters are only independent in the sense of the mathematical analysis of the two-state process. Parameters can still be connected on a mechanistic level of the molecular machinery as hypothesised for velocity and directional persistence of cell motion [54].

4. Controlling cell migration with micro RNA 200c

As we showed in chapter 3, ring-shaped microlanes are suitable for a detailed quantification of cell motility. The group of Andreas Roidl investigates the effects of miR-200c on cell migration (see section 2.4 for more information about miRNAs), thus we formed a collaboration and applied the multi-parameter quantification of cell motility on a target with possible relevance for clinical applications.
Expression of miR-200c is often lower in many cancer types and is described as *"watchdog in cancer progression"* [134]. It is involved in the regulation of many genes that play a role for example in EMT, drug resistance, proliferation and metastasis.
A recent study of the Roidl group analysed the changes in the proteome of MCF7 breast cancer cells when knocking out miR-200c. They found that about 50% of the genes with varied expression comared to the wild-type are connected to cell migration [157]. The most prominent axis of miR-200c interfering with migration and EMT is by regulation of E-cadherin via the protein ZEB1 (see Section 2.4). But, in MCF7 cells and also in other cancer types like MDA-MB-231 cells the ZEB/E-cadherin axis is not active due to epigenetic modifications [158–160]. A reduction of the miR-200c expression in MCF7 cells still led to an increased cell motilty. Thus, miR-200c shows effects independent of the ZEB/E-cadherin axis that where also found in other studies [141, 157]. However, there is no detailed quantifications of the changes in motility induced by miR-200c. Thus, we studied the effects of miR-200c on migration and morphology of the cells. Additionally, it is of interest which genes that show altered expression are responsible for the changes in cell motility. This is not an easy task as miRNAs can target many genes. Thus, we analyse also dynamic changes of motility parameters that could in combination with time resolved protein expression studies help to identify the important players of the regulation network.
Most of the results presented in this chapter is content of Publication [4].

4.1. Inducible expression of micro RNA 200c

The first step to study the effects of miR-200c on migration is to find a suitable model organism. Due to the fact that the ZEB/E-cadherin axis is not active in MCF7 and MDA-MB-231 cells, they both are suitable cell lines to study ZEB independent effects. MCF7 cells express miR-200c and show an epithelial phenotype, thus forming a closed cell layer with strong cell-cell contacts and usually do not migrate as single cells. In contrast, MDA-MB-231 cells do not express miR-200c, do not form cell-cell contacts,

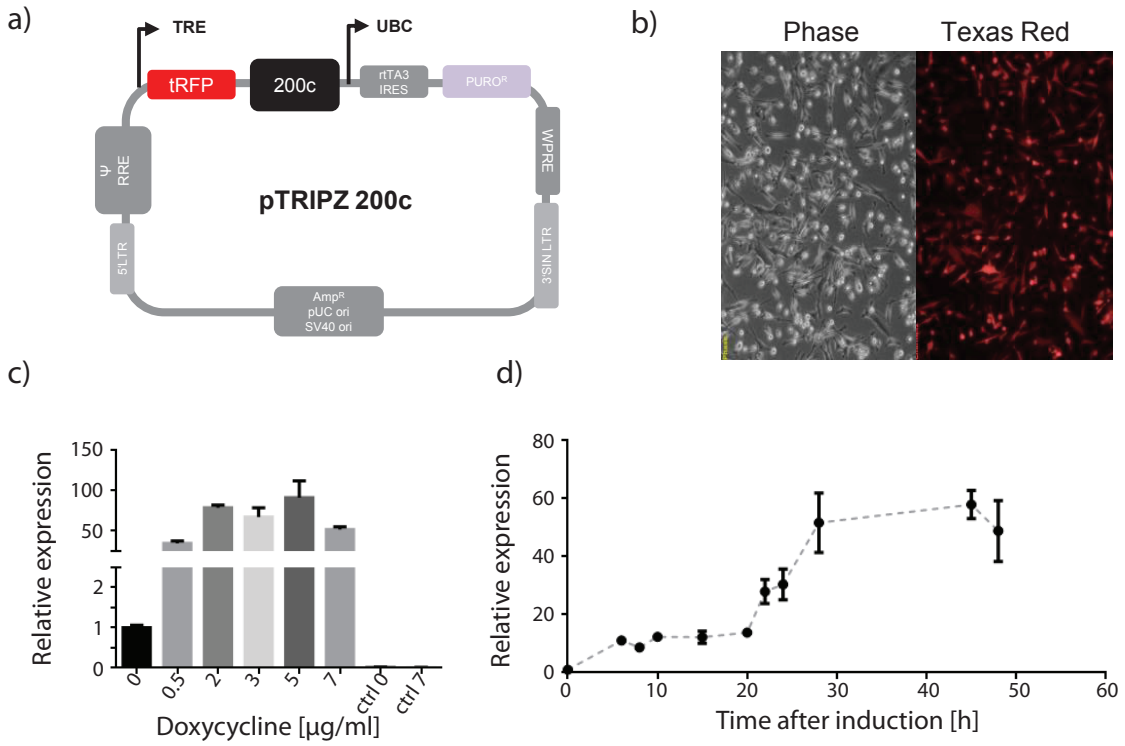

Figure 4.1.: Inducilble sytem for miR-200c expression. a) Schematic drawing of the plasmid used to create a cell line with inducible miR-200c expression. It is a modified TRIPZ plasmid where expression of RFP and miR-200c can be triggered by adding Doxycycline. b) Phase contrast and corresponding fluorescence image of MDA-MB-231 TRIPZ-200c cells treated with 5 μg/ml Doxycycline for 48,h. Cells express RFP and miR-200c. c) Expression of miR-200c in MDA-MB-231 TRIPZ-200c cells treated with different concentrations of Doxycycline for 48h relative to no Doxycycline. This is compared to miR-200c expression in MDA-MB-231 TRIPZ-Ctrl cells. d) Relative expression of miR-200c over time for MDA-MB-231 TRIPZ-200c cells treated with 5 μg/ml Doxycycline.

and are highly motile as single cells. Since MCF7 wild-type cells spend basically all of the time in the rest state, it is difficult to quantitatively compare the changes in the motility parameters. Additionally, in terms of applications *in vivo* it makes more sense to reduce the motility of invasive cancer cells instead of making cells more aggressive. Therefore, MDA-MB-231 cells were chosen for migration experiments.
The next problem is to find a suitable way of expressing the miRNA in cells. Usual methods like transient transfection of the cells with miRNA have the disadvantage that cells are stressed by the transfection procedure. This can also have an effect on migration, which makes it more difficult to identify the miR-200c induced effects. A stable transfection of miR-200c would minimize those effects. However, the selection process of the successfully transfected cells needs a lot of time. As many genes are regulated by miR-200c cells could change their phenotype dramatically. Such a transformation takes place fore example during EMT or the reverse mesenchymal-epithelial transition (MET). Those processes take usually several days [139]. Therefore, the changes in motility during the first days are of special interest as these are the direct effects of miR-200c on cell migration.
The Roidl group found a clever way to express miR-200c by stably transfecting cells

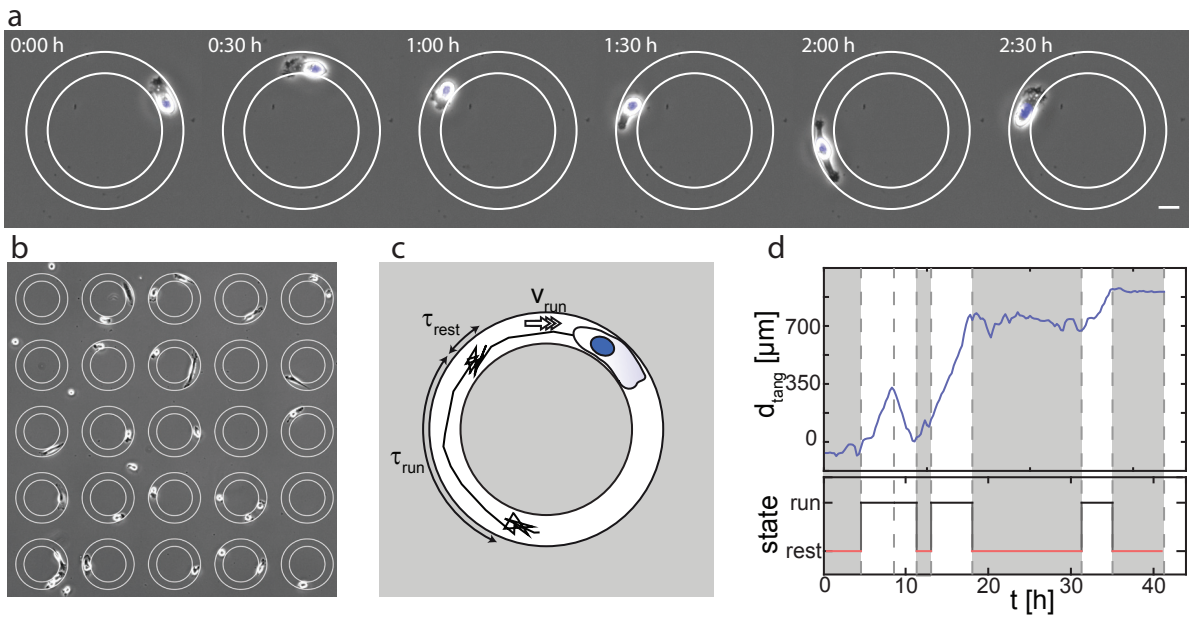

Figure 4.2.: a) Time series of a MDA-MB-231 TRIPZ-200c cell migrating on a ring-shaped microlane(white). Scale bar is 20 μm. b) Overview of many rings with cells seeded randomly. c) The migration on the rings without gap is characterized by three parameters: The mean velocity in the run state v_{run} and the typical durations of run and rest states τ_{run}, τ_{rest}. d) Angular position d_{tang} of a MDA-MB-231 TRIPZ-200c cell over time with classification into run and rest states.

with a inducible system (Fig. 4.1a). Therefore, a TET-off construct was chosen that leads to successful expression of miR-200c when adding the antibiotic Doxycycline (Fig. 4.1c). Additionally, a red fluorescent protein (RFP) is expressed to be able to check the functionality of the construct with florescence microscopy (Fig. 4.1b). A single clone was picked which resulted in the MDA-MB-231 TRPZ-200c cell line. Additionally, a cell line where the miR-200c was replaced was by a scrambled control was created for control experiments (MDA-MB-231 TRIPZ-Ctrl). The miR-200c expression increases with increasing Doxycycline concentration by up to a factor of 100. The MDA-MB-231 TRIPZ-ctrl cell line shows zero miR-200c activity (Fig. 4.1c). The low expression of miR-200c of the MDA-MB-231 TRIPZ-200c cell line shows that also without Doxycycline the construct has a low basal activity, but this is not enough to observe changes in the phenotype of the cells. The addition of Doxycycline resulted in an increase of miR-200c over time, starting already after less than 8 h of induction and saturating after about 30 h (Fig. 4.1d). This shows that this system is suitable to control the amount of miR200c produced and allows to study the effects of miR-200c expression at certain time points after induction and also in a time resolved manner.

4.2. Micro RNA 200c decreases cell motility

First, we use the time point 48 h after induction with Doxycycline to study dose dependent effects on migration when miR-200c already reached a plateau according to Figure

4.1d. Similar as described in chapter 3, cells are seeded on ring-shaped microlanes 48 h after starting treatment with Doxycycline and observed with time-lapse microscopy over 48 h with images taken every 10 min (Fig. 4.2a,b). As MDA-MB-231 cells show a higher tendency to span over the middle part of the ring than the MDA-MB-436 cells we increased the outer diameter of the rings to 150 μm but the width was kept constant at 20 μm. The nucleus was labelled with Hoechst to allow automatic cell tracking that was successful even with Doxycycline having some autofluorescence.

To see whether the amount of miR-200c is critical for the effects on migration we tested three different concentrations 0.5, 2, and 5 μg/ml Doxycycline, that lead to different miR-200c levels of a factor of two (Fig. 4.1c). To compare the results, we also performed experiments without Doxycycline and with the MDA-MB-231-Ctrl cell line. The resulting cell tracks show again a bimodal behaviour, thus we evaluated the three characteristic parameters of the two state motion τ_{run}, τ_{rest}, and v_{run} (Fig.4.2c,d). Additionally, we also analysed the probability of the cells to be in the run state P_{run}. This is not an orthogonal parameter as it basically can be expressed by τ_{run} and τ_{rest}. In the case of τ_{run} and τ_{rest} beeing perfectly exponentially distributed it would hold: $P_{run} = \frac{\tau_{run}}{\tau_{run}+\tau_{rest}}$. However, P_{run} is an interesting parameter as it shows the combined effects on the duration of run and rest states and most importantly is well defined on the single-cell level, which will be important later. In contrast, since the typical duration of run and rest states is only a bit shorter than the measurement time it is not very meaningful to define τ_{run} and τ_{rest} for a single trajectory. In the worst case cells can be in one state, either run or rest, for the whole observation time, which makes it impossible to define rest or run times for these cells.
Furthermore, we included the persistence path q in our analysis, that is a simple measure of the persistence which is often used [20]. It is defined as the maximal distance between two points of the trajectory divided by the contour length of the cell path.

$$q = \frac{max(d_{tang}) - min(d_{tang})}{\sum_i \mid d_{tang}(t_{i+1}) - d_{tang}(t_i) \mid} \tag{4.1}$$

Consequently, cells that move straight all the time have q = 1 and for random walkers q goes to zero.
In Figure 4.3 radar charts of the motility parameters for the different conditions are shown. To begin with, there is almost no difference between the miR-200c cells and the control cells in the absence of Doxycycline. This means that the small basal expression of miR-200c without Doxycycline seems to be irrelevant for migration behaviour. Therefore, this cell line is suitable for our study. With increasing Doxycycline concentration the control cells show only very small changes in the motility parameters. In contrast, with the expression of miR-200c cells get much less motile, which is visible in all the observed parameters. For the lowest dose of 0.5 μg/ml Doxycycline mainly rest states get longer and the run velocity is decreased a bit. For higher doses also run states get shorter and P_{run} goes down to only one third of its usual value.
This means that mir-200c mainly affects the ability of the cells to polarize and also decreases the stability of the polarized state. The run velocity is also decreased but not as far as the persistence of the cell motion. The decrease of persistence is also visible in the persistence path q. Thus, this cannot be an artefact of the two-state analysis.

In addition to the pooled population data, it is also possible to look at parameters

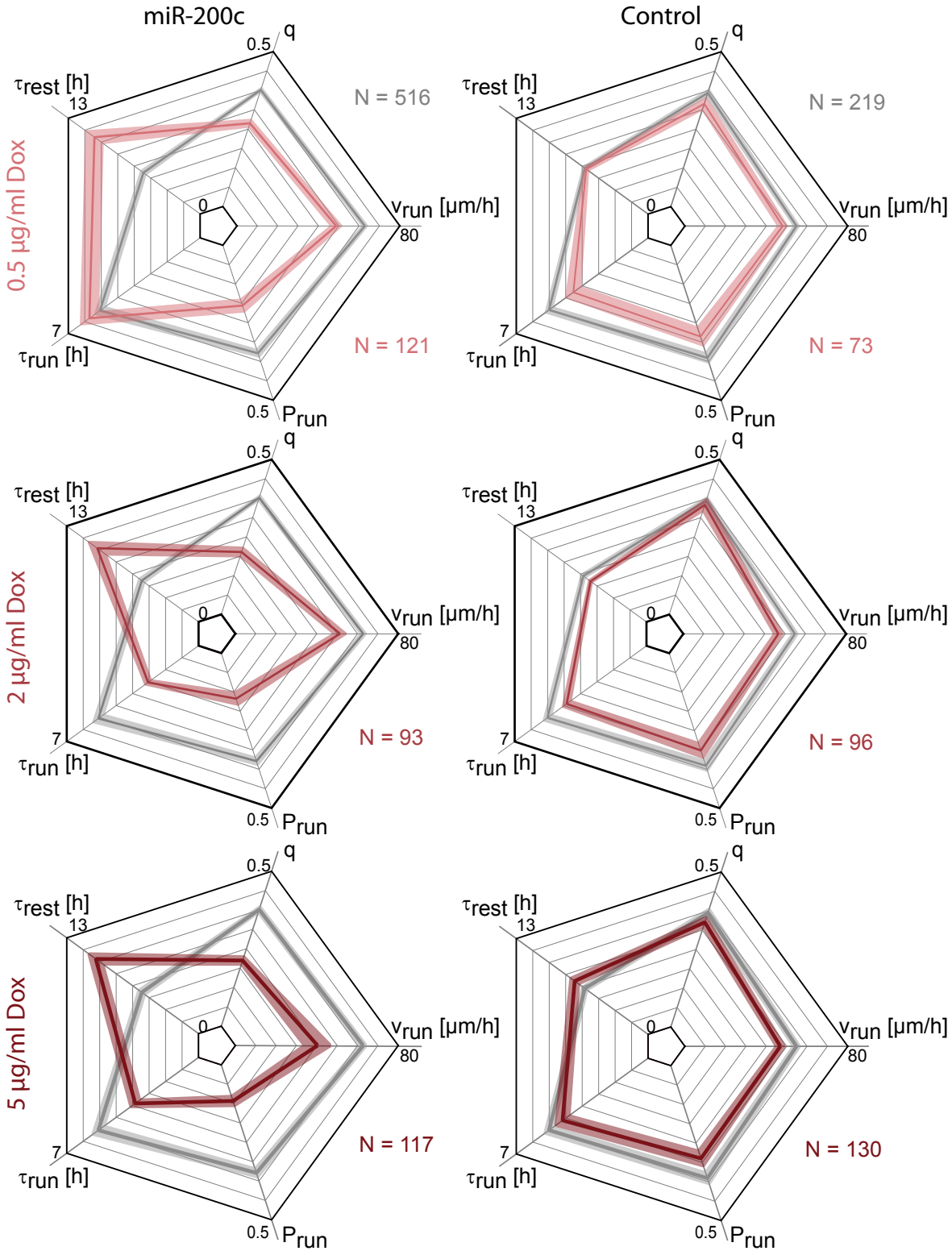

Figure 4.3.: Motility fingerprints of MDA-MB-231 TRIPZ-200c cells (left) and MDA-MB-231 TRIPZ-Ctrl cells (right) where miRNA expression is induced with different concentrations of Doxycycline (red) compared to no Doxycycline (grey). Doxycycline treatment was started 48 h before the experiment and was continued during the 48 h of measurement time. For each condition the three characteristic parameters τ_{run}, τ_{rest}, and v_{run} plus the probability to find a cell in the run state P_{run} and the persistence path q, which are not orthogonal are given. Control cells do not change their migratory behaviour much, whereas miR-200c leads to less motile cells with changes in all parameters. Shaded regions give the error range. N is the number of cells analysed.

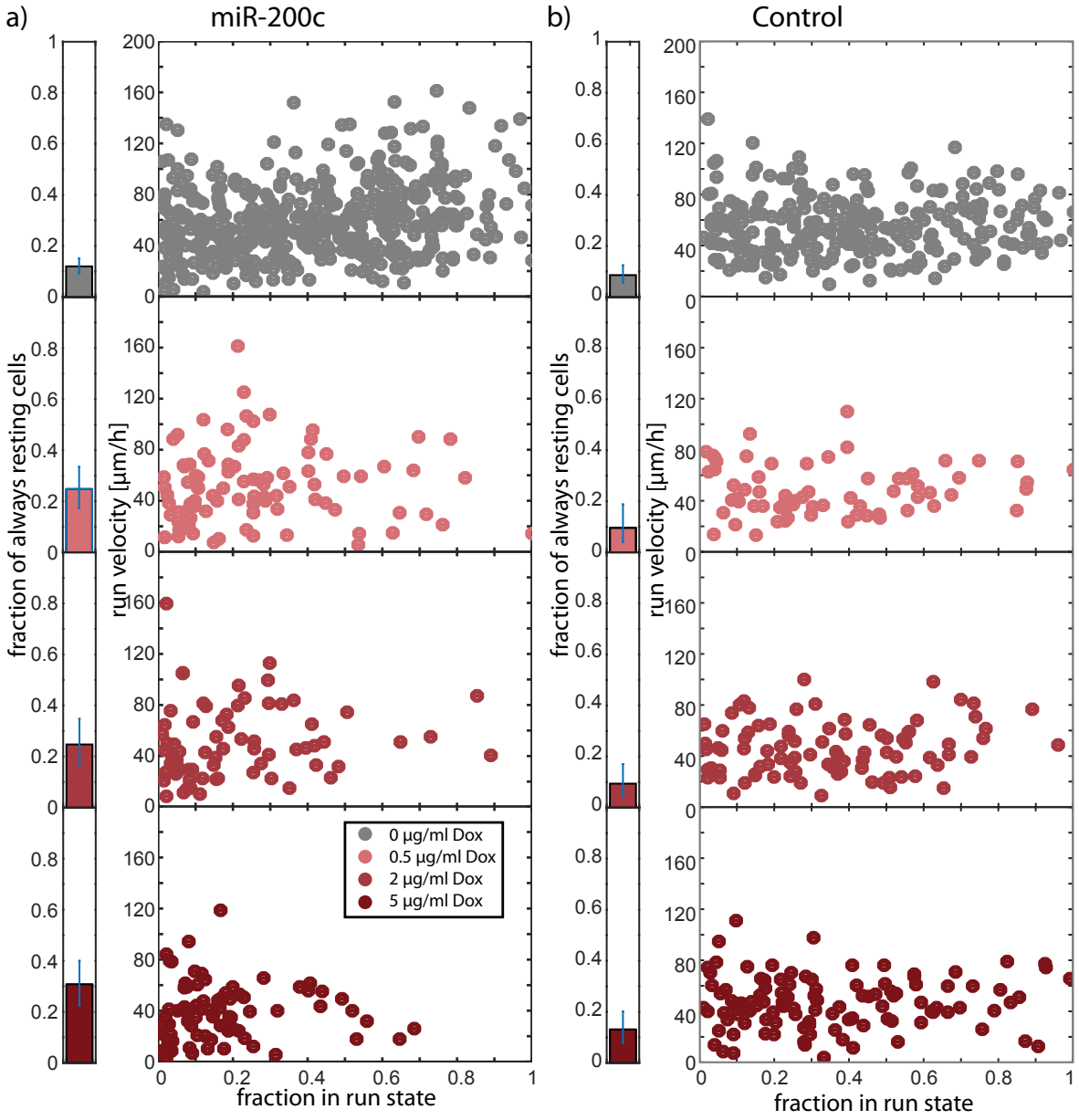

Figure 4.4.: Effects of miR-200c on single-cell level. Run velocity v_{run} plotted versus the fraction of time cells spend in the run state P_{run} for MDA-MB-231 TRIPZ-200c (a) and MDA-MB-231 TRIPZ-Ctrl (b) cells with different Doxycycline concentrations. Each dot represents a single cell from the dataset shown in Figure 4.3. The bar graphs at the side show the fraction of cells that are all the time in the rest state corresponding to $P_{run} = 0$. Error bars are 95% Clopper-Pearson confidence intervals.

at the single-cell level. To do this, scatter plots where P_{run} is plotted versus v_{run} are shown in Figure 4.4. Without Doxycycline it is clearly visible that there is great heterogeneity in the cell population. The run velocity varies from about 10 up to more than 100 μm/h. Thus, the fastest cells are up to 10 times faster than the slowest ones, although all should be genetically identical. Also in P_{run} the full spectrum is covered from $P_{run} = 1$ to cells that are in the rest state for the full time of observation (about 10% of the population). All in all there is a small positive correlation between velocity and P_{run}, which is basically a measure for persistence, that is in line with a study by Maiuri et al. [54].
With induction of miR-200c (Fig. 4.4a) the distribution gets narrower and shifted towards lower velocities and smaller P_{run}. Especially cells that spend more than half of the time in the run state get extremely rare. At the same time, the fraction of cells that are always resting increases to 30%. The control cells show now changes as expected.
Taken together the single-cell analysis shows, that there are no sub-populations, but the expression of miR-200c shifts the whole population to a less motile phenotype, by mostly reducing the time cells spend in a polarized state.

4.3. Micro RNA 200c affects morphology and regulates filamin A

As part of the collaborative project the morphology of the cells was analysed to get more hints what proteins could be important in the regulation by miR-200c. By staining the actin cytoskeleton of fixed cells 72 h after induction changes in cell shape can be investigated (Fig. 4.5a). With miR-200c expression cells get more round compared to Control cells which is quantified by the shape factor measured by the ratio of the long axis of the cell L and the width W perpendicular to this: shape factor = W/L. This shows that cells expressing miR-200c change their morphology and get more rounded. In 3D images (Fig. 4.5b) one can see that cells also get flatter.
Those quite drastic changes in morphology and migratory behaviour could be caused by many different proteins or by a combination of several proteins. From the many proteins, where the expression is altered by miR-200c [157] it is likely that proteins interacting with the cytoskeleton are involved in the structural changes of the cells. One protein that was found to be a candidate for this is filamin A. It is an important actin cross-linking protein and is known to play a role in cellular structure and migration [161–163]. By antibody staining for filamin A it gets visible that Filamin A expression is actually decreased in MDA-MB-231 TRIPZ-200c cells 72 h after induction with Doxycycline (Fig. 4.5c,d). Actually filamin A is not directly regulated by miR-200c as there is no suitable binding side at the filamin mRNA. Thus, the Roidl group explored further regulation path ways and found that miR-200c acts on filamin A via the two transcription factors MRTF and JUN.
The regulation of transcription factors makes once again clear that we are faced to a complex regulatory network with hundreds of proteins being involved. Filamin A affects cell migration by mainly interfering with the process of polarization which leads to a

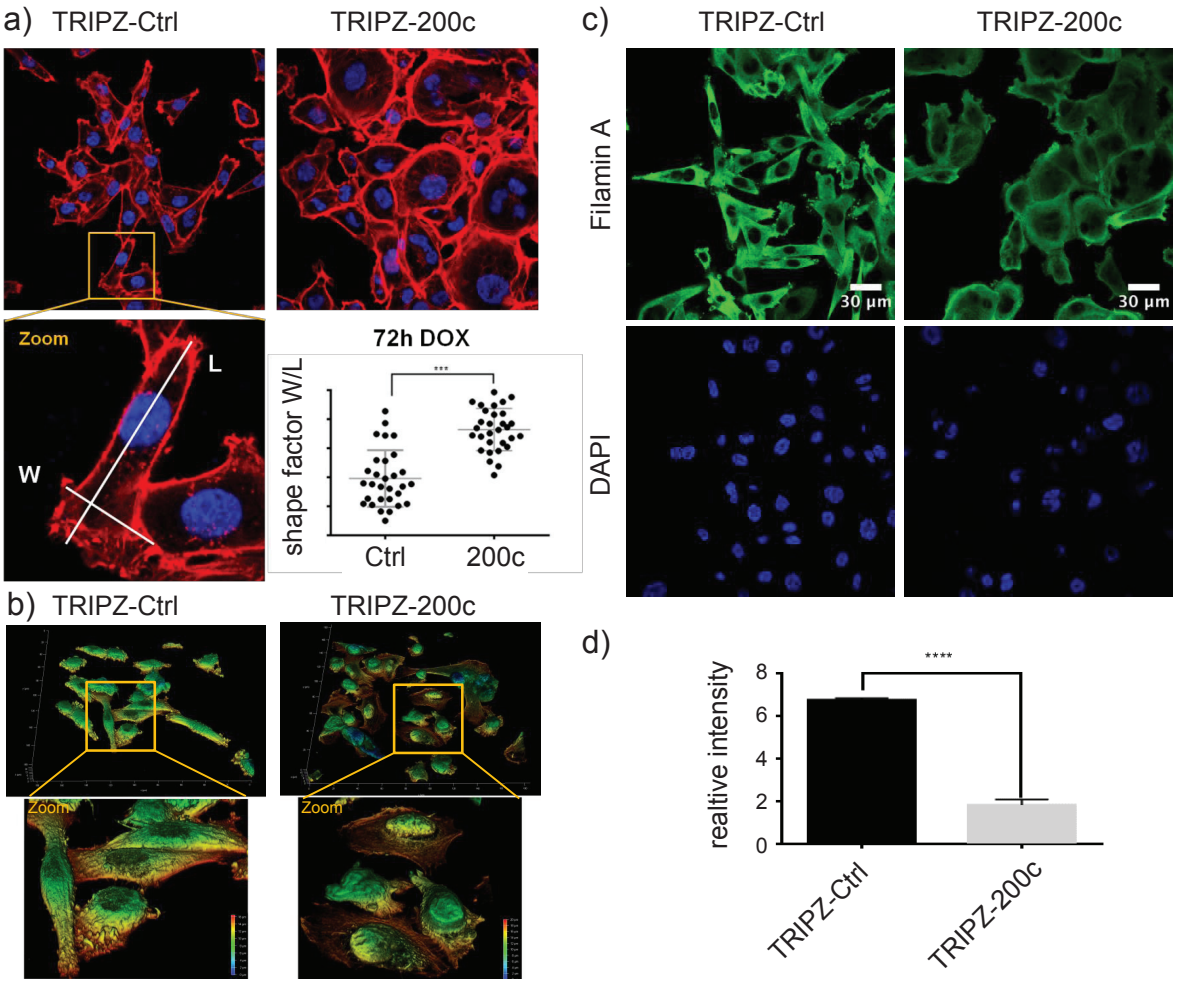

Figure 4.5.: a) Fluorescent image of actin stained with phalloidin (red) and the nucleus stained with DAPI (blue) of fixed cells 72 h after induction with Doxycycline. Analysis of the long axis L and the width in perpendicular direction W show that MDA-MB-231 TRIPZ-200c cells get more rounded up compared to MDA-MB-231 TRIPZ-Ctrl cells. Error bars are standard error of the mean, student t-test with $p < 0.001$. b) 3D rendered images of confocal stacks of the actin images. Colour codes for height. c) Fluorescent images of filamin A (antibody staining) and DAPI of Control and 200c cells 72 h after induction. d) Relative intensity of filamin A normalized by DAPI intensity. miR-200c reduces filamin A expression, student T-test with $p < 0.0001$.

high number of non moving cells [163]. This fits well to the observed effects of miR-200c. Therefore, the data presented here makes filamin A a hot candidate for the main player in the regulation of motility by miR-200c. Nevertheless, this is not a proof that filamin A is important at all and there are many more candidates like cortactin, AGR2, RAB-14, or tropomyosin [157]. The standard approach to test whether one of those proteins is causing the effects of miR-200c is to do a recovery experiment. Therefore, the expression of the protein of interest is readjusted to the normal level in miR-200c active cells. In the best case the effects of miR-200c could be reversed by this. To do those experiments is a great effort, thus every simple possibility to reduce the number of candidates is of great value.

4.4. Time resolved switching of cell motility

For now we analysed the effects of miR-200c at a certain time point. Due to simplicity this is done in many studies, but the time point is usually chosen at a rough estimate where effects are expected, which is rather random. When trying to resolve a complex regulatory pathway one could capture dynamic changes instead. For example dynamics in the motility parameters could tell at which specific time point changes in the phenotype are happening. The molecular players, that are causing this changes should show changes in expression or conformation at exactly this time point. Consequently, time resolved experiments could help to find important players in regulatory networks much more efficiently.
One problem in the analysis of many biological processes like cell motility is the high stochasticity. Therefore, large sample sizes are necessary to get meaningful measures. Thus, usually not only population averages are used but also time averages. This increases the statistics quite a lot for example when analysing velocities of cells. For a time resolved quantification of cell motility one has to abandon the time averaging, which makes it even more important to have large data sets.
The good thing of the velocity being a simple derivative is that it can be calculated for every time point. For other parameters that describe characteristics of time series, like for example the persistence in our case, it is not trivial to describe them in a time resolved manner. For instance it is not clear how the typical duration of the run state τ_{run} could be expressed with time resolution smaller than τ_{run}. Also for parameters like the persistence path q it is necessary to evaluate a certain time interval and the resulting values will depend drastically on the length of this interval. Therefore, changes in the time resolution might change the results, which is not favourable. In contrast, the two state analysis classifies whether the cell is in a run or a rest state for every time point. Consequently, P_{run} is well defined for every time point. The only restriction is that many cells have to be evaluated to get meaningful average values without averaging over time.

To study the effects of miR-200c on migration in a time resolved manner, we seed cells on the ring shaped microlanes and directly start the induction with Doxycycline. Cells need some time to adhere to the micropatterns and it takes some time until the measurement is set up at the microscope, thus cell tracking starts about 4 h after the begin of induction.
In Figure 4.6 the development of P_{run} over time is shown for 0, 0.5, 2, and 5 μg/ml Doxycycline. It is striking that even without Doxycycline for MDA-MB-231 TRIPZ-200c cells $P_{run}(t)$ is not constant. It starts at a low value and increases during the first 5 hours to about 0.4 where it stays more or less constant with a small decrease towards the end of the measurement. Interestingly, MDA-MB-231 TRIPZ-Ctrl cells show a much faster increase in the beginning. This increase is most likely a result of the seeding process. To do so, cells have to be detached from the culture flask, which involves an enzymatic cleavage of transmembrane proteins. Cells need to recover and spread on the micropatterns to be able to polarize and start running. It makes sense that this needs some time which can be seen in $P_{run}(t)$. For 0.5 μg/ml Doxycycline there are no significant differences visible during the observed 1.5 days after induction. But

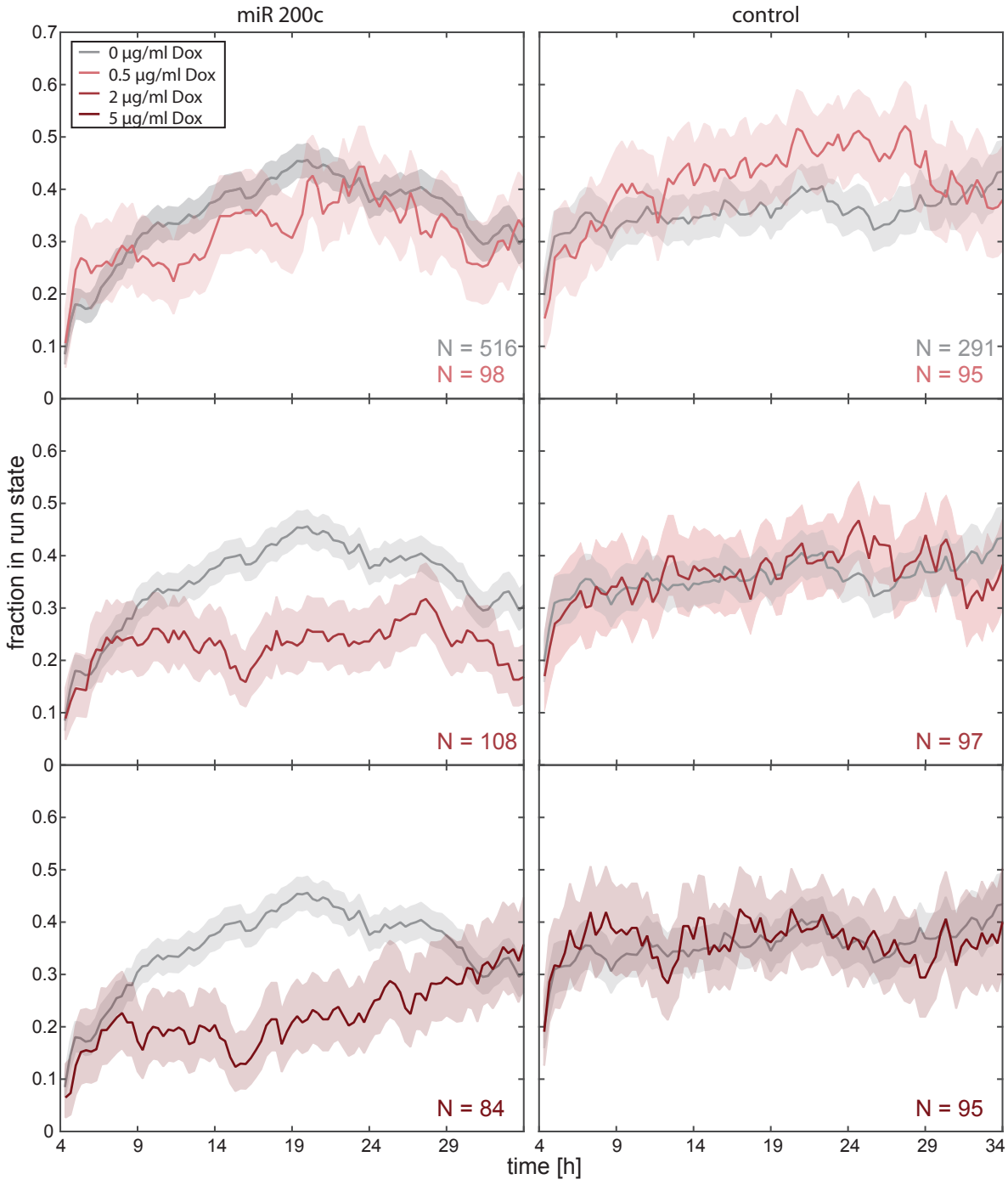

Figure 4.6.: Dynamic changes of P_{run} induced by miR-200c. Cells are seeded on ring-shaped microlanes and Doxycycline treatment is started at the same time. Cell tracking is started 4 h later. The fraction of cells is the run state P_{run} is evaluated for MDA-MB-231 TRIPZ-200c cells (left) for different concentrations of Doxycycline (red) and without Doxycycline (grey). The same is shown for MDA-MB-231 TRIPZ-Ctrl cells on the right. Data of two subsequent time points is taken together resulting in a time resolution of 20 min. Shaded areas correspond to 95% confidence intervals. N corresponds to the number of cells analysed.

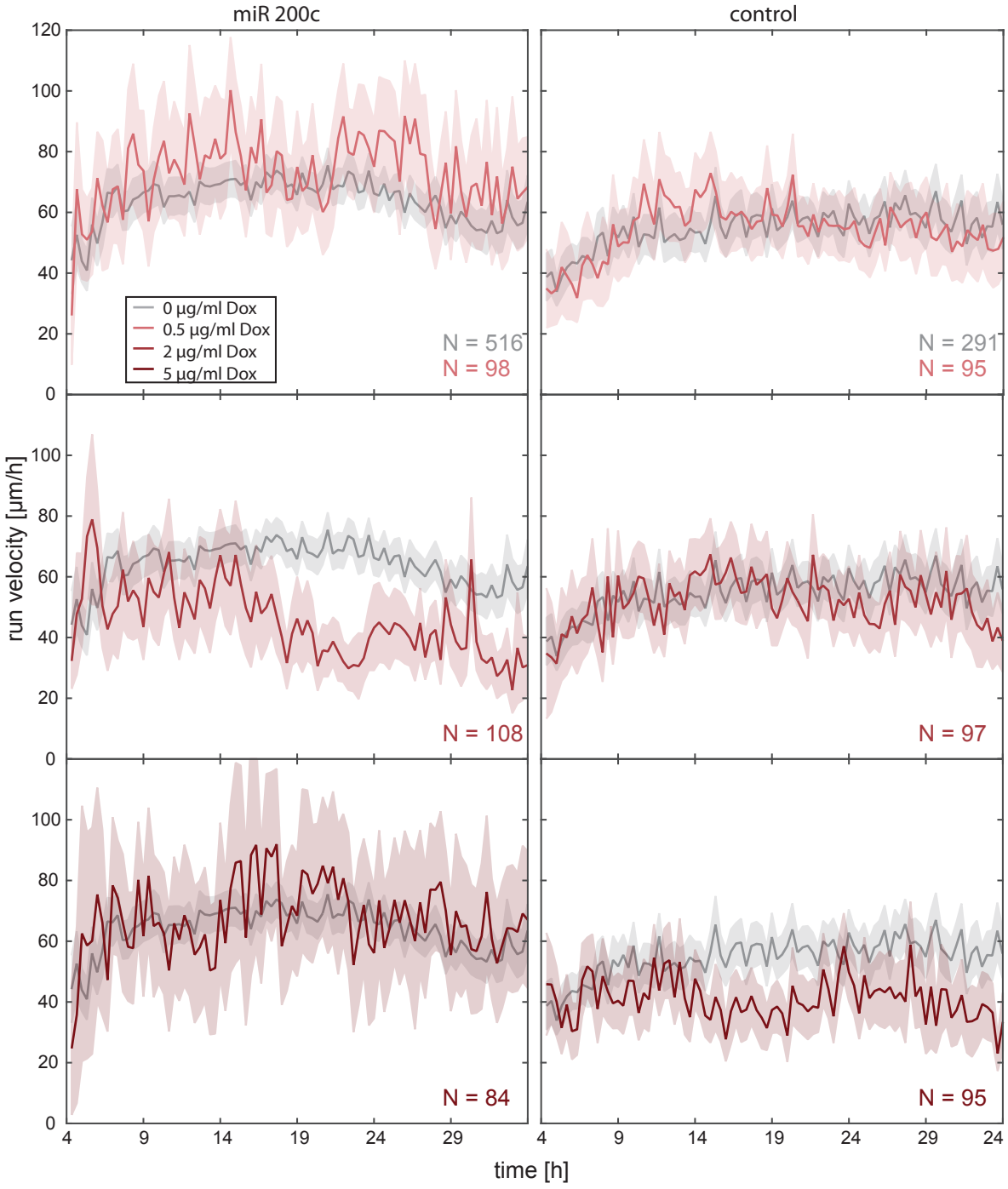

Figure 4.7.: Dynamic changes of v_{run} induced by miR-200c. Cells are seeded on ring-shaped microlanes and Doxycycline treatment is started at the same time. Cell tracking is started 4 h later. The run velocity v_{run} is evaluated for MDA-MB-231 TRIPZ-200c cells (left) for different concentrations of Doxycycline (red) and without Doxycycline (grey). The same is shown for MDA-MB-231 TRIPZ-Ctrl cells on the right. Data of two subsequent time points is taken together resulting in a time resolution of 20 min. Shaded areas correspond to 95% confidence intervals. N corresponds to the number of cells analysed.

for the higher concentrations a significantly lower P_{run} is observed. In the first hours P_{run} shows also an increase, but it never reaches the usual amount, but stays constant slightly above 0.2. The deviations to no miR-200c inductions get significant for 8 h or 12 h after start of induction. For control cells no large influences of Doxycycline is observed.
The same analysis is performed for the run velocity $v_{run}(t)$ and can be seen in Figure 4.7. $v_{run}(t)$ also shows a small increase in the first hours but the data is much more noisy than for $P_{run}(t)$. With induction of miR-200c mostly no differences in the velocity can be found. Only for the data set with 2 μg/ml Doxycycline a significantly lower v_{run} was measured 16 h after induction. Due to the high noise level in the velocity data and due to the fact that the results are not reproduced in the other data sets this can be also a statistical outlier and should not be over interpreted.
Nevertheless, the data for $P_{run}(t)$ shows a consistent effect. Therefore, we get a defined time window from 8 to 12 h after induction where effects of miR-200c are visible depending on the Doxycycline concentration. We would expect that the proteins responsible for this should show changes in the expression exactly at this time point. Thus, together with protein expression studies at a few time points around that time window, this can help to narrow down the potential candidates in the regulation network.
With an effect already after 8 h it is quite fast until miR-200c affects migration. During this time several processes have to take place. First of all, the miRNA has to be produced and processed. The production of a miRNA should be in the range of one hour. In Figure 4.1d, it is visible that the miR-200c level increases only slowly during the first hours, thus this low level seems to be enough to trigger an effect. In the next step, in case of direct regulation, the miRNA binds to the mRNA which can be fast. However, for indirect regulation for example via transcription factors it should take at least half an hour to several hours until the mRNA level of the target is changed. On top of this, in case of a down regulation of the respective protein the degradation rate of the protein has to be considered to know at which time point a reduction in the expression level gets visible. Degradation rates of proteins can vary a lot and can be also many hours or up to days. As all these numbers are often not known, and also active degradation of proteins could be changing, it is not possible to link a certain time to a specific protein. But we can conclude that the time of 8 to 12 h could be caused by both direct or indirect regulation of a protein. [164]

To investigate the role of filamin A the Roidl group performed q-PCR measurements of the filmain A mRNA levels. They found no change in expression of the mRNA during the first 12 h after induction. Consequently, it is unlikely that filamin A is responsible for the early drop of P_{run}. Nevertheless, it can still play an important role in the later processes. To find other suitable candidates a broader analysis of the proteome at several time points is planed and this will in the end show whether time resolved motility measurements can be successful in providing more information that help to explore complex regulatory networks.
One interesting part of the results is that we observe two overlapping processes. One is the process of cells starting to run on the ring-shaped lanes, and the other one is caused by miR-200c. Interesting experiments to separate these two processes would be

either to start the induction at a later time point so that most cells are already running. Or alternatively it is also possible to do the reversed study and stop the production of miR-200c after some time. However, we could also speculate that there might be a connection between the two processes. As transmembrane proteins like integrins have been cleaved before seeding it is possible that cells need some time to go into the run state because they need to produce new integrins. If miR-200c would down regulate integrins it could just stop the production of new ones. Consequently, this would mean that the degradation rate becomes irrelevant and could be an explanation for such a fast response. In these terms also the slower starting time of the miR-200c cells compared to the Control cells could be a hint that the low basal expression of miR-200c interferes with the recovery process. After all further experiments will hopefully clarify these points and the role of miR-200c in cell migration.

5. Cell migration depending on substrate adhesiveness

In Chapter 3 we study cell migration on lanes with uniform fibronectin coating and introduce PEGylated non adhesive areas. This means that we create defined interfaces where the adhesive properties change to learn how cell adhesion defines the migratory behaviour of cells. There are many studies showing that adhesions or the number and type of possible adhesion sites provided by the substrate is crucial for cell migration. [33, 82, 165–167] But there is still no fundamental understanding of how adhesion controls the process of cell migration and how the coupling to the substrate defines parameters like cell speed.
The situation studied in Chapter 3, with an interface between fibronectin coated and PEGylated surface is an extreme case. The number of possible adhesion sites on the PEGylated surface is so low that cells usually do not migrate much on this surface. Thus, cells move only over small areas of this non adhesive surface, which makes it difficult to properly compare differences in migration parameters like velocity. In order to produce interfaces between two areas in a more physiological regime of adhesiveness, a new patterning technique was developed. This basically allows producing step functions of different adhesives. Other studies, where cells are faced with differences of adhesiveness have focused on gradients of adhesion molecules [25, 166, 168, 169]. Studying cell migration at the step function has some interesting features that distinguish it from other experiments. First of all, single cells can probe two different environments with homogeneous coating, where the motility can be compared for the exact same cell. But most importantly the interface defines a specific position in space where we can look for changes in cell behaviour. As cells perform stochastic motion it is usually very difficult to connect the behaviour of single cells at a certain time point to external influences. Only the statistical analysis of a cell population reveals certain changes like for example on the gradients or for the effects of miR200c described in Chapter 4. In this Chapter, we show that interfaces can help to find specific responses to environmental cues on the single-cell level. The content of this Chapter is summarized in Manuscript 1.

5.1. A two protein patterning technique

To study controlled interactions of cells with interfaces between fields with different adhesive properties we need a technique that can create the two different protein coatings combined with the confinement to 1D lanes. Most of the techniques that are available relay on sequential coating with different protein solutions [70, 74, 78, 82, 84] or alternatively subsequent stamping steps would require perfect control over the positioning of

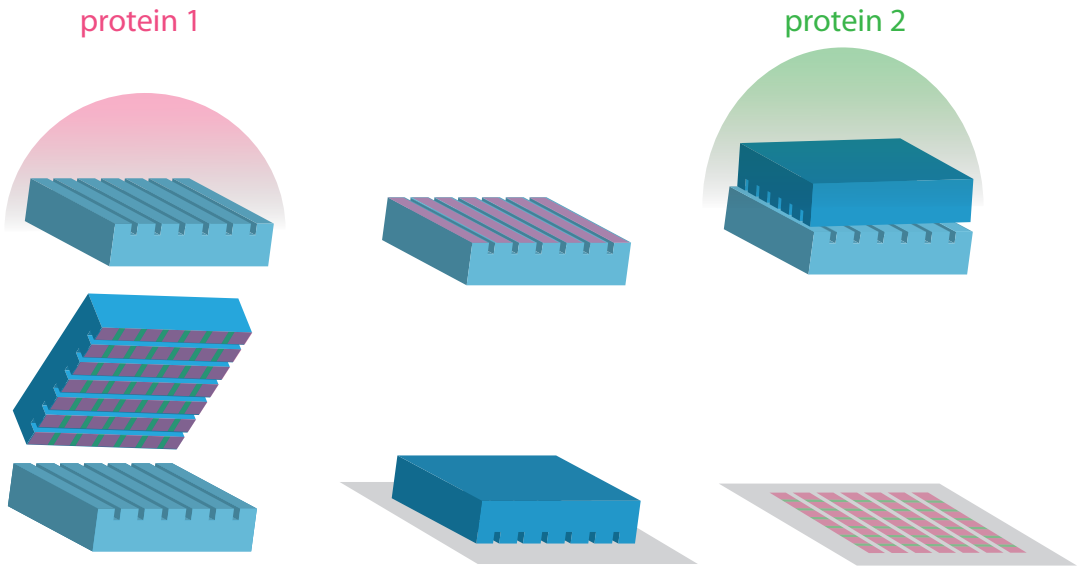

Figure 5.1.: Two step microcontactprinting technique to produce stripe micropatterns with alternating protein coating. A PDMS stamp is inked with protein solution 1, dried and stamped on a second stamp with lines perpendicular to the first ones. After a short plasma treatment a second protein solution can flow into the room between the two stamps and coat the unprotected parts. After drying the second stamp can be lift off and shows the favoured alternating protein pattern which can be transfered to the substrate. The surrounding is subsequentially coated with pll-PEG to prevent cell adhesion.

stamps. The sequential coating of the surface has the disadvantage that possibly the proteins could bind to each other, which would exclude for example the combination of fibronectin with collagen [170]. In the case of patterns of the same protein but with different concentrations during the second inking step proteins could also bind to free areas in the firstly coated areas, which makes it difficult to control the surface concentration there.

We developed a technique that is based on two stamping steps, which keeps the inking of the different fields completely separated (Fig. 5.1). To this end, a first PDMS stamp with line patterns is coated with the desired protein. This is stamped on a second stamp with lines oriented in perpendicular orientation. A second protein solution with another protein or a different concentration is put in the room between the stamp to coat the remaining areas of the stripes. Consequently, this already creates the alternating fields with different coatings on the stamp and the pattern can be transferred to a substrate. A detailed protocol is given in section A.1.4.

With this protocol it is possible to create patterns with different proteins (Fig. 5.2a) or with different concentrations for example of fibronectin (Fig. 5.2b). In the further experiments we focus on stripes with different fibronectin concentrations. To estimate the surface concentration of fibronectin, it is labelled with a fluorescent dye. With the help of microfluidic channels of a defined height it is possible to compare the fluorescence of labelled fibronectin solutions with various concentrations to the fluorescence of the micropatterns (Fig. 5.2c, and Section A.4). Thereby it is possible to get the absolute fibronectin surface concentration from the median florescence intensity of each

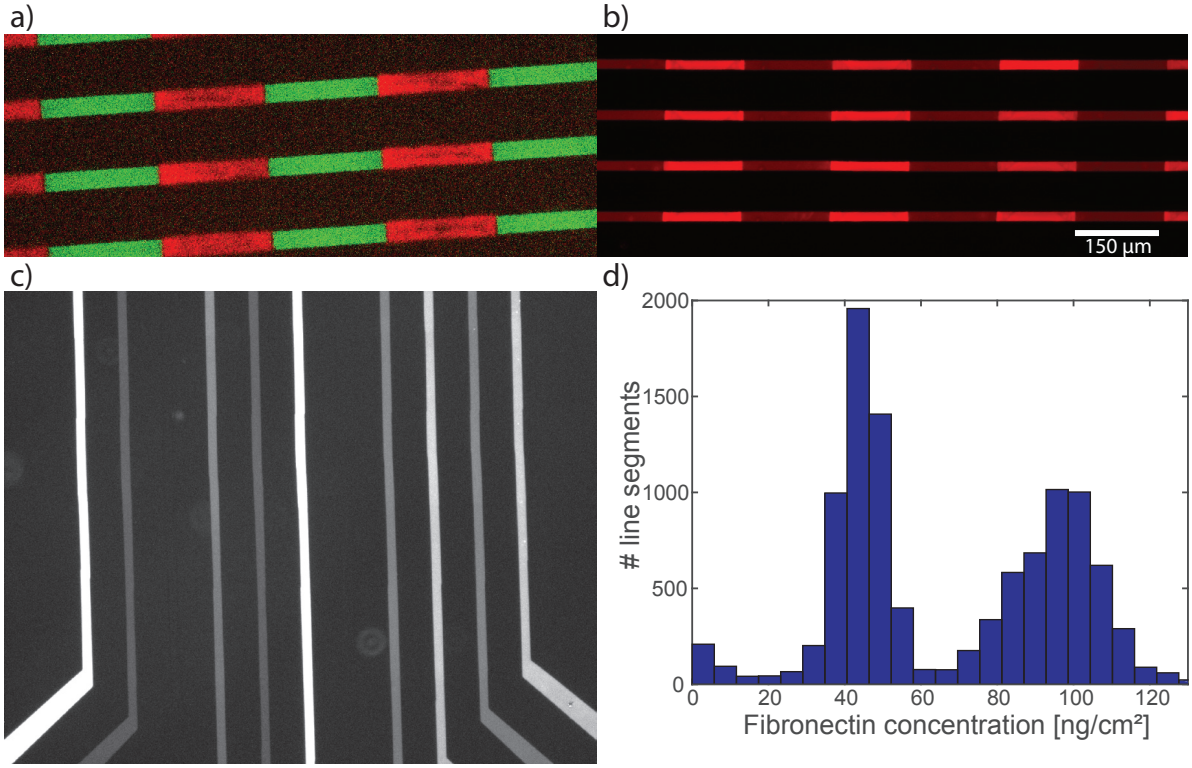

Figure 5.2.: a) Fluorescent image of patterns consisting of two different proteins (fibronectin and fibrinogen). b) Fluorescent image of line pattern with alternating fibronectin concentration. The intensity of the florescence codes for the surface concentration of fibronectin (labelled with Alexa 647). c) Microfluidic channel are filled with a solution of labelled fibronectin with different concentrations. By comparing the florescence intensity of the channels with the patterns the absolute surface concentration can be estimated. d) Histogram of the median fibronectin concentration of the individual line segments of one sample. Two peaks are visible representing the higher and lower fibronectin concentration seen in b). The width of the distributions show the heterogeneity.

line segment individually. For one set of parameters such as the concentration of the fibronectin solutions, the resulting surface concentration can still vary from stamp to stamp and also across the stamps. Thus, for each combination of parameters we get a distribution of surface concentrations (Fig. 5.2d). By varying the concentrations of the fibronectin solutions we can cover the whole range of possible surface concentrations. For analysis of the cell motility in dependence of the substrate it is important to measure the concentration of each line segment individually. This is done by automatically detecting the line patterns and evaluating the fluorescence intensity and also the homogeneity, which is described in more detail in Section B.3.
The measured fibronectin surface concentration only considers the fibronectin that is bound to the surface during the patterning process. However, it is also possible that the surface changes during the experiment. For example, cell medium is supplemented with serum which includes proteins that potentially could bind in between fibronectin molecules if these spaces are not fully covered by PLL-PEG. The most abundant protein in serum is serum albumin to which cells usually do not adhere to but it can also contain fibronectin [171]. In addition, cells could also modify the surface. It is known that during the retraction of the rear some parts can be left behind which mostly consist of

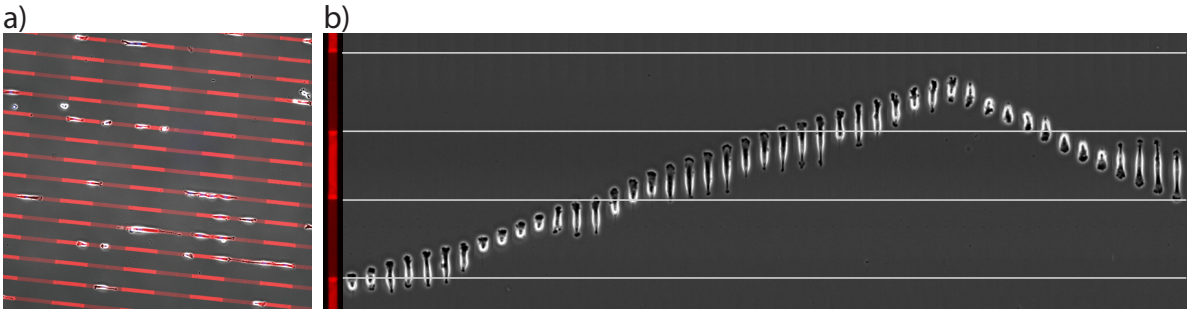

Figure 5.3.: a) Phase contrast image of cells seeded on line micropatterns (red) with segments of alternating fibronectin concentration. b) time series of a single MDA-MB-231 cell on the micropattern shown at the left. White lines indicate the interfaces between the line segments. Time between individual images is 20 min.

integrins and membrane patches [172]. Furthermore, some cell types also secrete ECM proteins such as collagen or fibronectin [173]. However, we did not observe that cell behaviour was affected when areas where visited previously by other cells. Also over time the cell behaviour was quite constant, thus we assume that there are no drastic surface modifications, although more experiments would be necessary to verify this.

5.2. Maximal velocity for intermediate fibronectin concentrations

We use microlanes fabricated as described above with a width of 15 μm and a segment length of 150 or 200 μm to study the migration of MDA-MB-231 cells in dependence of fibronectin concentration. Cells are seeded on the micropatterns and migrate similarly as on the ring-shaped microlanes (Fig. 5.3). In contrast to the ring-shaped microlanes, on the stripes we often find that cells are colliding with each other and cells are repeatedly leaving or entering the field of view. To get single-cell tracks out of this we used automated cell tracking of the labelled nuclei. Time points when individual cells are not on the lanes or have a distance of less than 66 μm to their neighbours are excluded. Remaining tracks with a duration of at least 5 h are used for further analysis.

The scanning time-lapse measurements together with automated cell tracking allows performing high-throughput measurements. In a range of different fibronectin surface concentrations lying, except for some outliers, between 5 to 120 ng/cm^2 a total number of 19,861 tracks was analysed. The evaluation of the run velocity of the cells in dependence of the fibronectin concentration shows that there is a maximal velocity for intermediate fibronectin levels as also found by other studies [21–24]. This can be seen in the population average of the run velocity as well as for the mean velocity also including rest states (Fig. 5.4a,b). Due to the limited length of the segments it is not possible to evaluate τ_{run} and τ_{rest} for a certain fibronectin concentration. However, we can define the persistence path q (Equation 4.1) for each part of a track that is on one segment. A study by Maiuri et al. [54] predicts that velocity and persistence should be

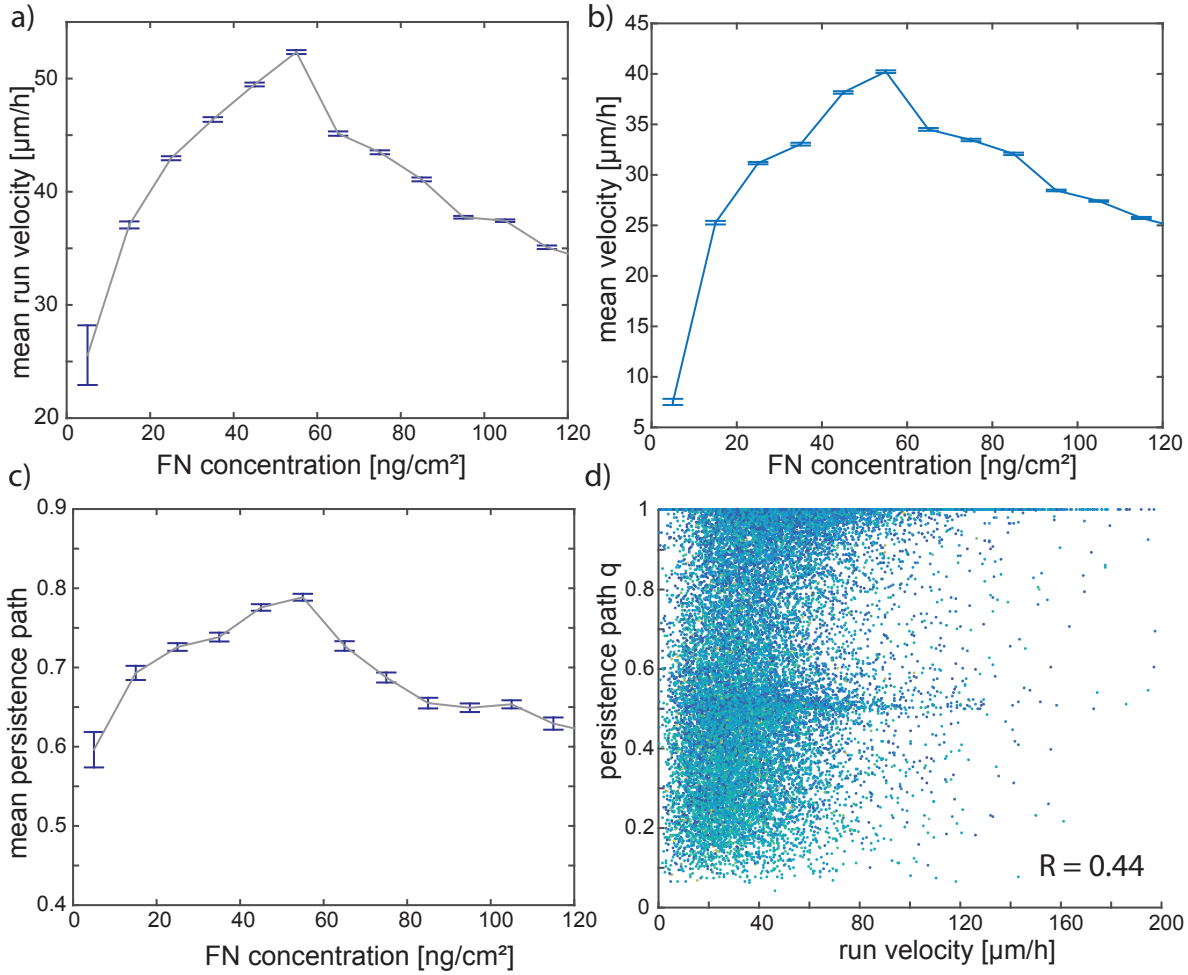

Figure 5.4.: a) Run velocity of MDA-MB-231 cell migrating on the microlanes in dependence of the fibronectin concentration (at the nucleus position) averaged over the population b) Mean velocity averaged over both run and rest states in dependence of fibronectin concentration. c) Mean persistence path in depence of fibronectin concentration. For the evaluation, tracks that go over several segments are cut into parts that are only on one segment. d) Persistence path versus run velocity for every part of a track that is on one segment. Colour codes for fibronectin concentration with bright means low and darker blue means high concentrations. Pearson correlation coefficient R = 0.44. All error bars represent standard error of the mean.

correlated. And indeed we find a very similar behaviour for the persistence (Fig. 5.4c) with a maximum at a fibronectin concentration between 50 and 60 ng/cm^2 as found for the velocity. This correlation is also visible on the level of the single tracks (Fig. 5.4d). However, due to the size limits of the segments cells can also interact with the interface to the next segment which can distort the measure for the persistence. The accumulation in Figure 5.4d at q = 0.5 is most likely caused by very persistently migrating cells turning around at the interface. Consequently, interpretation of the persistence data should be taken with care.

All earlier studies that found the maximal velocity for intermediate fibronectin concentrations did separate experiments on the different substrate coatings. Thus, not the exactly same cells are used in the different conditions. With this assay it is possible to find out how the velocity of single cells is actually changing when migrating

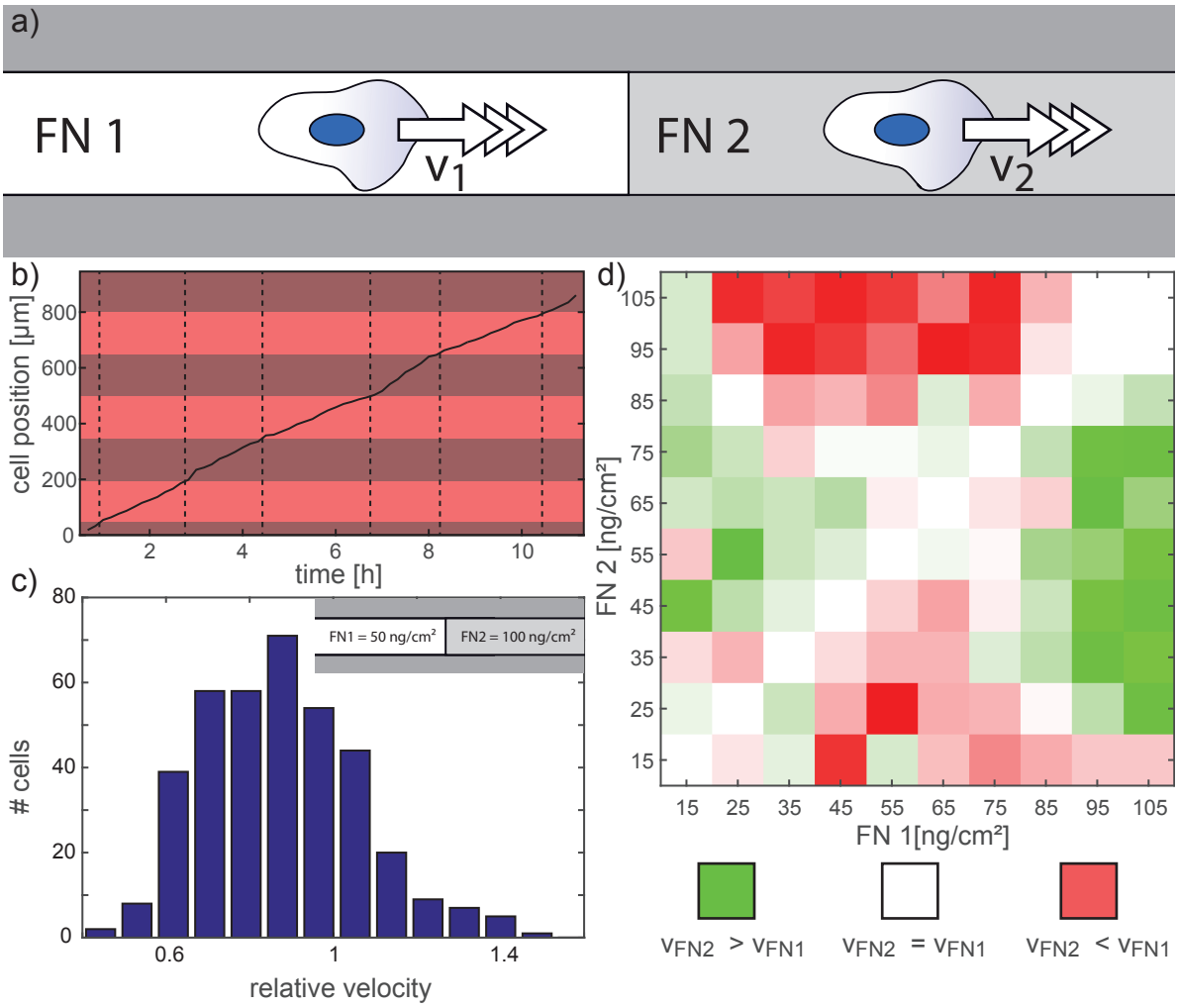

Figure 5.5.: a) Drawing of a single cell migrating first on one segment and then on another. The velocity on the first and on the second segment can be compared. b) Track of the nucleus of a single cell migrating over several segments with high (bright red) or low (darker red) fibronectin concentration. Dotted lines mark the transitions between the segments. c) Histogram of the relative run velocities v_2/v_1 of single cells migrating on segments of about 50 ng/cm^2 and about 100 ng/cm^2. The mean relative velocity is 0.8. d) The symmetrized version of the relative velocity (Equation 5.1) for all possible combinations of fibronectin concentration is calculated. For each field this is done from an underlying distribution like in c).

on two different substrates (Fig. 5.5a). Looking at single-cell tracks (Fig. 5.5b), it becomes apparent that cells actually change their velocity when migrating on different fibronectin concentration. When calculating the relative velocity on two fields with a defined fibronectin concentration for example 50 and 100 ng/cm^2, we get a quite broad distribution that is centred around 0.8 in this case. Although this means that mostly cells are slower on 100 ng/cm^2 than on 50 ng/cm^2 the distribution is sufficiently broad that also the opposite case can be found. We can now do this for all possible combinations of fibronectin concentrations. For each of these cases we can calculate the mean relative velocity, but averaging over relative velocities leads to the problem that the result depends on whether we calculate the velocity relative to v_1 or v_2. Thus, to get a formula where v_1 and v_2 are interchangeable we average over the relative inverse

velocities:

$$\langle v_{rel} \rangle = \langle \frac{\frac{2}{v_{FN2}}}{\frac{1}{v_{FN1}} + \frac{1}{v_{FN2}}} \rangle^{-1} \tag{5.1}$$

This leads to a map of the relative velocities shown in Figure 5.5d. The map shows that in general the maximum velocity is always found around 50 to 60 ng/cm^2 independent of what concentration it is compared to. Thus, this implies that the behaviour found on the population level is one to one reassembled on the single-cell level. However, the single cell analysis reveals the high noise level of this stochastic behaviour. This means that it is important to not draw conclusions from the behaviour of one single cell. One has to investigate large sample sizes and in this case it is fine to average over the population.

5.3. Velocity changes during traversals

Next, we want to put some attention on the cell behaviour at the interface between two segments, and in particular on cells traversing the interface. In the experiments discussed previously images where taken every 10 minutes. With this time resolution the transition happens in only a few time steps. Between the images cells can move several μm which means that we are missing many of the details of the cell motion. To get a more detailed view of the migration process we performed experiments with a time resolution of 20 s. In this case it is not possible to take fluorescence images of the nucleus because to image the Hoechst stain the illumination with UV-light is needed that would stress or even kill cells at this exposure rates. Therefore, only phase contrast images are acquired. Due to the confinement to the 1D microlanes, it is easily possible to create kymographs of the cells, which means that for every time point one takes only the middle line of one line pattern and sets it together forming a new image. Thus, Kymographs are images with one time axis (here drawn always from left to right) and one space axis. These kymographs give basically all important information of the 1D motion. In Figure 5.6a a kymograph is shown. Two cells are on this stripe, one is in the run state and in the end collides with the second one that is mostly resting. It is visible that the front of the polarized cell moves with a relatively constant velocity whereas the rear shows more intricate dynamics. A zoom in on one transition (Fig. 5.6b) shows that the motion of the front shows two kinks during the traversal. The velocity is changing once when the front traverses to another segment and a second time when the rear traverses. In the kymographs, the lamellipodia at the front shows an characteristic pattern of dark stripes which correspond to actin ruffles moving backward. The back of the cell shows basically two different modes. In one mode the back shows an oscillatory spreading behaviour (Fig. 5.6c). This means that at the rear of the cell a transient lamellipodia is formed, that often also shows the characteristic dark ruffles. The spreading towards the back does not last too long and is terminated by a fast forward slipping of the rear. In the other mode a more constant forward motion of the rear end is observed without the formation of lamellipodia spreading backwards (Fig. 5.6d).
With the time resolution of 20 s it is not possible to resolve the retraction protrusions

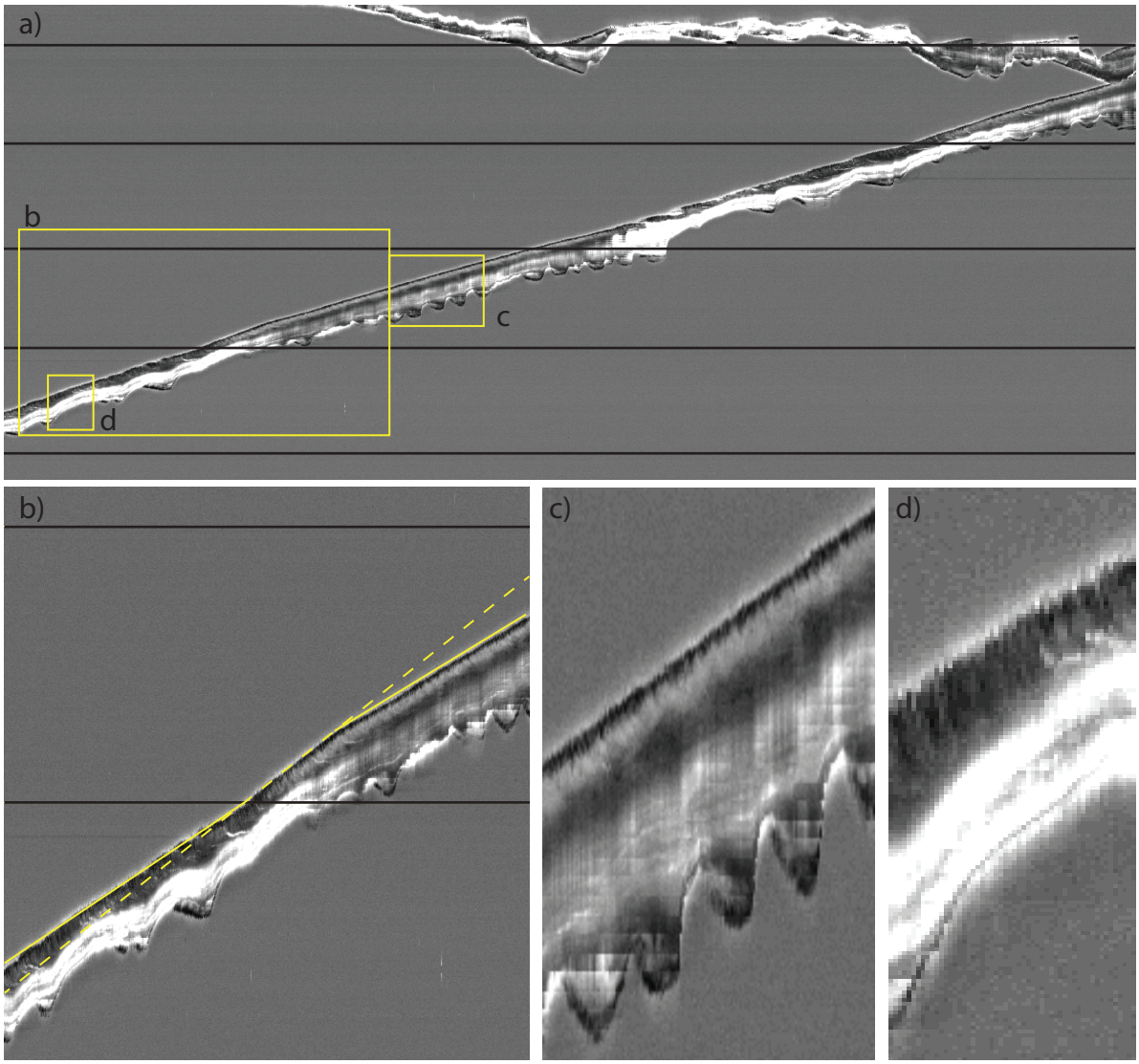

Figure 5.6.: a) Kymograph of phase-contrast images of two MDA-MB-231 cells migrating on microlanes (one in the run state, one mostly resting). Transitions between segments of different fibronectin concentration are marked by black lines (distance of 200μm). Time goes from left to right. b,c,d are zoom ins. In b) the slope of the yellow lines represents the cell velocity. During the transition the slope changes (dashed line).

cycles taking place at the front of the cell [34]. For that reason the front moves very smoothly and therefore the front velocity v_{front} is a good measure for the migration behaviour. One could assume that the velocity of the front is mainly governed by local influences on the lamellipodium. Indeed, we find that the speed of the front changes very abruptly in many cases when it traverses to a segment with different adhesiveness.Perhaps even more surprising is the fact frequently, when the back traverses, the velocity of the front changes as well. During the transition the cell is moving over the interface, which means that the part of the cell that is already on the next segment is getting larger and larger. Although the adhesion properties underneath the cell are changing permanently during this process we still observe a constant velocity of the lamellipodium at the front.

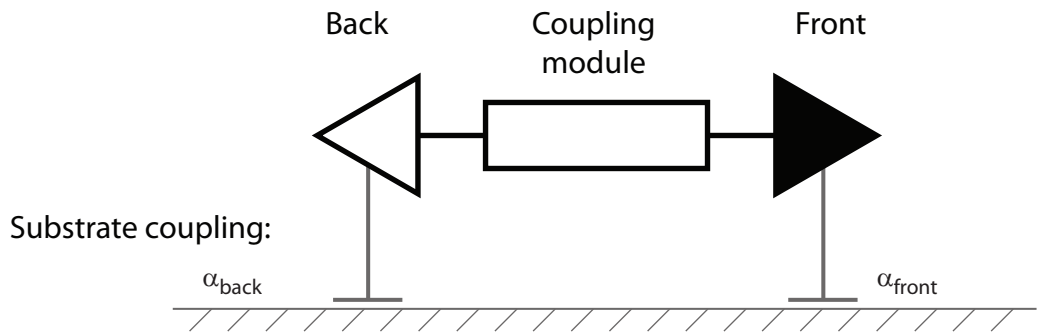

Figure 5.7.: A simplified model of a migrating cell. The cell couples to the substrate at front and back with coupling parameter α_{front} and α_{back}. In principle we assume a symmetric structure of the cell, but when it is polarized the symmetry is broken, leading to a defined front and back. The information of the binding to the substrate at the back has to be transported to the moving front, which is done by a coupling module.

5.4. A two-point model of a migrating cell

Taking these observations together we can make a very simplified phenomenological model of a cell to get a more intuitive view on the migration behaviour of cells (Fig. 5.7). First of all we can assume that a cell couples to the substrate only at the very front and at the very back, since the transitions show that the fibronectin concentration at these points defines the velocity of the cell. The coupling strength to the substrate at front and back can be parametrized by α_{front} and α_{back}. The fundamental structure of a cell migrating in 1D should be symmetric, because in the rest states we usually observe a symmetric cell body. Only with polarization of the cells the symmetry is broken which defines front and back of the cell. At the back we also see the transient lamellipodia forming thus the back still seems to be similar to the front but with the difference that retraction is taking place here. Furthermore, we know that the adhesion at the back influences the velocity at the front. This information has to be transmitted somehow through the cell. Therefore, front and back have to be connected. As we do not exactly know what this connection looks like we assume that front and back are connected by a coupling module that is not specified further for now.
The general understanding of the migration mechanism assumes that the lamellipodium of the front is the main driving force of a cell. (see also section 2.1) The coupling of the actin cytoskeleton to the substrate at the front is important to transmit forces that are needed to push the membrane forward. Thus, in a simplified few, the front lamellipodium can be described as a motor and it needs grip to efficiently drive the cell forward. Consequently, a stronger substrate coupling at the front should lead to faster velocities: $v_{front} \propto \alpha_{front}$.

At the back of the cell strong adhesions hinder the cell rear from moving forward. In our simplified picture of a cell the coupling to the substrate at the rear should therefore decrease the velocity with a linear dependence in the simplest case: $v_{front} \propto -\alpha_{back}$.

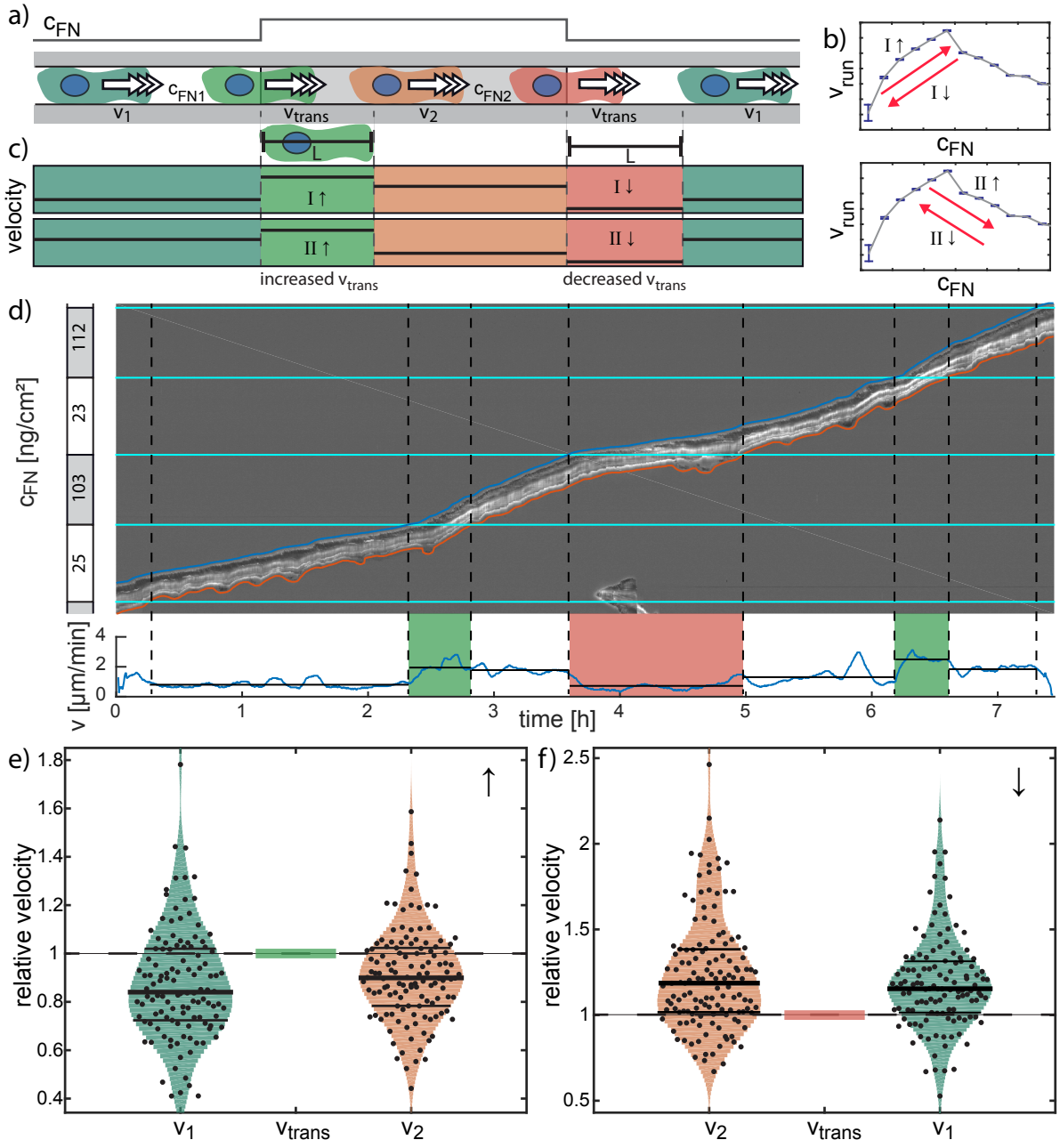

Figure 5.8.: a) Sketch of a cell migrating from less to more and back to less fibronectin. We distinguish phases where cells are completely on one segment and transitions phases where the cell front is already on the next segment whereas the back still remains on the previous segment. b) Transitions can either take place in the low c_{FN} regime I, where cells are faster on more fibronectin or in the high c_{FN} regime II where cells get slower with increasing c_{FN}. Transitions towards more c_{FN} are denoted by ↑ and reverse transitions by ↓ c) The model predicts increased transition velocities for I↑ and II↑ and decreased transition velocities for I↓ and II↓. d) Kymograph of a cell performing transitions to different fibronectin concentrations (given on the left). Front (blue) and back(red) are traced and front velocity is given. For each phase mean velocities are calculated. e,f) Front velocity before and after relative to v_{trans}. Violin plots show the velocity distribution with dots representing the mean front velocity during one phase. Median and quartile values are marked by black lines. At transitions to more fibronectin, v_{trans} is increased, at transitions to less fibronectin, v_{trans} is decreased.

With the simple assumption that the coupling to the substrate α_{front} and α_{back} increases monotonically with fibronectin concentration c_{FN} we can now make qualitative predictions for the velocity of cells traversing the interface between two segments. When a cell is fully on one segment it migrates on a homogenous fibronectin coating and should on average have a velocity described by the velocity relation in Figure 5.4a. During the transition cell front and rear are on different fibronectin concentrations which we define as the transition phase (Fig. 5.8a). Depending on the range of the fibronectin concentration, the absolute change of velocity after the transition is different. We can therefore differentiate two regimes (Fig. 5.8b): In the range of low coupling to the substrate, cells are faster on more fibronectin (transitions of type I), whereas in the case of high coupling cells get slower when the fibronectin concentration is increased (type II). Independent of this, cells traversing from low to high fibronectin (transitions I↑ and II↑) should always show an increased velocity during the transition, v_{trans}, acording to the model. This is due to the fact that the front motor works more efficient on more fibronectin and the cell still has weak adhesions to break at the back. The opposite behaviour is expected at the transition from high to low fibronectin (transitions I↓ and II↓). Here, the motor works less efficient and strong adhesions at the back have to be overcome, which should lead to a decreased transition velocity (Fig. 5.8c).
To test these predictions we analysed 99 kymographs of cells in the run state that are traversing over one or several interfaces. We used an automated image analysis algorithm to identify the position of the front and the rear of the cell over time. The algorithm is based on calculating the variance of the image, which is higher in regions occupied by a cell than in the background where there are no cells. This allows examining the front velocity over time (Fig. 5.8d). Additionally, we calculate the average velocity for each phase where cells are on one segment and for the transition phases. The velocity during transitions from low to high fibronectin is actually shifted to higher velocities (Fig. 5.8e) and shifted to lower velocities for inverse transitions (Fig. 5.8f). When looking at single transitions we find that in 75% of the cases v_{trans} is really larger than v_1 and v_2 for $c_{FN1} < c_{FN1}$ or smaller than v_1 and v_2 for $c_{FN1} > c_{FN1}$ respectively. Thus, the simple model can qualitatively predict the average changes of the front velocity during transitions. But again we find very wide distributions of the relative velocities, which means that there is a high level of noise in this stochastic system that can even show single cases where the relative changes are not in line with the predictions for the average.

5.5. A mechanical approach to describe the velocity relation

The presented simple model can qualitatively predict the transition velocities with only few assumptions. However, it is not possible to get a formula for the global velocity dependence on fibronectin concentration without making further assumptions about how exactly the coupling to the substrate and the coupling of back to front is accomplished. Of course, this is all in an oversimplified view of the cell and actually much more compli-

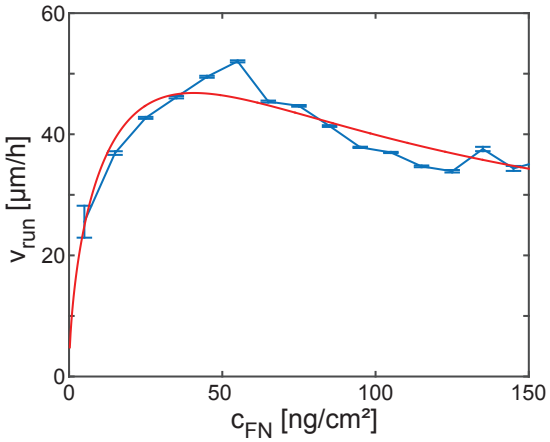

Figure 5.9.: Simple approach to explain the velocity relation (data in blue). The force ansatz assumes that the front pulls with a constant force $\overrightarrow{F}_{front}$ proportional to the substrate coupling α_{front}. The back opposes an effective friction force $\overrightarrow{F}_{friction}$ that is proportional to the velocity v and the substrate coupling α_{back}. This leads to Equation 5.2 for the velocity relation which is fitted to the velocity in dependence of the fibronectin concentration (fit in red with $q \approx 0.5$).

cated models are needed that incorporate cytoskeleton dynamics, adhesion generation and breaking, mechanical forces, membrane tension and so on. It is not clear how all these components could lead to simple rules that we recover with our simple approach. Thus, in this paragraph we discuss assumptions that we can make for the simplified model and test whether they can be validated by the experimental findings. In the end this could help to get an intuitive understanding of the relations in the migration process, and give some constraints to more sophisticated models, that would be needed to get a more detailed understanding of this process.

A simple mechanical ansatz that we can make is that the lamellipodium at the front produces a constant force pulling the cell forward. With this we reduce the complex processes in the lamellipodium that include actin polymerization and pushing the membrane forward, contraction of the actin network, and adhesion to the substrate, to a simple forward force generating process. This depends on the adhesion strength at the front and therefore we can assume $\overrightarrow{F}_{front} \propto \alpha_{front}$. To move the back forward the force has to be transmitted throughout the cell. We can assume that the back exerts an opposing friction force that is proportional to velocity and to the substrate coupling $\overrightarrow{F}_{friction} \propto v \cdot \alpha_{back}$. This would be in agreement with theory on the nature of viscosity that shows that binding and unbinding events can indeed lead to an effective velocity dependent friction force [52].

As cell migration is very slow, the inertia of the cell motion can be neglected and we can assume overdamped dynamics and mechanical equilibrium at all times $\overrightarrow{F}_{front} = -\overrightarrow{F}_{friction}$. To get a formula that can describe the velocity relation in dependence of fibronectin concentration, we have to make further assumptions how the coupling α depends on c_{FN}. For a simple linear relation at front and back it is not possible to get the maximum in the velocity relation. Besides, there are physical limits like the maximal binding energy or the maximal force and the number of myosin motors that limit the force exerted by the lamellipodium. Thus, it makes sense to assume a saturating force

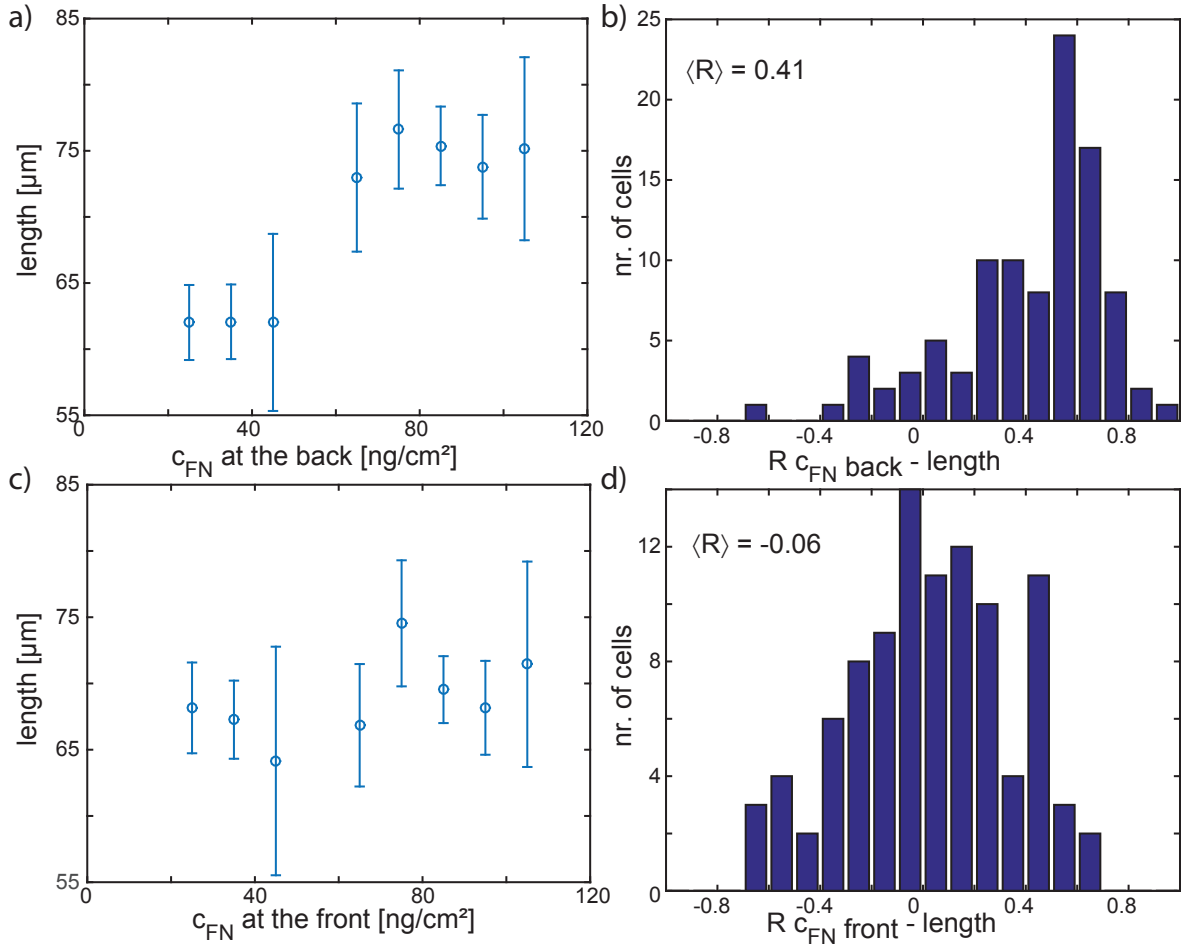

Figure 5.10.: a) In the kymographs position of front and back are determined. The average length dependent on the fibronectin concentration at the back or at the front (c) is shown. For each individual cell the Pearson correlation coefficient of length and fibronectin concentration at front or back is calculated in b,d) histograms of the correlation coefficient are shown and mean correlation coefficients$\langle R \rangle$ are given.

depending on the fibronectin concentration $F_{front} = a_{front} \cdot exp(\lambda c_{FN,front})$ with the free parameters λ and a_{front}. One way to get the maximum in the velocity relation is to introduce a power law dependency of the friction force on $c_{FN,back}$ where we leave the exponent q as a free parameter. $F_{friction} = a_{back} \cdot {c_{FN,back}}^q$. When setting the Forces equal we get the following formula for the front velocity in the case of having the same fibronectin concentration at the front and the back:

$$v(c_{FN}) = \frac{a_{front}}{a_{back}} \frac{1 - exp(-\lambda c_{FN})}{{c_{FN}}^q} \tag{5.2}$$

This can be fitted to the observed velocity relation with an exponent $q \approx 0.5$ (Fig. 5.9). Although this fits quite well we can think of other implications of the approach that could be tested. One implication is that the total tension of the cell is completely governed by $c_{FN,front}$ as this defines the force exerted at the front. If the cell is a body with elastic properties, the length of the cell should depend only on $c_{FN,front}$ and not

on $c_{FN,back}$. This is strengthened by studies showing that cell tension is indeed proportional to cell length [174]. We analysed the kymographs and found that the mean cell length does not change with $c_{FN,front}$ but increases with larger $c_{FN,back}$. (Fig. 5.10a, b). Also on single-cell level we calculated Pearson correlation coefficients that show that the cell length is governed by the fibronectin concentration at the back (Fig. 5.10c, d). Consequently, we observe a behaviour of the length that is qualitatively different to the predictions of the force ansatz.
Another problem of this approach is the difficulty of getting it consistent with the dynamics at the back. To get a constant friction force we assume that the back is moving forward with a constant velocity. But in reality this is not the case with the back even spreading in the opposite direction from time to time. In principle this could all be saved by the coupling module that could average the friction forces and adapt the cell length. However, this would require a very complex coupling module that on the one hand transmits forces but on the other hand shows no elastic properties, but regulates cell length totally independent of cell tension. It is unclear how this could be realised and it contradicts other studies, thus we have to reject this model of frontal towing with a constant force combined with effective friction of the back. This approach also explicitly needs a tight mechanical coupling of front and back. A study with cells migrating on lines of pillars found that for example during rear release forces are not transmitted throughout the cell [175] which also contradict the assumptions.

5.6. A phenomenological model explains the velocity relation

This showed that it is not easy to formulate a mechanistic model that is in line with the data and with literature. An alternative approach is to construct a phenomenological model directly from the data. To this end, we can right away look for a relation for the velocity instead of considering forces and other mechanistic details.
We can assume that $v_{front} \propto \alpha_{front}$ and $v_{front} \propto -\alpha_{back}$ but we have to find relations how the coupling constants depend on c_{FN}. Therefore, we can take a look at the magnitude of the velocity changes during transitions in the different c_{FN} regimes (Fig. 5.11a). We find that in regime I, where the coupling to the substrate is lower, on average there is a great change of v_{front} when the front crosses the interface. When the rear is traversing there is also a change of v_{front} but with a smaller magnitude. For the second regime this changes dramatically. Here the average v_{front} shows almost no change when the front is traversing. In contrast, when the rear traverses changes in v_{front} are not disappearing but are even getting a bit larger compared to regime I.
This behaviour implies, that α_{front} is saturating very fast with increasing c_{FN}, whereas α_{back} does not show a saturation in the c_{FN} range we are investigating. Consequently, we can assume a saturating dependence of α_{front} on c_{FN}: $v_{front} \propto 1-exp(-\lambda c_{FN,front})$. For the rear, we can assume a simple linear dependence on the fibronectin concentration for the sake of simplicity $v_{front} \propto -\alpha_{back} = a_{back} - b_{back} c_{FN,back}$ which leads to the following

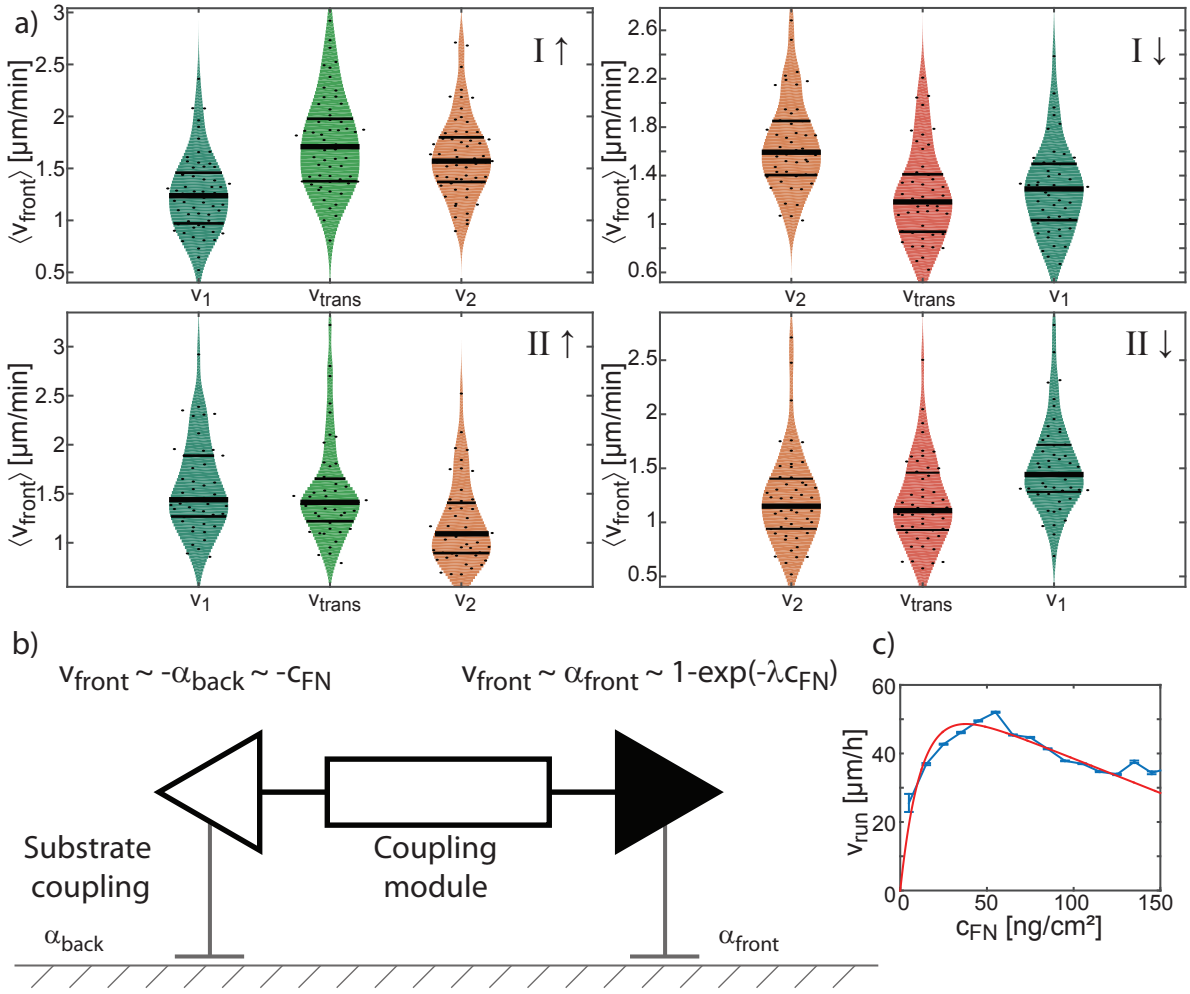

Figure 5.11.: a) Distributions of the mean front velocity in phases before, during, and after transitions separately for the low c_{FN} (I↑ and I↓) and for high c_{FN} regime (II↑ and II↓). Black lines indicate median and quartile values of the distributions. b) Phenomenological ansatz to describe the velocity relation. We assume that the velocity increases with increasing c_{FN} at the front and saturates. v_{front} decreases linearly with increasing c_{FN} at the back. This results in Equation 5.3, which can be fitted to the velocity (c).

equation:

$$v(c_{FN}) = (a_{back} - b_{back}c_{FN}) \cdot a_{front}(1 - exp(-\lambda c_{FN})) \tag{5.3}$$

This reproduces the maximum in the velocity relation and fits to the velocity in the observed range of the fibronectin concentration (Fig. 5.11b). But of course the linear relation at the back can not hold true for higher fibronectin concentrations because a negative α_{back} would not make sense.

For the front these assumptions are in line with the theory by Maiuri et al. [54] that assumes that the velocity is proportional to the retrograde actin flow V and the substrate coupling α: $v = \alpha V$. In this framework α_{front} can be interpreted as an efficiency of the cell to transform actin polymerization into forward motion. In the case of perfect adhesion $\alpha_{front} = 1$ the velocity of the cell is equal to the retrograde actin flow in the

frame of the moving cell. In the lab frame this would mean that the retrograde flow is zero, and thus there is no slipping back of the actin network. In this context α_{front} is limited to 1, thus a saturation of $\alpha_{front}(c_{FN})$ makes sense.

In this approach we did not make assumptions on how exactly the information of the coupling to the substrate at the back is transmitted through the cell and influences the velocity at the front. Albeit this is a very interesting question, there is no clear answer to this, and the phenomenological model leaves a lot of room for different possibilities. For example if mechanical forces are needed to break the adhesions at the back, the cell would elongate until enough force is built up. The higher tension for stronger adhesions at the back could affect the efficiency of the forward motion (although this is not perfectly in line with the study showing that changes in forces are not transmitted through the whole cell [175]). Alternatively, it is also possible that a biochemical coupling for instance via small GTPases is responsible for the regulation of the velocity of the front by adhesion at the back. Additionally, membrane tension could also be an important player in the coupling of front to back.
All in all, the phenomenological two-point model describes the transition behaviour and the maximum in the velocity relation very well. However, due to the phenomenological nature of the model there are no further straight forward predictions that could be tested. It rather gives a constraint to mechanistic models that should reproduce these emerging laws and gives an intuitive view on the cell migration behaviour.
The coupling of front to back is revealed very clearly in these experiments with cells performing transitions at the interfaces. This certainly needs more attention in further studies to get a better understanding of how processes at the front and at the rear are interconnected.

5.7. Dynamics of the rear

To learn more about the processes at the back of the cell and how they are connected to the velocity of the front we look for characteristic parameters describing the motion of the rear and their correlations to other values. Therefore, we can look again at the kymographs and the dynamics of the front and back motion (Fig. 5.12a). The motion of the back looks quite irregular, but when we separate the motion into phases where cells are only on one segment and into transition phases, we often find a more regular motion of the back. Zooming into one of those phases (Fig. 5.12b), we find a quite clear oscillatory behaviour of v_{back}. By performing a Fourier transform, we find that there is indeed a peak at a finite frequency verifying the oscillatory nature. The position of the maximum gives us the dominant frequency of the retraction behavior at the back. However, cells do not always perform the regular cycles of spreading backwards and retracting, as we also find a constant sliding motion of the back. Those phases that show maybe only one or two events of spreading backwards and retracting give rise to rather small retraction frequencies. Thus, there are retraction frequency ranging from about 1 to $6\,\mathrm{h}^{-1}$. In conclusion, we can interpret the dominant retraction frequency

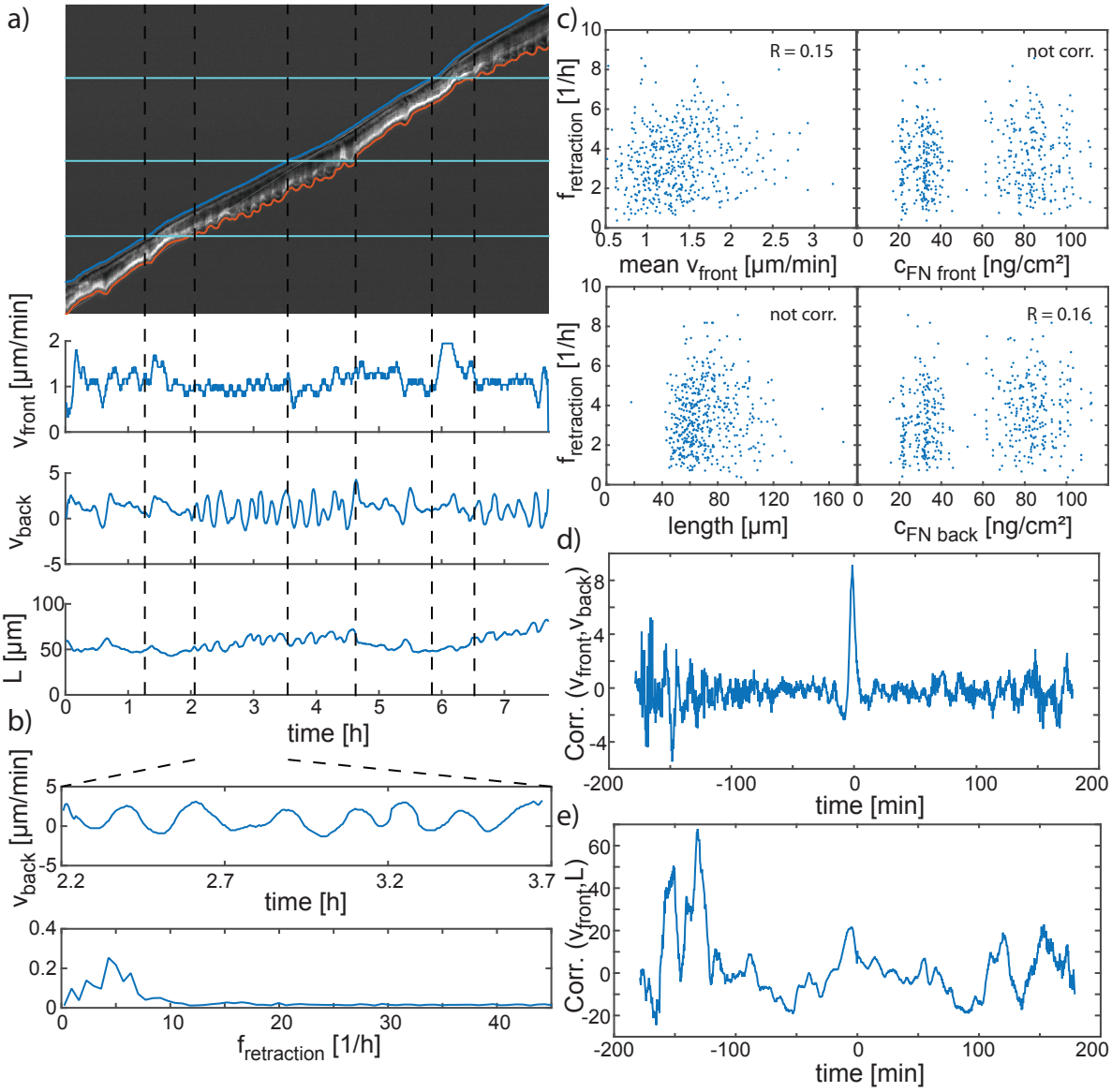

Figure 5.12.: a) Exemplary kymograph of a MDA-MB-231 cell migrating on the microlanes. Interfaces between two different segments are marked by horizontal lines. Front (blue) and back (red) are identified. Phases where cells are on one segment and transition phases are marked by dotted lines. Velocities of front and back smoothed over 5 min and cell length is plotted over time. b) Zoom in for the velocity of the back on one segment shows oscillatory behaviour. A Fourier transform is performed which has a maximum at frequency $f_{retraction} \approx 5h^{-1}$. c) For each phase (like seen in (a)) the dominating retraction frequency $f_{retraction}$ is calculated. Scatter plots with the average front velocity, average length, and fibronectin concentration of front and back are shown to reveal correlations. Pearson correlation coefficient R is analysed. d) To find temporal correlations, the cross correlation function between v_{front} and v_{back} or between v_{front} and the cell length L (e) is calculated for each phase and averaged over all phases.

$f_{retraction}$ as a probability of those back spreading events.
For each phase we can now quantify $f_{retraction}$ and other parameters like v_{front} the mean cell length L or the fibronectin concentration of the substrate. By calculating Pearson correlation coefficients we find that $f_{retraction}$ is not correlated with L or $c_{FN,front}$. But there is a small positive correlation with $c_{FN,back}$ (Fig. 5.12c). This implies that $f_{retraction}$ is mostly dependent of the local adhesion strength at the back, which makes sense. Interestingly, there is also a small positive correlation between $f_{retraction}$ and v_{front}. Intuitively we did not expect this, because the backwards spreading of the cell rear seems to be a process acting against the forward motion of the cell. When interpreting the correlations it is also important to have in mind that the fibronectin concentrations that where used are not equally distributed. The arbitrary choices of c_{FN} for the experiments could be also a cause for correlations. Thus, more experiments would be needed to clarify the role of the retraction behaviour.
To further investigate the coordination of front and rear we can look at the time courses of v_{front}, v_{back}, and L in Figure 5.12a. Although the front velocity looks quite smooth in the kymographs, we can see that there are some fluctuations that seem to be on a similar time scale as the fluctuations in v_{back} and L. Consequently, we evaluate the cross correlation between v_{front} and v_{back} or L (Fig. 5.12d,e). Indeed there is a positive correlation between v_{front} and v_{back} without any time delay that decays in about 5 min which is on the order of the time scale of the oscillations at the back. For the length in contrast, there is no clear correlation visible.
This means that there is a direct connection of front and back that coordinates the movement. But when looking at the size of the fluctuations of front and back velocity it is obvious that the fluctuations of the rear are one magnitude larger than at the front. Thus, for the rear the changes of the velocity on a short time scale are larger than the changes that come from the transition to different fibronectin concentrations. Therefore, it is possible that there a two processes involved. One that leads to the correlation of front and back velocity, but leads to only small modulations of the front velocity over time. And a second one that leads to a dependence of v_{front} on $c_{FN,back}$. Or alternatively, the process that leads to a dependence of v_{front} on $c_{FN,back}$ could also be influenced by v_{back}.

Taken together, we find no clear evidence that the changes of v_{front} due to different fibronectin concentrations at the back could be caused by changes of the retraction dynamics of the back. Although there is a direct coordination of v_{front} and v_{back} it is unlikely that changes in v_{back} can mediate the changes in adhesiveness at the back. As the coordination of v_{front} and v_{back} is very fast, a mechanical coupling like through membrane tension would be a good explanation. It seems that in addition to this there is a second process coupling front and back that transmits the adhesiveness at the back through the cell. This could also be a mechanical coupling for example via the cytoskeleton or also a biochemical coupling. On top of this, there are retraction dynamics at the back that depend on $c_{FN,back}$, but otherwise do not seem to influence the motion of the front too much. Taken together, these implications by the presented data highlight the need for a better understanding of how cell front and back are coupled. To this end, the data gives some clear correlations and restrictions that can help to create a more comprehensive model.

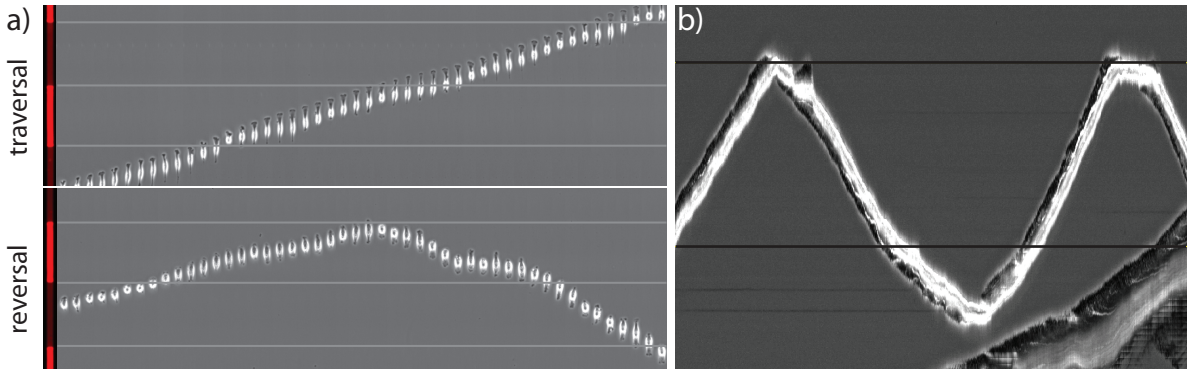

Figure 5.13.: a) Time series of MDA-MB-231 cells migrating on microlanes with segments of high and low fibronectin concentration (fluorescence images of the pattern on the left). Cells can either traverse the interface (above, time step between phase-contrast images 10 min) or reverse at the interface (below, time step between phase-contrast images 30 min). b) Kymograph of phase-contrast images of a cell reversing at the interface (time resolution 20 s)

5.8. Stochastic reversals at the interface

In the last sections we considered mostly the velocity changes during transitions. Therefore, we only investigated running cells, and thus the simple model was used to describe cells that deterministically move in one direction. But cell migration is of course a stochastic process that also includes reversals of the cells and switching between run and rest states. Consequently, in this section, we study stochastic reversal and traversals at the interface between two segments with different fibronectin concentration (Fig. 5.13a). On a phenomenological level, we can look at reversal events and find that at the interface the lamellipodium invades a bit into the next segment (Fig. 5.13b), thus probably probing the adhesiveness of the substrate.

In order to investigate the reversals with proper statistics, we analysed the behaviour of the tracks of the cell nuclei. A simple definition of a traversal or reversal event is to define a region of 50 μm in front of the interface. When a cell (cell nucleus position) enters this region we define a reversal event when it leaves the region on the same side and a traversal when it actually crosses the interface. As cells can also turn around without an interface present we additionally define a control traversal probability for traversals in the middle of the segment (Fig. 5.14a,b). The control traversal probability $P_{trans,ctrl}$ is more or less constant for different fibronectin concentrations. It only decreases for very small concentrations, a low number of data points in this regime leads to a large error range (Fig. 5.14c). Next, we compare the traversal probability at an interface for all possible combinations of c_{FN1} and c_{FN2} with the respective traversal probability without barrier $P_{trans,ctrl}(c_{FN1})$ (Fig. 5.14d). Below the diagonal, where cells traverse to less FN, the traversal probability decreases, whereas for equal or more FN the traversal probability stays more or less unchanged (In the first column the value of $P_{trans,ctrl}(c_{FN1})$ has a huge uncertainty, thus this is not very meaningful). The symmetry of the matrix, with different values in one row suggests that cells make relative measurements of the

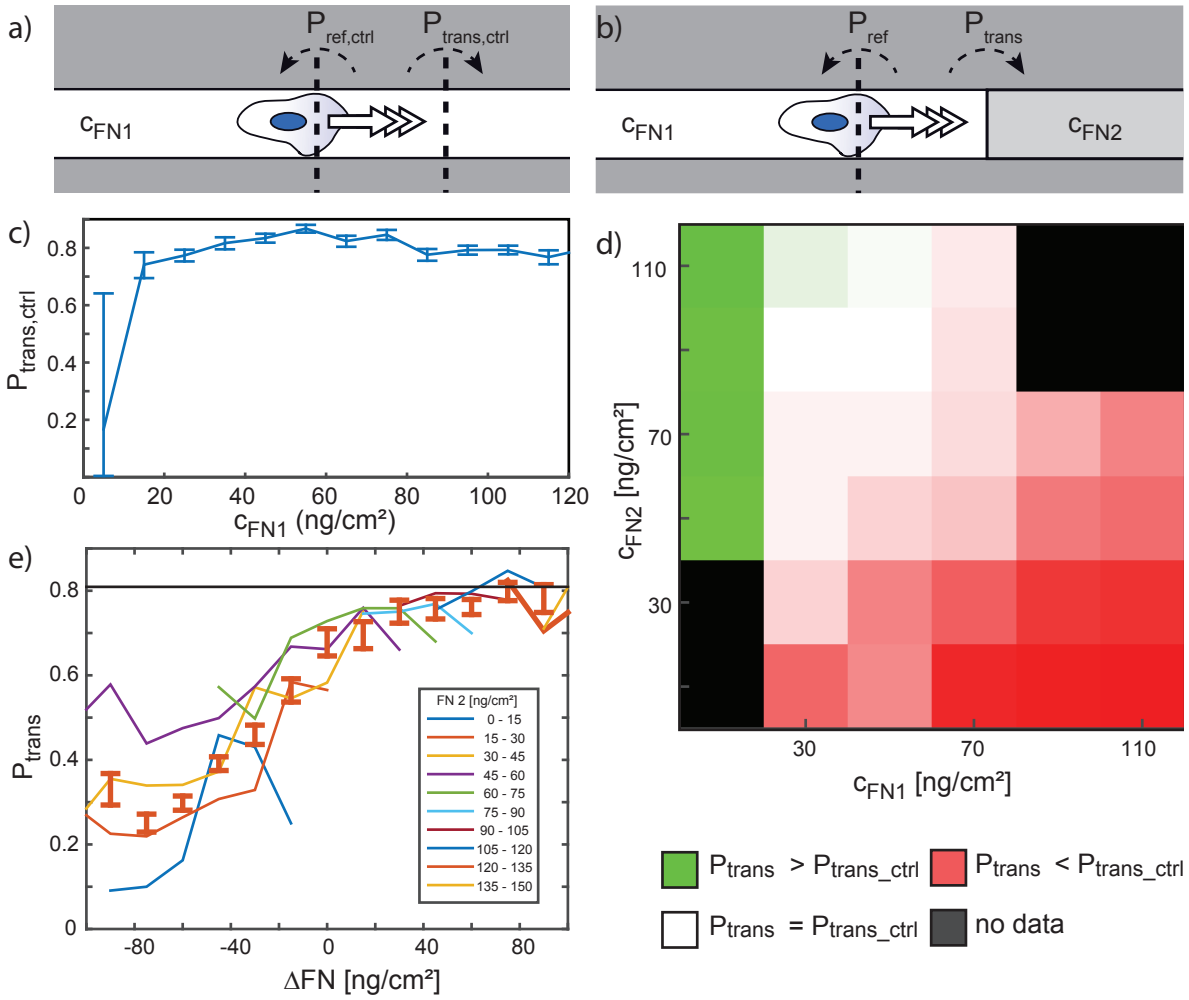

Figure 5.14.: a) Definition of reversal and traversal probabilities without a barrier present. To this end, a 50 μm region in the middle of the segments is observed. For cells entering this region, leaving the region on the other side is counted as a traversal, leaving on the same side is counted as a reversal and the probability of each event is calculated. b) Analogous to (a) reversal and traversal probabilities at the interface are calculated. c) The transition probability without a barrier $P_{trans,ctrl}$ for different fibronectin concentrations with 95% Clopper-Pearson confidence intervals. c) Map of P_{trans} at interfaces between all possible concentrations of c_{FN1} and c_{FN2}. The color code compares P_{trans} with $P_{trans,ctrl}(c_{FN1})$. e) P_{trans} in dependence of the difference between c_{FN1} and c_{FN2} (red with 95% Clopper-Pearson confidence intervals). Additionally, values for different regions of c_{FN2} are plotted in various colours.

FN concentration. Therefore, it is mainly Δc_{FN} that defines the traversal probability (Fig. 5.14e). Interestingly, the traversal probability is not becoming much higher when cells are traversing to more fibronectin. In contrast, they reverse much more often at interfaces to areas with less fibronectin. This defines a new guidance principle for cell motion. Although the absolute value of c_{FN} is not that crucial, it plays a role in the extent of the drop of P_{trans} when faced to less fibronectin, which makes sense as in the extreme case of zero fibronectin we would expect the cells to never go there.

It is known that cell migration can be guided by an unequal distribution of surface bound proteins, which is called Haptotaxis. Haptotactic behaviour plays an important role in processes like angiogenesis [176], and cancer cell migration [177]. On surface bound gradients of fibronectin, haptotactic behaviour has been observed that is usually described as cells move *"preferentially towards regions of higher adhesion ligand concentration"* [25]. At the interfaces we also observe haptotactic behaviour that lets us make the statement a bit more precise. Cells seem to not care so much about regions of higher ligand concentrations but they usually turn from regions with lower ligand density. This refined guidance principle is of interest for example for applications of self sorting of cells that should arrange in a certain way. This could be of special interest in the growing field of creating artificial organs.

A first approach that could be thought of to explain the reversal behaviour at the interface is that the persistence of cell motion is dependent on c_{FN} and therefore this could lead to the increased number of reversals at the interface. However, we found in Figure 5.4c that the persistence shows a maximum for intermediate fibronectin concentrations just like the velocity. In contrast the traversal depends on Δc_{FN} and this is does not flip with increasing fibronectin levels. Therefore, the stochastic traversal behaviour is not just a cause of changing motility parameters at the interface, but cells are really performing a relative measurement at the interface.
If we want to incorporate stochastic behaviour in our simplified phenomenological model, this can be easily done by defining probabilities to switch between run and rest states that are dependent on the fibronectin concentration. In order to get also the stochastic behaviour at the interfaces, the probability to switch from run to rest states definitively needs a term depending on Δc_{FN}. With this, cells can stop at the interface, but to get very high reversal rates also the probability to polarize (thus the rate of switching from rest to run states) in a certain direction needs to get a bias. This is also supported by the polarization behaviour of cells at the PEGylated areas studied in Chapter 3.
A simple mechanistic explanation for the reversal behaviour at the interface would be a mechanical breakage of adhesions, similar to the model by DiMilla et al. [21] where they assume an asymmetric adhesion strength at front and back with stronger adhesions at the front. Through mechanical tensions more adhesions at the back are broken, which leads to a net forward motion of the cell. In our case, newly formed adhesions at the front could be broken if a cells moves to a field with less fibronectin, which would stop the cell. However, a study of cells on pillars showed that forces are not transmitted very far throughout the cell [175]. Therefore, also other, more complicated, mechanisms to do relative adhesion measurements could be implemented by the cells.

All in all, the investigation of cell migration at steps of different adhesiveness reveals much more about the functionality of a migrating cell compared to homogeneously coated substrates. It also raises important questions like: What is the nature of the coupling between the front and the back of the cell? To answer this, more experiments are needed that include the measurement of forces and the dynamic of the cytoskeleton and of adhesions. In the end, this will hopefully lead to a comprehensive model that explains how cell migration depends on the coupling to the substrate via adhesions.

6. Conclusion and outlook

We find that microlanes are a versatile tool that is well suited to study several aspects of single-cell migration. First of all they provide a defined environment that allows obtaining many single-cell trajectories of high quality and of long duration. This is the basis to get a good quantification of the cell migration behaviour of a heterogeneous cell population. By restricting the motion of cells to 1D, we greatly simplified the analysis. Instead of the many models used for quantification of the cell motion in 2D that often are very complicated and have many parameters, we used a simple two-state analysis that turned out to be a good approximation for the cell behaviour. The extracted parameters are orthogonal, thus they really contain distinct information about the cell migration behaviour. Furthermore, the two states seem to have their according counterpart in the morphology of the cell. In run states cells are polarized and in rest states cells are unpolarized. This makes the multi-parameter quantification a powerful tool as changes in the parameters are not just changes in a mathematical description, but can actually give hints which biological processes are affected.
Here, we demonstrate that this fingerprint like characterization allows distinguishing different cancer types or determining drug effects. However, one is of course not limited to the parameters that we investigated. It is also possible to extend the fingerprint by incorporating for example parameters like the cell length or other parameters that quantify the morphology or other aspects of the cell.
Furthermore, this characterization could be used to compare many more cell types to build up a database which could be used to study whether a certain migration behaviour correlates with the ability of cells to form metastasis or similar aspects of different diseases. The microlanes could also be used to screen for drugs that affect the migration behaviour of the cells in a desired way. For these applications of the assay a very high throughput is necessary. Therefore, a fully automated data analysis would be needed which we showed in Chapter5 is possible. However, also the experiments would have to be optimized to decrease the effort of conducting the measurements. For now, the micropatterns were created manually which includes positioning the stamps by hand. To scale up the production of micropatterns an automation of the microcontactprinting process would be necessary. This could be done by using a cylindrical rolling stamp as proposed by Xia et al. [178]. There are even some companies that offer automated microcontactprinting machines. An automation of the printing process might also improve the quality of the patterns. For the manually produced patterns, there are often some small inhomogeneities in the surface coating and also across one stamp there can be some variations of the protein transfer efficiency. When manually placing the stamps and performing the pipetting steps it is not possible to always apply the exact same pressure or waiting times between steps, which could be a reason for the inhomogeneities. Furthermore, there are also other possible micropatterning techniques that could be well suited for an automated fabrication. One possible option is patterning

based on photoactivation [19, 75–78], which has the advantage that it can be performed contactless. Or alternatively, there are already several companies that offer patterned surfaces ready to use.

An important feature of the analysis of cell migration on microlanes is the possibility to get a time-resolved characterization of the motility. In combination with the ability to switch on the expression of miR-200c we were able to find the time point where the migration behaviour is changing. By combining time resolved studies of protein expression and of changes in the phenotype it could be possible to disentangle complicated regulation networks. To do so, also tight control over activity of the pathway of interest is needed. For miR-200c this was performed by using a TET system where the expression of miR-200c can be controlled by adding Doxycycline. In order to optimise the control over such a system, TET systems that can be controlled by light have been developed [179], which could lead to a sharper switching and therefore a more precise determination of time points where changes in the cell behaviour occur.

For the comparison between MDA-MB-436 breast cancer cells and the HUH7 liver cancer cells that we performed, the observed motility and ability to overcome PEGylated barriers correlated with the invasive potential of the cells. However, the *in vivo* situation of a migrating cell is quite different to our artificial setup, thus it is not that simple to quantify the invasiveness of cancer cells in the lab. In the body cells are in a 3D environment and to get into blood or lymph vessels cancer cells need to digest dense structures of the ECM and squeeze through small pores [180,181]. Usually, these abilities are measured by a Boyden chamber assay, in which cells are seeded on a dense matrix, and the number of cells that succeed to cross it is investigated [182, 183]. Thus, this is an endpoint assay that does not provide single-cell resolution or a time resolved investigation. By incorporating obstacles into the lanes it could be possible to create an assay that allows studying single-cell migration in defined environments that mimic the 3D situations. Therefore, a 3D confinement by channels with bottlenecks, similar as in the dumbbell patterns could be used to probe the ability of cells to squeeze through small constrictions [184–186]. In order to measure also the potential of cell to digest ECM, new patterning techniques would have to be developed that can create defined ECM barriers. Or alternatively other methods that allow to probe the presence of ECM digesting proteases for example by fluorescence based methods would have to be incorporated.

Another aspect that is different in our artificial micropatterns compared to the natural environment is that the plastic substrate is much stiffer than the natural environment. These mechanical properties can also play an important role in cell migration [187–189], thus it would be interesting to study cell motility on microlanes also in dependence on the substrate stiffness. To obtain such micropatterns, there are several techniques available [190–193], but the fabrication is more complex, which makes it more tedious to do high throughput experiments.

In this thesis, we used the approach to study cell migration at interfaces of changing

substrate coatings in order to get a better understanding of the underlying mechanism and of the influence of adhesions. Therefore, we used microlanes with discrete steps of the fibronectin concentration where a single cell can be observed in different microenvironments. We find that there is a maximum of the cell velocity for intermediate fibronectin concentrations. Moreover, during transitions the cell front changes its velocity two times. Once, when the front and a second time when the rear traverses the interface. The observed transition behaviour can be well described by a phenomenological two-point model that interacts with the substrate only at the front and the back. The interaction strength with the substrate at the rear end has a great influence on the velocity of the front, thus there needs to be some kind of coupling that transmits this information throughout the cell. It is not clear how this coupling of front and back is implemented and could it be a mechanical or a biochemical coupling, as well as a combination of both.

The transfer of the system onto soft substrates, mentioned before, would be an interesting way to investigate this coupling, as if allows incorporating beads into the substrate that can mark deformations caused by forces that the cell is applying. This technique is called traction force microscopy and is widely used in cell research [194–196]. This could clarify the role of mechanical forces in the coupling between front and back.

In our phenomenological model, a stronger coupling to the substrate at the front leads to higher velocities most likely because forces can be transmitted to the substrate more efficiently. In contrast, stronger adhesion at the back reduces the velocity of the cell. Since the rear reduces the velocity of the front it is interesting what would happen if we could cut the cell in half while it is migrating. Would the cell front be able to migrate much faster without the decelerating influence of the back, or would the back side of the cell front act like the former cell rear so that we just get a shorter cell? For keratocytes it is known that sometimes the lamellipodium can separate from the cell body and is able to migrate individually for some time without the nucleus and other cell organelles [133]. For keratocytes, it is even possible to induce the formation of this fragmented lamellipodia by some drugs [197], but also for the breast cancer cells we observed a ripping of lamellipodia in very rare cases. By studying these solitary lamellipodia at the interfaces we could learn more about the influence of the rear and whether organelles like the nucleus play an active role in the migration process.

Also for a mechanistic understanding of the cell migration process those fragments are interesting, as they provide a minimalistic model system of a migrating cell. For example, the fragments are believed to not contain microtubules and are still able to migrate, although it is known that microtubules are involved in the regulation of cell migration [198, 199]. To create a mechanistic model that is able to describe the process of cell migration on the molecular level such simplified systems might be useful.

Also in a reduced setting it is still very difficult to get a comprehensive model of the cell migration process, because there are so many different molecules involved. However, also new methods have been developed in the last years that will most likely contribute to a better understanding of some parts of the process. For example with the development of super-resolution microscopy techniques [200–203] it is now possible to resolve the structure and interaction of protein complexes with nanometer resolution as demonstrated for example for focal adhesions [204]. Further progress has been made also in how biological systems can be manipulated by gene editing for example by the famous

CRISPR Cas system [205]. One approach that could be used to specifically manipulate certain processes are optogenetical tools [206]. There, light sensitive proteins are expressed in the cell that allow precise manipulations with response times in the millisecond regime. For example this has been used to manipulate the activity of rho family GTPases to influence protrusion formation or forces generated by the cells [207–209]. Using such optogenetical tools it could be possible to tune the adhesion to the substrate at front and back individually by using selective illumination. In combination with the microlanes, the influence of the coupling to the substrate could be further investigated and maybe also the directionality of the cell motion could be controlled.

Furthermore, we found that steps in the fibronectin concentration have an influence on cell guidance. It is remarkable that cells only show clear changes of the reversal probability when faced with a relative decrease of the fibronectin concentration. In order to investigate how cells can do an apparent comparison of the adhesiveness at front and back, the number and size of focal adhesions could be studied. A better understanding of such cell guidance mechanisms could be used to build devices where cells can autonomously arrange in a certain formation. In order to brake the symmetry and achieve cell guidance in one direction, gradients of fibronectin have been used [25, 131, 168]. However, it is not possible to generate steep gradients over large distances, as soon the whole surface is covered with fibronectin. To get an infinitely long lane with biased cell migration one could think of a sawtooth profile of the fibronectin concentration. This is basically a connection of many segments with gradients and intuitively one would think that the cells move along the gradient in the direction of increasing concentration. However, we found that at the steps, where the fibronectin concentration is decreasing, cells turn around very frequently. Thus, in the end it is not clear how cells would behave in such a setting and in which direction the motion would be biased.
The patterning technique that we developed allows also to create fields with different protein coatings. The biggest advantage, compared to other micropatterning methods, is that coating of the two different fields is completely separated, which allows patterning of proteins that can bind to each other like fibronectin and collagen I. In the experiments we performed at the steps between different fibronectin concentrations, the ligand density for certain integrins changed. However, the integrin types that bind to the substrate stayed the same. When using different proteins this would be different and it could be studied whether cells need some time to adapt when faced with a different type of ligand. Additionally, it is also possible to use cell signalling molecules like ephrins to mimic cell-cell interactions. For example, when cells touch front to front, there is a process called contact inhibition of locomotion that leads to a repolarization of cells [95,210–212]. Thereby, it is possible that very high reversal rates could be achieved, although the functionality of signalling molecules that are usually incorporated in the cell membrane has to be ensured when bound to a surface.
In the frame of a bachelor thesis conducted by Maximilian Kreft we explored whether MDA-MB-231 breast cancer cells have preferences for certain protein coatings, which means that they spend more time on areas coated with this protein. For MDA-MB-231 cells we can make a ranking of ECM proteins. Cells showed high preference for collagen IV, low preference for laminin and intermediate values for collagen I and fibronectin.

Depending on the integrin expression we would expect different preferences for different cell types [213]. Therefore, further studies on this could lead to applications that allow a self sorting of various cell types.

In conclusion, the fingerprint like characterization of cell motility on microlanes can be used to get refined analysis of the effects of drugs by quantifying velocity and duration of running and resting times. This could be utilized to develop anti-migratory drugs that may be applied in cancer therapy. Furthermore, the introduction of defined interfaces allows studying single cells in two different micro-environments and at transitions. The cell behaviour could be explained by a phenomenological model that can give new insights into the function of the migration mechanism of cells and provides clear constrains for a bottom-up model of cell migration.

A. Methods and experimental details

A.1. Micropatterning

A.1.1. Stamp production

All used micropatterning techniques are based on PDMS stamps. The masters that are used to cure the stamps are produced by photolithography. For this purpose, silicon wafers were coated with TI Prime adhesion promoter and AZ40XT (MicroChemicals) photoresist. Areas of the favoured geometry were exposed to UV light using laser direct imaging (Protolaser LDI, LPKF). The photoresist was then developed (AZ 826 MIF, MicroChemicals) and silanized (Trichloro(1H,1H,2H,2H-perfluoro-octyl)silane, Sigma-Aldrich). For the creation of PDMS stamps, PDMS-monomer and cross-linker (DC 184 elastomer kit, Dow Corning) were mixed in a 10:1 ratio, poured onto the stamp master, degassed in a desiccator, and cured overnight at 50°C.

A.1.2. Protein labelling

To be able to image the micropatterns it is essential to label fibronectin with a fluorescent dye. This makes it possible to find the patterns, to identify defects, and to perform automated identification of pattern position and quality.
For the labelling, two different dyes where used. First (for experiments in Chapter 3) Alexa 488 was utilised, but this resulted in compounds with low photo stability. This allowed to check whether there are defects, but to get an image quality that enables automated pattern detection and evaluation of the surface concentration via fluorescence intensity I switched to Alexa 647 for further experiments.

Labelling Protocol: 50 μl of 1M sodium bicarbonate buffer was added to 500 μl of 1mg/ml fibronectin solution (Yo Proteins). 34 μg of Alexa Fluor 488 SDP ester or 50 μg of Alexa Fluor 647 NHS ester (Thermo Fisher Scientific) was dissolved in 3 μl ultra pure dimethyl sulfoxide (DMSO) and mixed with the fibronectin solution. Next, I waited 2–4 h for the labelling reaction to take place at room temperature and protected from light. Then, free dye and labelled protein are separated by size-exclusion chromatography using a PD MiniTrap G-25 (GE Healthcare) and phosphate-buffered saline (PBS) as buffer solution. The concentration of the resulting fractions of labelled fibronectin solution was measured with a spectrophotometer (NanoDrop, Thermo Fisher Scientific).

A.1.3. Microcontactprinting

Microcontact printing was used to produce fibronectin-coated ring-shaped lanes for the experiments in Chapter 3 and 4. This method is widely used to create protein patterns on various substrates. There are several protocols available in literature [19, 70, 72, 214] and I adapted them for the conditions used here to improve the results:
PDMS stamps were treated with UV light (PSD-UV, novascan) for 5 min. Then, the stamps were incubated for 45 min in a solution containing 40 μg/ml fibronectin (Yo proteins) and 10 μg/ml labelled fibronectin dissolved in ultrapure water. Next, stamps were washed with ultrapure water, dried and placed on a petri dish (μ-Dish, Ibidi), which had been treated with UV light for 15 min. A droplet of a 2 mg/ml (or 1 mg/ml in Chapter 3) poly-L-lysine-grafted polyethylene glycol (PLL-PEG) (2 kDa PEG chains, SuSoS) solution (dissolved in 10 mM HEPES containing 150 mM NaCl was placed at the edge of the stamps and drawn into the spaces between surface and stamp by capillary action. Stamps were removed and a glass coverslip was placed on the dish surface to ensure complete coverage of the surface with PEG solution. After a 30-min incubation, the coverslip was removed and the surface was washed three times with PBS and stored in PBS until cells were seeded (maximum storage time: 1 day).

A.1.4. Two protein patterning

In order to create stripes with segments of alternating fibronectin concentration, which were used in Chapter 5, a new protocol was developed. This cannot only be used to create fields of different fibronectin concentrations like described here, but also patterning with two different proteins is possible (see also Fig. 5.1 and 5.2):

Stamps with a relief structure of 150 or 200 μm wide stripes were activated for 3 min in a UV cleaner (PSD-UV, novascan) and inked with a fibronectin (Yo Proteins) solution ranging from 6.3 μg/ml to 50 μg/ml for 45 min. (Fibronectin was labelled with Alexa Fluor 647 NHS ester (Thermo Fisher)). Stamps were washed with deionized water and dried. During the drying process of the first stamps, a second type of stamps with lines of 15 μm width were UV treated for 7 min. When stamps were dry, they were stamped on the second stamps with lines orientated perpendicular to each other. Subsequently, when stamps were still in contact with each other, they were treated with O_2-plasma for 1 min to change the unprotected surface between the stamps to hydrophilic. A drop of the second fibronectin solution ranging from 50 to 300 μg/ml was put next to the stamps and got drawn into the free space between the stamps. After 30 min the second solution dried and the stamps could be separated and stamped on a Petri-dish (μ-dish uncoated, Ibidi) that was treated with UV for 15 min before. A drop of Pll-PEG (2 kDa PEG chains, SuSoS) was put next to the stamp and got drawn into the free space under the stamp. After waiting for 2 hours, stamps were removed and the pattern was washed with PBS three times and stored in PBS at 4°C until cells were seeded on the next day.

A.2. Cell culture

MDA-MB-436 breast cancer cells were cultured in DMEM-F12 medium (c.c.pro) containing 10% fetal bovine serum (Invitrogen) and 2.5 mM L-glutamine (c.c.pro). HuH7 cells were cultured in RPMI medium (c.c.pro) containing 10% fetal bovine serum (Invitrogen), 2 mM L-glutamine, 5 mM HEPES, and 1 mM sodium pyruvate (c.c.pro). Cells were incubated at 37°C in a 5% CO_2 atmosphere.
MDA-MB-231 breast cancer cells (DSMZ) were cultured in L15 medium containing 2 mM glutamax (Thermo Fisher) plus 10% fetal bovine serum (Thermo Fisher). MDA-MB-231 TRIPZ-Ctrl cells and MDA-MB-231 TRIPZ-200c cells were cultured in L15 medium containing L-glutamine (Sigma-Aldrich) and 10% fetal bovine serum that was tested for compatibility with TET-systems (ClonTech) at 37°C without CO_2.
All cell lines were passaged every 2-3 days. For experiments cells were trypsonized and cell solution was centrifuged at 800 rcf for 3 min (except for MDA-MB-436 that were just bumped off). Subsequently about 3,000–10,000 cells were seeded per dish. After 2-3 h cells adhere to the micropatterns and medium was exchanged to L15 medium without phenol red with extra 25 nM Hoechst 33342 (Invitrogen) for experiments, during which cell nuclei were tracked. Then, samples were transferred to the microscope and experiments were started within 1–2 h.

A.3. Microscopy

In order to realize automated tracking of the cell nuclei with a time resolution of 10 min, scanning time-lapse measurements were performed. For experiments in Chapter 3, an automated inverted microscope (iMIC, Till Photonics) with a 10x Zeiss objective, a oligochrome lamp (Till Photonics) and an ORCA-03G camera (HAMAMATSU) was used. Cells were maintained at 37°C using a temperature-controlled mounting frame (Ibidi temp. controller, Ibidi). For further experiments, two different Nikon TI setups were used equipped with a 10x Nikon objective, a SOLA or Spectra-X LED lamp (Lumencor), a pco.edge 4.2 sCMOS camera (PCO), and a Okolab heating chamber. At every time-point, phase-contrast and fluorescence images of the nuclei were taken. Fluorescence images of the patterns (and of RFP expression for MDA-MB-231 TRIPZ cells) were taken before or after the experiment. For experiments in Chapter 5, a 2x2 binning was used to decrease the data size. The time-lapse movies acquired at the Nikon microscopes were converted from 16 bit to 8 bit before processing. For experiments of cells migrating on a homogeneous 2D surfaces always four images were combined to effectively get a larger field of view.
For experiments with higher time resolution only phase-contrast images were acquired to reduce photo damage of the cells. In Chapter 3, high resolved images of cell protrusions at the interface were taken with the IMIC microscope and a 40x Zeiss objective with a frequency of 5 s.
In Chapter 5, images were taken with a time resolution of 20 s on the Nikon microscope with 10x objective.

A.4. Determination of fibronectin surface concentrations

In Chapter 5 the cell migration behaviour in dependence of the fibronectin concentration of the substrate is studied. Therefore, a quantification of the surface concentration of fibronectin is needed. The surface concentration of proteins can be measured for example by ellipsometry [215], isotopic labelling of the proteins or plasmon frequency measurements [216]. However, these techniques are difficult to apply to the micropatterns on plastic dishes as they often require metal surfaces. Furthermore it would be difficult to perform measurements with high spacial resolution that is needed to measure the surface concentration of every line segment. Additionally, if the measurement is conducted on a different setup than the time-lapse microscopy an alignment of the measured concentrations to the microscopy images of the cells would have to be done. Therefore, I chose to use fibronectin labelled with a fluorescent dye and to determine the surface concentration via the fluorescence intensity.
In order to measure quantitative surface concentration and not only relative values, a calibration curve that translates fluorescence intensity into absolute concentrations is needed. To obtain such a calibration curve, I filled microfluidic channels with fibronectin solution of different concentrations and measured the fluorescence intensity. Preliminary experiments on the calibration of the fibronectin surface concentration were performed in the course of a Bachelor thesis by Michael Redl.

The height of the microfluidic channels (designed by Rafal Krzysztoń and made by Charlott Leu) has to be smaller than the focus depth of the objective used to ensure a proper calibration. Otherwise some of the fluorescence intensity would not be detected by the camera which would lead to deviations. To be able to fill the thin channels they are connected with larger channels that lead to inlets and outlets. (Fig. A.1a)
For the creation of the calibration slide, the PDMS with the desired structures was cut and 1.2 mm holes where punched at inlets and outlets. A glass slide with an approximate height of 180 μm was cleaned in the sonicator for 10 min in isopropanol and for 10 min in deionized water. The glass slide was dried and the PDMS was cleaned using nitrogen flow. Both were cleaned for 0.3 min in oxygen plasma and pressed together. Afterwards the slide was kept at 50°C overnight to ensure adhesion of the PDMS to the glass slide.
The filling process was performed in a clean room, to avoid blocking of the channels. Tubes where connected to the inlets (Fig. A.1a) and channels were first filled with 10 mg/ml Pluronic F127 using a syringe pump (filling speed: 0.2 ml/h) to passivate the channels. After at least 4 h of incubation channels where washed with PBS and then filled with fibronectin solution. The connecting tubes were not removed for the different filling steps, as this can create PDMS crumbs (Fig. A.1b) that can potentially block the channels. The height of the PDMS channels was measured by Charlott Leu using

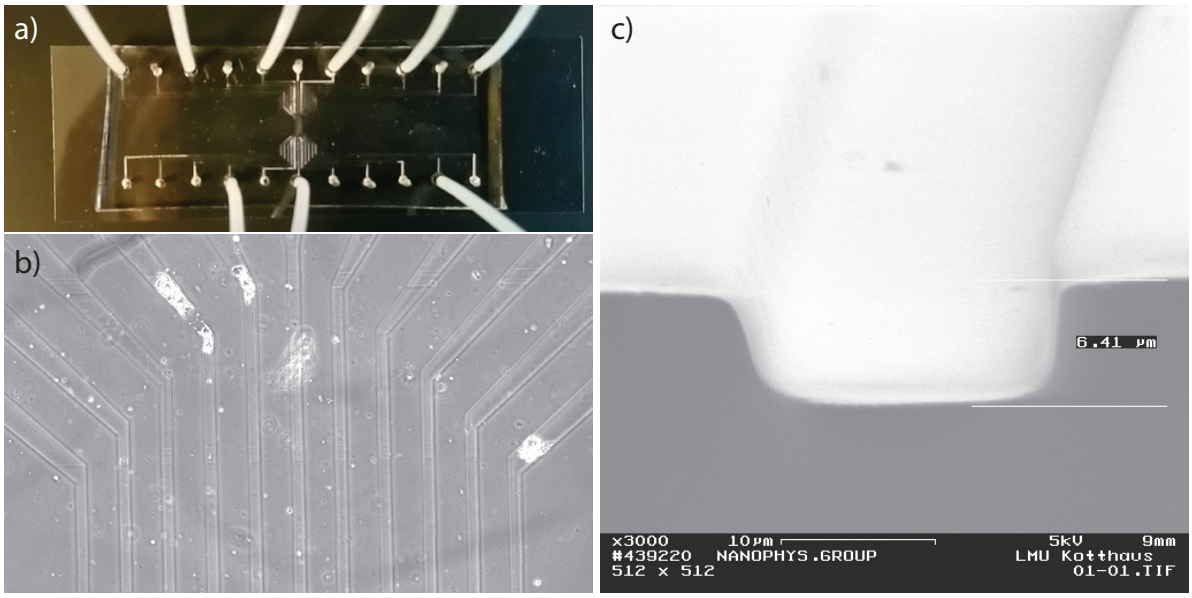

Figure A.1.: Calibration slide: a) Image of microfluidic channels in a PDMS block glued to a glass slide. The individual channels are connected to tubes to allow filling with fibronectin solution. b) Microscopy image of microfluidic channels. From the inlet large channels lead to the middle part where they merge into smaller and flatter channels. Crumbs of PDMS can get stuck there and block the channel. c) Scanning electron microscopy image of one channel formed with PDMS. Thereby the channel height is determined. (Image provided by Charlott Leu)

scanning electron microscopy (Fig. A.1c).
The fluorescence intensity was measured at the microscopes using the 10x objective, 500 ms illumination time, 75% lamp intensity, with and without binning (Fig. A.2a). The concentration of the different fibronectin solutions was measured with fluorescence correlation spectroscopy (three dilutions for each solution). A two component fit to the correlation curve showed that there was about 11% free dye in the sample. By dividing the concentration by the height of the channel, we get the corresponding surface concentration, which together with the background corrected intensity provides the desired calibration curve (Fig. A.2b,c). We find a linear relation between intensity and concentration $I = a \cdot c_{FN}$ that can be used to calculate the fibronectin concentrations of the micropatterns.

The calibration process can be affected by several sources of errors that complicate the estimation of the precision of the calibration. Fluorescent dyes can influence each other which leads to quenching when they are in close proximity to each other. The linear relation between concentration and intensity implicates that quenching does not play a role in this concentration regime, but it is unclear whether this is changing when proteins are not in solution but coated on a 2D surface. Furthermore it is difficult to check whether the passivation of all used components was successful so that no protein is lost during the filling process. Additionally, the protein concentration in the channels can change due to evaporation. I give an error range that is an statistical error, but I cannot exclude that there are also systematic errors that decrease the precision of the determination of absolute fibronectin concentrations.

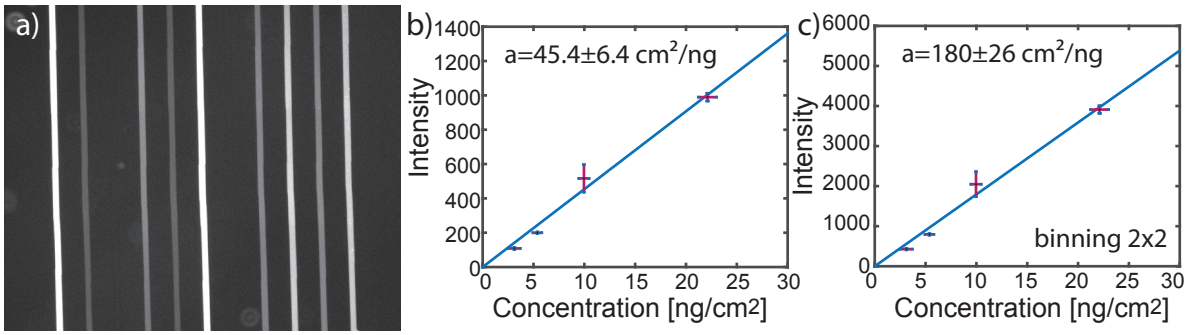

Figure A.2.: a) Fluorescent image of channels filled with different fibronectin concentrations. By measuring the concentration of the solution and the height of the channels, a calibration curve of the surface concentration is generated (b, c). This is done individually for specific microscope settings. Here at the UNIKON with 10x objective, 75% lamp intensity, 500 ms illumination time, without (b) and with 2x2 binning (c). A line through the origin with slope a is fitted to the data.

B. Image and data analysis

B.1. Semi-automated tracking of nuclei

In Chapter 3 and 4, tracking of the nuclei of cells migrating on ring-shaped microlanes was performed with a basic semi-automated tracking algorithm implemented in *ImageJ*.
In order to study only cells that are alone on one ring, the time lapse movies were analysed by eye. Additionally, the cells should meet the following criteria to allow a meaningful study of cell motility: Cells should have only one nucleus and should show no signs of cell death. Furthermore they should be well confined on the micropatterns. Due to the curvature of the ring, the cell body is often shifted a bit to the inner border of the ring-shaped lane, but cells should not really span over the passivated middle part of the ring. Furthermore the pattern should not show clear defects and there should not be larger pieces of dirt visible that could affect the cell motion. To ensure that cells are alive they should show a minimal sign of motility.
Cells that meet these conditions for a time interval of at least 20 h (mostly cell division terminates these phases) are selected manually. Subsequently, a bandpass filter is applied to the image of the labelled nucleus and a fixed threshold is used to create a binary image. The geometric centre of the nucleus is further used as proxy for the cell position calculated with the *analyse particles* plug-in from *ImageJ*.

To be able to change from Cartesian coordinates to polar coordinates, it is necessary to determine the centre of the ring-shaped lane. In the beginning of the experiments, I had problems with the image quality of the fibronectin patterns because the dye used for labelling bleached very fast. Therefore, it was not possible to apply an automated detection of the micropatterns. As an alternative I fitted a circle to the cell trajectories (using *Matlab*), which successfully identified the centre. Solely for cells that move only a little this method is not very robust. Therefore, only cells that move at least one quarter of the circle where analysed. This is not a large additional restriction because for most cells that show a little bit of movement, this criterium is met.
With better image quality of the patterns, it is now definitively possible to detect the rings automatically, for example by using the circular Hough transform. For further migration experiments on rings this should be incorporated to save time that is otherwise needed for manually selecting cells. Additionally, this allows also to investigate non-moving cells which can give a more complete view on the cell population.

B.2. Change point analysis

In Chapter 3, I describe how cell motion on a quasi 1D microlane shows clear characteristics of a two state process. To analyse this process in more detail, a classification scheme that is capable to distinguish between the run and rest states is needed, which is also described in Publication [1].
Here, we are using the cell nucleus as an estimator for the cell position. Since it is difficult to automatically segment bright-field images of the cell, tracking the nucleus is a very efficient way to gain large data sets. However, this means that we do not have any information of the cell morphology or polarization. To separate the different states of cell motion we are left with just the dynamics or in other words the angular velocity ω(t) of the nucleus.
A simple velocity threshold is not a robust method to distinguish between states as the velocity in the rest states can also show very high peaks (Fig. B.1a). Additionally, this means that slow running periods are not allowed. Moreover, cell populations can be quite heterogeneous, thus the threshold would have to vary for individual cells. When comparing the velocity of different cell lines, results could be very sensitive on the chosen threshold.
In order to avoid this, we implemented an iterative change-point analysis based on cumulative sum (CUSUM) and classified the motion using a fit of the mean squared displacement (MSD) (Fig. B.1).
We first calculate the CUSUM of the angular velocity ω(t) for each time point t within a track:

$$S_t = \sum_{i=1}^{t} (\omega_i - \overline{\omega}) \tag{B.1}$$

Here, $\overline{\omega}$ is the average velocity within the tracking interval t = 0,...,T. To decide whether a change-point occurred within an interval, we estimate a confidence level for existence of a change-point via bootstrap analysis. Therefore, we define the estimator for the existence of a change as

$$S_{diff} = (\max_{t=0,...,T} S_t) - (\min_{t=0,...,T} S_t) \tag{B.2}$$

that is calculated for the CUSUM of the actually measured velocity and also for a set of bootstrapped CUSUMs where the order of $\omega_t : t \in \{0, ..., T\}$ is permuted randomly (Fig. B.1). Next, we calculate a confidence level for the occurrence of change-point in the interval:

$$L_{conf} = \frac{S_{diff} < S^0_{diff}}{N_{perm}} \tag{B.3}$$

Here $S_{diff} < S^0_{diff}$ denotes the number of permuted CUSUMs for which S_{diff} is smaller than the estimator of the original CUSUM S^0_{diff} and N_{perm} gives the total number of bootstrap samples. For the analysis we used $N_{perm} = 10,000$. If L_{conf} is above a certain threshold level L_{th}, we assume that there is a change-point. The position of the change-point can be found by evaluating

$$S_{CP} = \max_{t=0,...,T} |S_t| \tag{B.4}$$

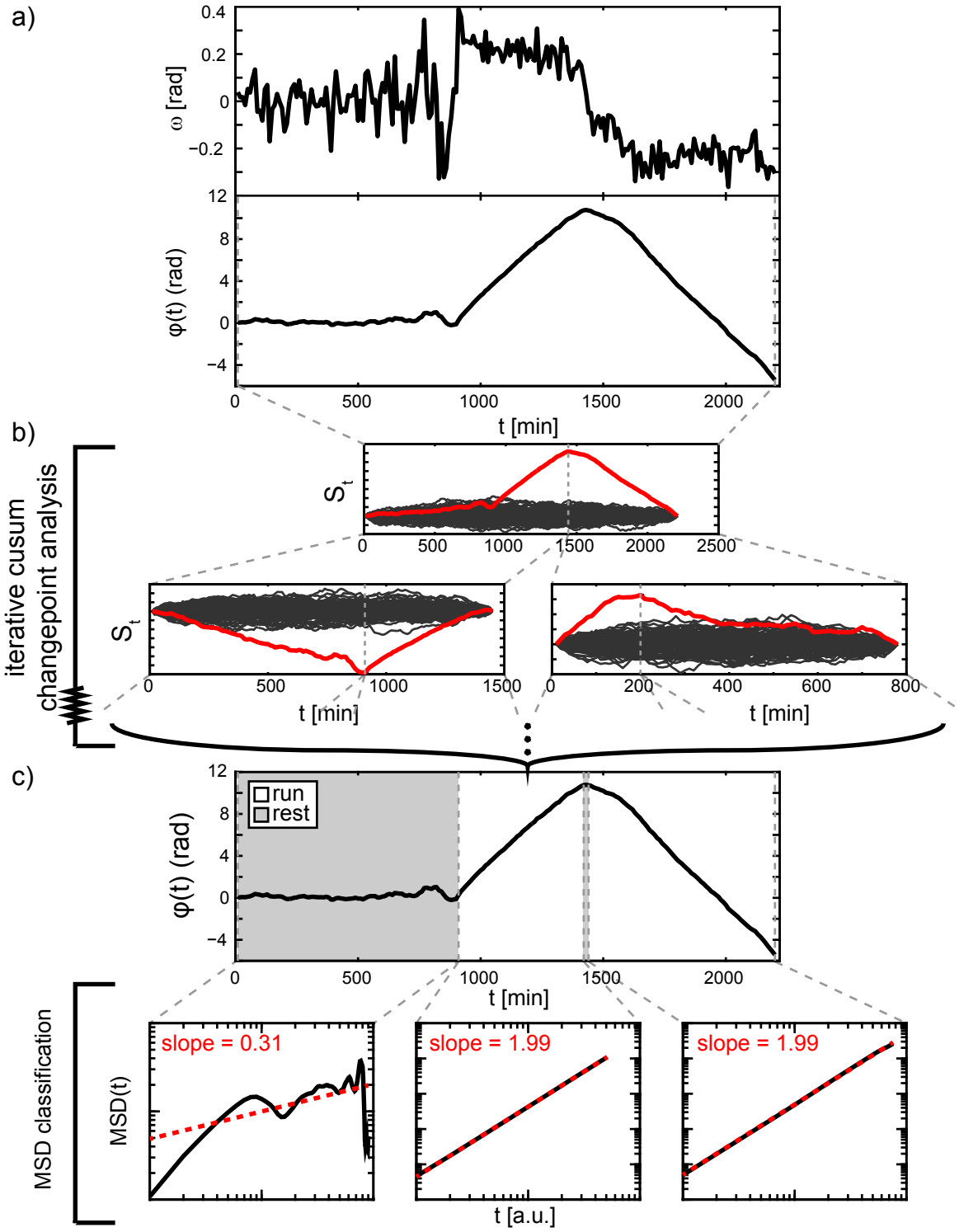

Figure B.1.: Two-state data analysis: a) Angular position φ(t) (with respect to the initial position $\varphi(0)$=0) and the angular velocity ω(t) of a MDA-MB-436 cell migrating on a ring-shaped microlane. b) Iterative change-point analysis. In order to find change-points and their position, the CUSUM S_t of ω(t) (red) is evaluated and compared to bootstrapped CUSUMs of the same time period (black). This is repeated for intervals between two change-points until no more change-points are found. c) The state of motion in each interval is classified by evaluating and fitting the corresponding MSDs. The MSDs (black) are plotted in log-log scale and fitted by $f(t) = a \cdot t^b$ (red). In the log-log representation the slope b of the fit function is used to discriminate run and rest states. Figure adapted from Publication [1] permitted by the creative commons licence.

We choose $L_{th} = 0.7$, which is a trade-off between missing some change-points and getting false positive change-points. If a change-point is detected with confidence $L_{conf} > L_{th}$, this change-point detection is repeated iteratively for the two resulting intervals adjacent to the change-point until no further change-points are found.
In the next step, the phases between the change-points are investigated and classified as run or rest states. Therefore, the time averaged MSD is calculated for each interval between two consecutive change-points via:

$$MSD(t) = \frac{1}{T-t+1} \sum_{\tau=0}^{T-t} [\varphi(\tau + t) - \varphi(\tau)]^2 \tag{B.5}$$

For run states with persistent motion, the MSD(t) should behave like a ballistic particle, thus in a log-log plot it should have a slope of two. For rest states, one would expect random motion which would correspond to slope one of the MSD(t). Consequently, we fit the function $f(t) = a \cdot t^b$ where the fitting exponent b gives the slope in log-log representation (Fig. B.1c).
To distinguish periods during which a cells shows directional persistent motion, we choose a threshold of b_{th}=1.75. All intervals where $b < b_{th}$ are show non-ballistic motion and therefore classified as rest states. All intervals with ballistic motion, where $b > b_{th}$ are classified as run states. Note that for very short intervals (< 60 min) with only a very limited set of accessible data points, the fit to the MSD is not a very robust measure. Hence, for such short intervals we set the criterion in a way, that if ω_t is increasing or decreasing strictly monotonically within the interval, the interval is considered a run state, and as rest state otherwise. Finally, all change-points that are in between two rest state states or between two run state periods with a cell moving in the same direction are removed.
This classification turned out to be very robust and parameters did not have to be changed for the different cell lines analysed in this thesis. This is due to the strength of the bootstrapping algorithm, which compares the real data set to permuted sets. Therefore, it does not depend on absolute velocity values and is applicable for cells with greatly different velocities.
In this classification scheme, it is possible that in a run state the nucleus moves backwards for a few time steps. This could be caused by internal reorientation events or by the formation of a transient lamellipodium at the back that pulls on the nucleus. But it is likely that some of those events also include a retraction event of the front like we see in the kymograph analysis in Section 5.3. In the kymograph analysis, I have information about front and back motion and run states can be defined as periods without retraction at the front. This classification might be more accurate but it needs much more effort and measurements with a very high time resolution. The classification via the cell nucleus position and CUMSUM analysis is a good estimate and in contrast to the kymograph analysis compatible with high throughput measurements.

B.3. Pattern detection and automated cell tracking

For the experiments described in Chapter 5, cells are migrating on micro lanes with segments of alternating fibronectin concentration. In order to analyse the motion of cells in dependence of the substrate coating and to study the behaviour at the interface, it is important to know the position and composition of the microlanes. A manual evaluation of the position of the lines would be time consuming and therefore an automated line detection algorithm was implemented using *Matlab* (MathWorks).
On the ring-shaped microlanes we aimed for one single cell per ring to avoid cell-cell interactions. When analysing the single-cell trajectories, cell tracking is trivial as there is always only one cell in the region of interest. On stripes the situation is more complicated. Cells are colliding and they can leave or enter the field of view. Therefore, we need to distinguish between cells and assign cell positions tot the correct cell at the next time point. Consequently, a semi-automated method like the one used for the experiments in Chapter 3 and 4 would be a great effort that would not allow to do high throughput measurements. Hence, an automated tracking algorithm was applied.

B.3.1. Line detection

In order to detect the position of the lines in the fluorescence image of the microlanes (Fig. B.2a), the images are first smoothed with a Gaussian filter with a width of 1.5 pixels. Thereby fluctuations in the image are minimized. Subsequently, edges in the image are detected using the sobel edge detection algorithm. It successfully detects the edges of the lines, although sometimes for large differences in fibronectin concentration only edges of the bright segments are detected (Fig. B.2b). The resulting image is transformed to Hough space. The Hough transformation [217] is a method widely used in image analysis and computer vision to detect patterns in an image [218]. To go to the Hough space, gray values along all possible lines with a certain angle φ and the distance to the origin ρ are summed up (Fig. B.2c). When one hits a bright line in the image, this leads to a maximum in Hough space at the specific combination of φ and ρ. For the variation of φ a step size of 0.2° is used, which produces good matches with the patten. Due to the regular order of the line patterns, we obtain, for the correct φ value, maxima that posses the same distance as the microlanes (Fig. B.2d).
The exact dimensions of the patterns were measured once, thus we can use this information to find the maxima in the Hough space that correspond to the patterns. Therefore we create step functions with the dimensions of the patterns. We can now calculate the cross correlation functions of the step function with the values in Hough space for each φ value (vertical lines in Fig. B.2d). The correlation reaches a maximum for the correct φ and ρ value. Consequently, the grid position that corresponds to these values marks the position of the microlanes (Fig. B.2e). Edges between the two line segments are not always detected. Thus, to make it more robust the Hough transformation of the original image was used for the detection of the vertical lines. However, for similar concentrations of the segments the algorithm sometimes fails to find the interfaces between segments. Therefore, all detected lines are inspected by eye. In the case of errors, line positions are corrected manually.

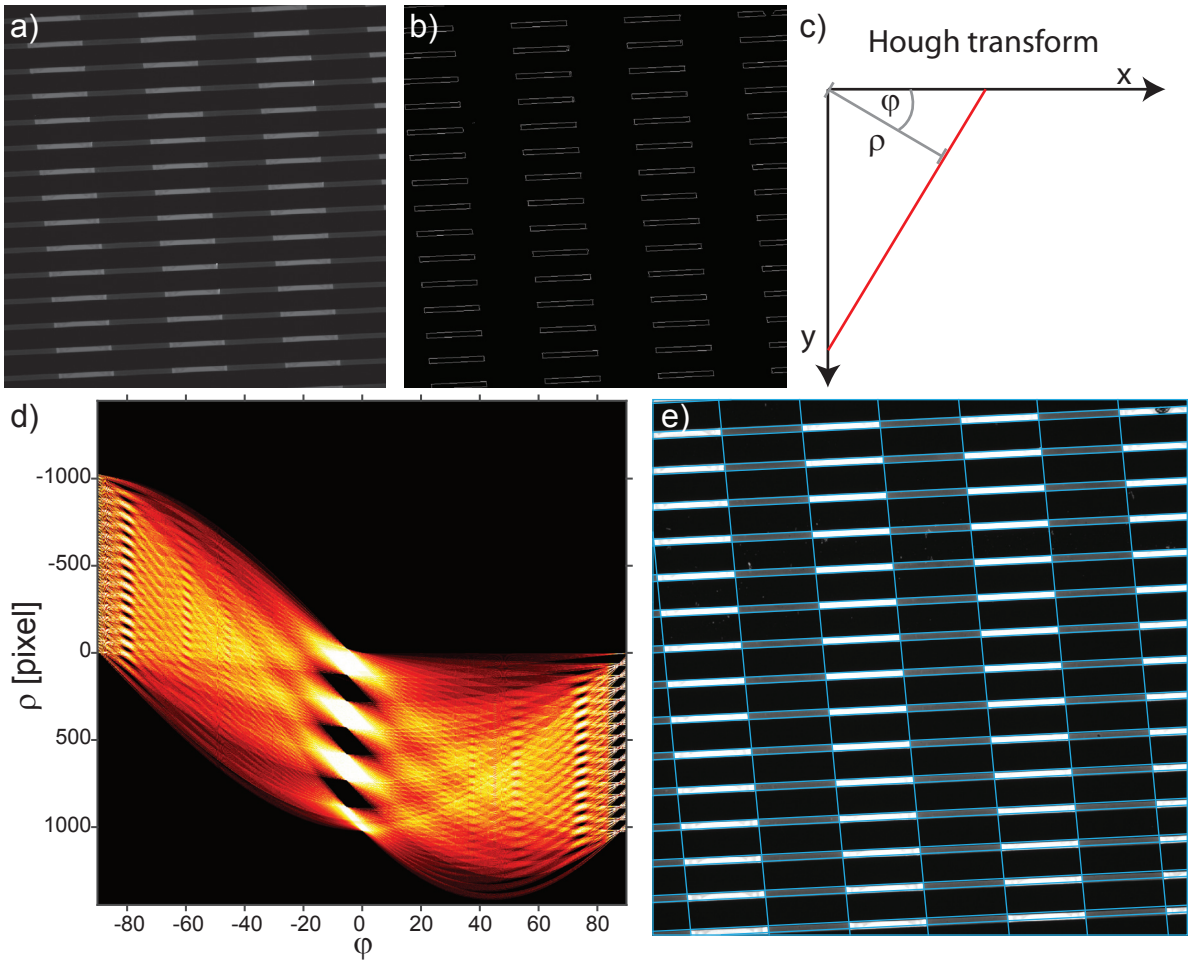

Figure B.2.: a) Fluorescence image of microlanes coated with fibronectin labelled with Alexa 647. Lanes have a width of 15 μm and segments have a length of about 200 μm b) To detect the borders of the lines the sobel method for edge detection is used. c) Visualisation of the Hough transform. For each value of φ and ρ the grey values of the original image that lie on the corresponding red line are summed up. If there are bright lines in the image this leads to maxima in the φ - ρ space. d) Hough transform for the image in (b). The maxima at $\varphi = 87.2°$ have the same distance as the microlanes and therefore correspond to the horizontal lines. The maxima for the vertical lines are less pronounced and lie at $\varphi = -5.4°$ e) The detected lines (blue) match with the micropatterns.

B.3.2. Evaluation of pattern homogeneity

Since we want to study the effect of fibronectin concentrations on cell motility, it is important to have fairly homogeneously coated micropattens. When producing the microlanes, it is always possible to maintain some defects in the patterns. Thus, we have to identify imperfect areas and exclude those segments from the analysis.
Due to the fact that the fluorescence intensity correlates with the fibronectin concentration, we can determine the standard deviation of c_{FN} within one of the line segments that are detected automatically. For each segment we can calculate the median fibronectin concentration (Which is more robust than the mean). We find that standard deviation and median are strongly correlated as often found in stochastic processes. Thus, we use the coefficient of variation which is the standard deviation divided by the median (or

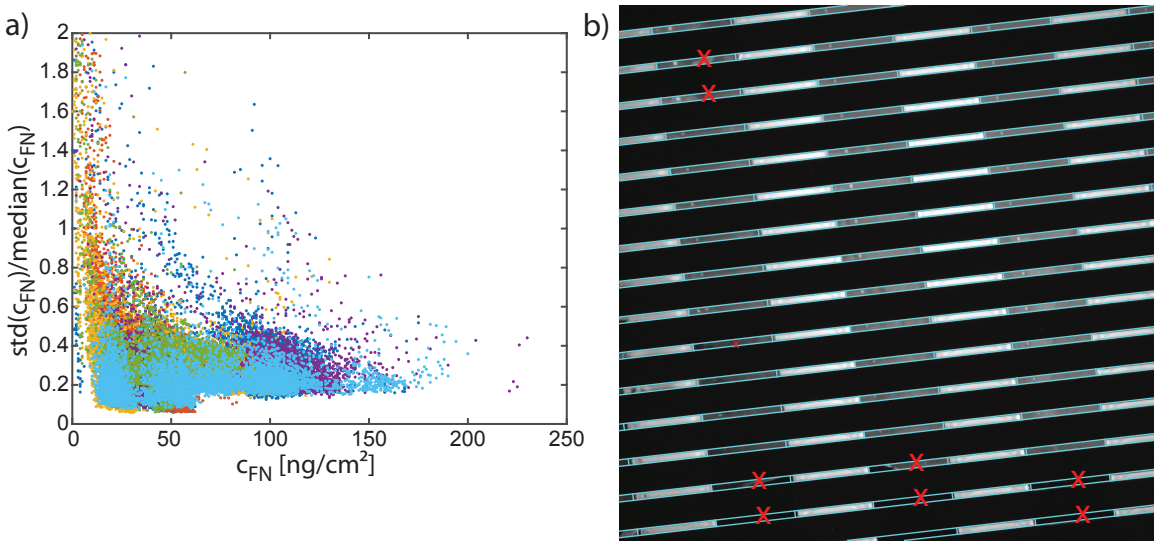

Figure B.3.: a) Variations of fibronectin concentrations inside the individual segments of the microlanes. Standard deviation divided by the median of the fibronectin concentration measured by the fluorescence intensity plotted via median fibronectin concentration. Each dot represents one single segment. Different colours code for different experiments. Each experiments can include several inking concentrations which leads to different clusters. To exclude inhomogeneous pattens a threshold of 0.3 was chosen. b) Fluorescent image of microlanes (borders detected in blue). Segments that are excluded due to inhomogeneities are marked with a red cross.

mean) as a measure for the extend of the inhomogeneity (Fig. B.3a). The coefficient of variation is mostly between 0.1 and 0.5 and increases almost only for very small surface concentrations for which we divide through very small median values. In Figure B.3a clusters are visible that correspond to certain inking concentrations. It is striking that for median concentrations up to 70 ng/cm^2 a higher maximum homogeneity is achieved. This concentration regime corresponds to the segments coated by the first inking step where the protein is transferred from the first to the second stamp. Higher surface concentrations were created by the second inking step that takes place in between the two stamps. This separation of the concentration regimes was conducted because firstly lower inking concentrations in the second step produced only very inhomogeneous patterns. Secondly, for creating high surface concentrations in the first inking step a lot of fibronectin would have to be used as large volumes of solution are needed here. Due to these limitations, it is difficult to obtain a totally equal distribution of the homogeneity for all concentrations.
We defined a threshold of the coefficient of variation to exclude inhomogeneous segments of 0.3. This is a trade-off between homogeneity and the amount of data that is excluded. In the end, we have to accept that the patterning method is not perfect in this and if we set the threshold too low there is no data left to analyse. With a threshold of 0.3 we exclude drastic inhomogeneities, but we keep segments with smaller variations (Fig. B.3b).

Interestingly, we often find some brighter spots at similar positions in adjacent segments. One explanation could be that these spots are drying artefacts where unbound fibronectin or maybe also free dye is concentrated in drying droplets. But, to learn more

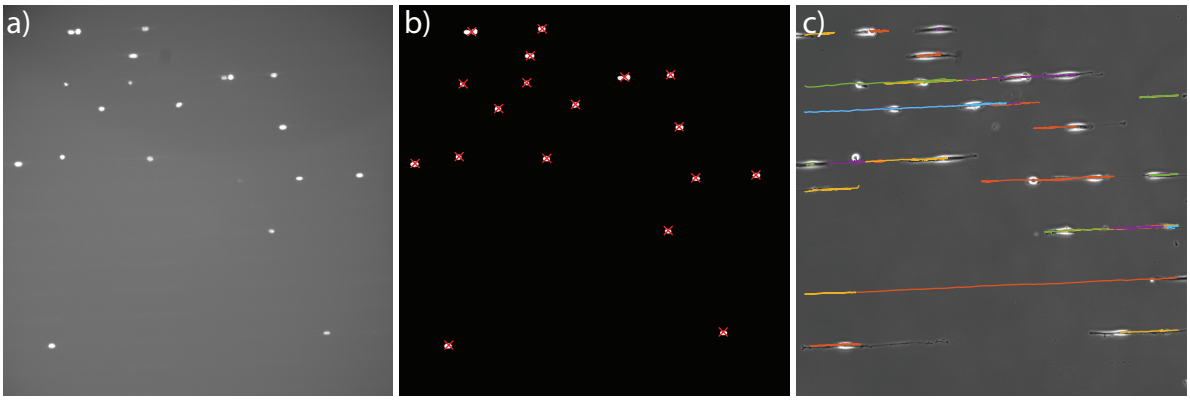

Figure B.4.: a) Fluorescence image of cell nuclei stained with Hoechst. b) To determine the positions of the nuclei (red crosses) a segmentation of the nuclei is performend. c) Phase contrast image of the cells migrating on microlanes. The cell tracking results in single-cell trajectories that are shown in multiple colours.

about the nature of the artefacts, more studies would have to be performed. At least, cells do not show clear reactions on these artefacts, thus in a large data set possible small effects should not have a large influence. However, these inhomogeneity can definitively be one possible source of the high noise level observed in the cell motility parameters.

B.3.3. Cell tracking

For determining the positions of the cells, we start with the images of the labelled nuclei (B.4a). To correct for uneven illumination of the image, a background image is created using morphological opening in *Matlab* (size of the disk 10 pixel). Subsequently, the background is subtracted from the original image. A bandpass filter is used to filter out noise and then a threshold is applied to create a binary image of the nuclei. The geometric center of each nuclei is calculated (Fig. B.4b), which gives the positions of the cells.

Now, we use the information of the location of the patterns to track cells individually on each stripe. (An overview of the image analysis is shown in a flow chart in Figure B.5.) To track the cells over time, we use an adaption of the IDL particle tracking algorithm [219, 220] (The same algorithm was also used to track cells on 2D homogeneous surfaces). The resulting cell tracks include collision events where cells could possibly get interchanged. Since we want to investigate exclusively single-cell migration, time points where cells have a distance to the next neighbour cell of below 66 μm are excluded. This solves also the problem of cell interchanges. The resulting cell tracks are often very short. To get meaningful parameters of the cell trajectories very long trajectories would be preferred. Single cells that run on one line straight through the image sometimes need only slightly more than 5 h. Because we do not want to exclude those tracks, we decided to take all tracks with a minimum duration of 5 h. Note that it is possible that one cell contributes to several tracks. For example when it collides with another

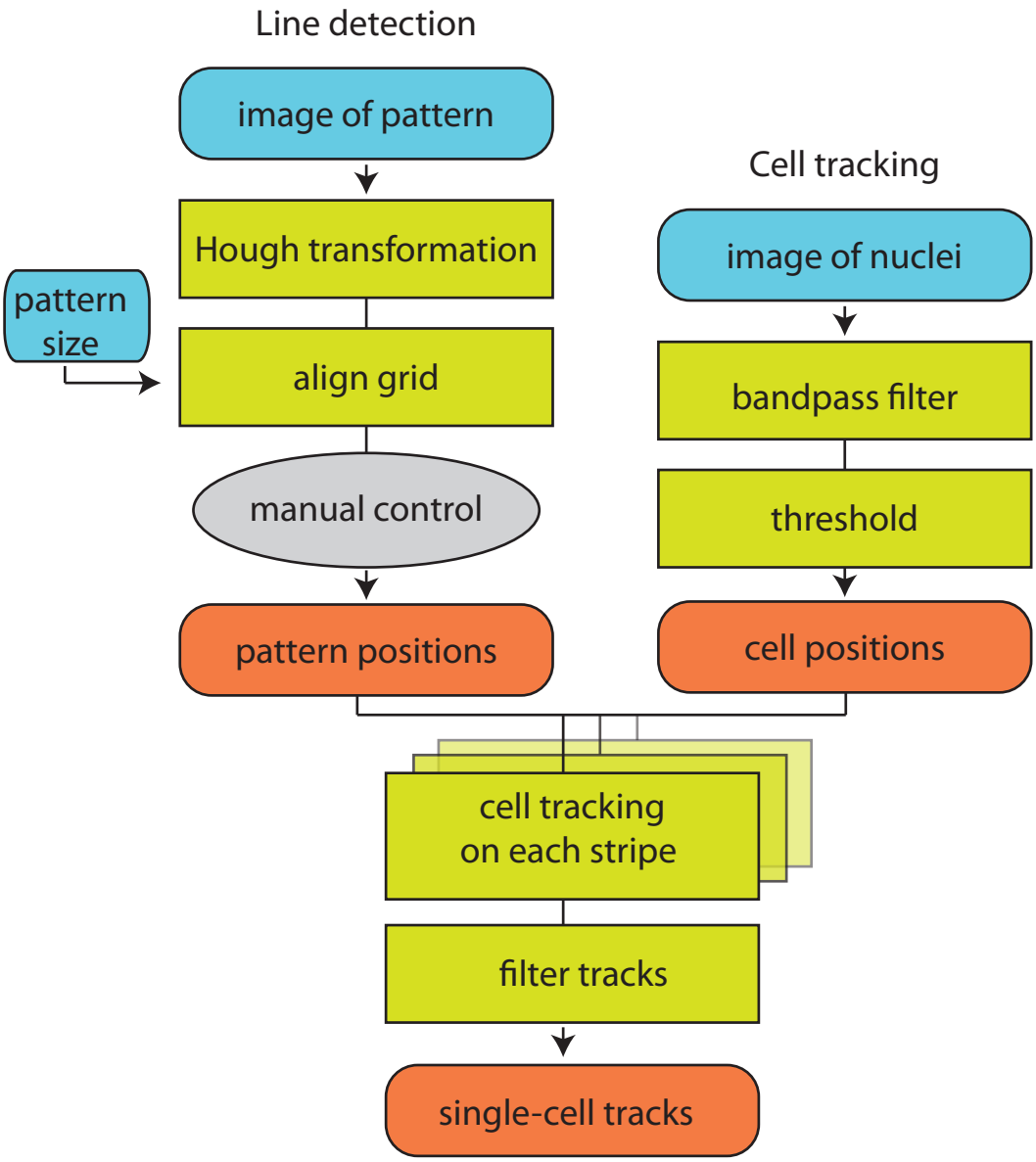

Figure B.5.: Flow chart describing image analysis. For the detection of the lines, the images and the dimensions of the patterns are used as input and we obtain the pattern position as output. Here, a manual examination is performed to correct possible mistakes of the algorithm. To find the positions of the cells the images of the nuclei are used as input. Nuclei are segmented andthe information of the cell position is combined with the information of the patterns to do cell tracking for cells on each stripe separately. The resulting tracks are filtered to get trajectories of single cells in the end.

cell in the middle of the experiments, we can get a first track before the collision and a second one when the two cells have separated again. These filtered tracks are shown for one exemplary position in Figure B.4c.
This way of cell tracking worked quite well. As a further step to filter out more unwanted tracks, one could also include a data clearing step where the cell tracks are examined manually. For cells with a length that is above average, it is possible that the minimal distance we implemented, is not enough to exclude all events where cells interact with each other. Also dying cells or the interaction with dirt particles could be eliminated by this. Of course such a step would be quite time consuming. A rough examination of the data led to the impression, that most of the automatically generated tracks are fine and we omitted such a data clearing step.

B.4. Kymographs

The transition behaviour at the interfaces was studied with a time resolution of 20 s and kymographs of the phase-contrast images were used for a detailed study of cell motion. Due to the high time resolution, a lower number of positions can be scanned in one measurement which leads to a lower number of cells observed. Also, the size of a single 48 h movie increases to 33 GB which makes image data handling more complicated and leads to longer image processing times. In this case, a semi-automated analysis was used as it promised to be less time consuming.
Therefore, middle lines of microlanes with migrating single cells were selected by hand (Fig. B.6a). The corresponding fluorescence intensity of the fibronectin patterns along the line is evaluated and correlated with a step function with the dimensions of the line segments to determine the position and the fibronectin concentration of the microlane (Fig. B.6b). The same line is selected for the phase-contrast images of the cells (Fig. B.6c) and lines for each time point of the movies are put together using *ImageJ* (Fig. B.6d) to get the kymograph.

In these kymographs one can find a rich variety in the behaviour of the cells. For example, cells can be running or resting, and one can see cell reversals or cell division events. Phases during which cells are running in one direction, which means that no retraction event takes place at the front, and they do not interact with other cells and perform at least one transition to another line segment, are selected manually. For those parts of the kymographs a variance filter was applied that calculates the variance in the grey values in a radius of 4 pixels. The resulting variance image (Fig. B.7a) was smoothed with a Gaussian filter with radius 3 pixels. Usually, the variance of the brightness of the image is much higher in regions of the kymograph that are occupied by the cells. Thus, this can be used to detect the cell outlines. Therefore, a threshold is applied to get a binary image of the cells. As we have to apply the variance filter over a region with finite size, the result is usually a bit larger than the actual cell. Therefore, the regions are eroded by two pixels and subsequently the outlines of the detected area represent the front and back position of the cell (Fig. B.7b).

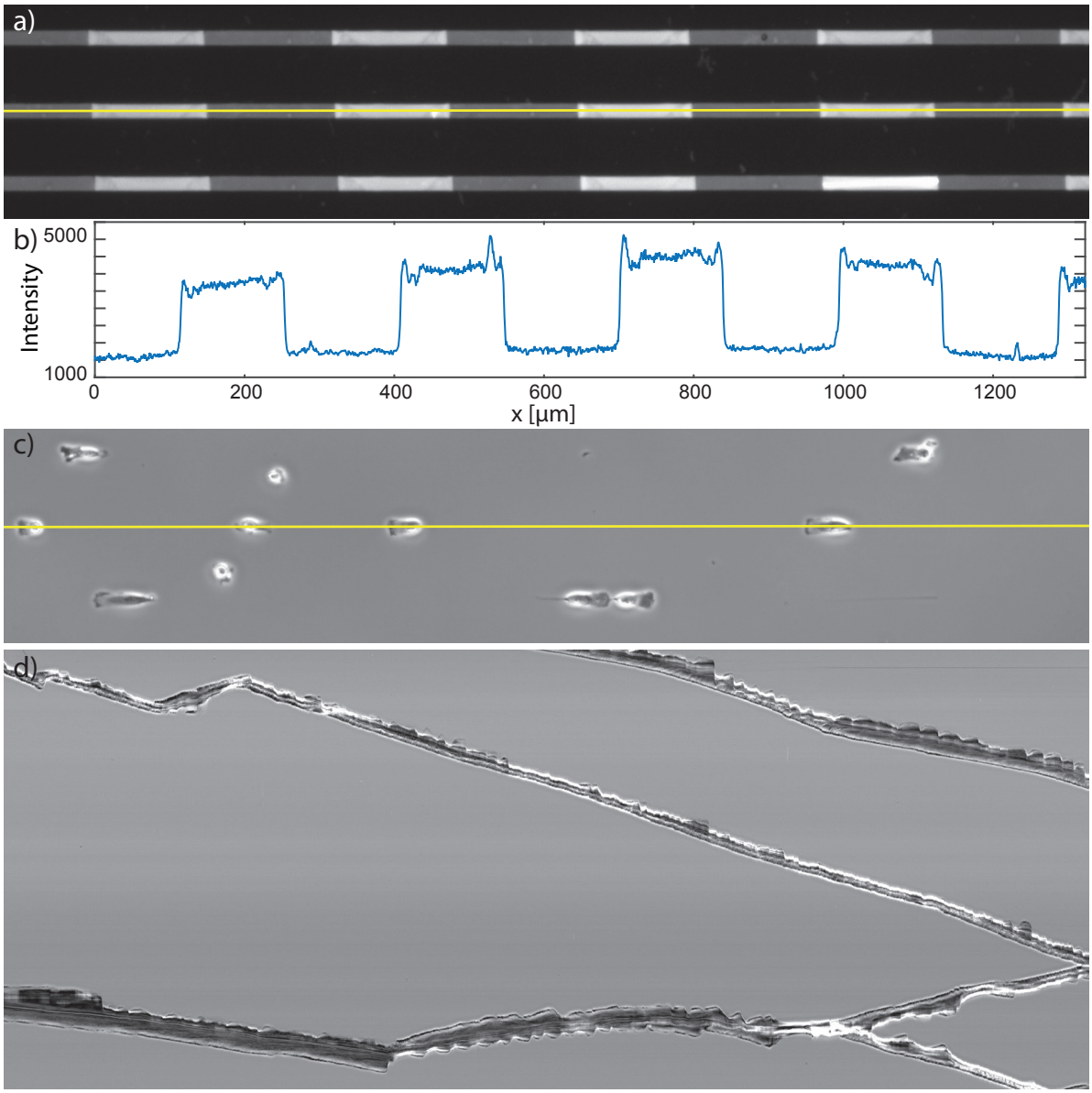

Figure B.6.: a) Fluorescent image of microlanes. The middle of a line is selected manually (yellow) to create a kymograph. b) Florescence intensity along the selected line. c) Phase contrast image of cells with the selected line (yellow). d) Part of the resulting kymograph. Time axis goes from left to right.

This works quite well, but sometimes when cell protrusions have very low contrast, which is mostly the case at the back, some parts of the cells are missed. In some cases, this can leads to some holes in the cells (like in Fig. B.7b at the very right) that have to be filled afterwards. At the front, the cells usually have some dark ruffles that give a very good contrast. But normally, there is also a region of a few μm in front of the ruffles that has lower contrast. This region can possibly be missed by the algorithm. However, due to the fact that the variance filter is calculated with a radius of about $3\,\mu$m, the accuracy of this method is limited to this scale anyway.
Another possible source of errors in detecting the cell front and the back lies in the nature of the kymograph analysis. Of course, the width of the cells is larger than one

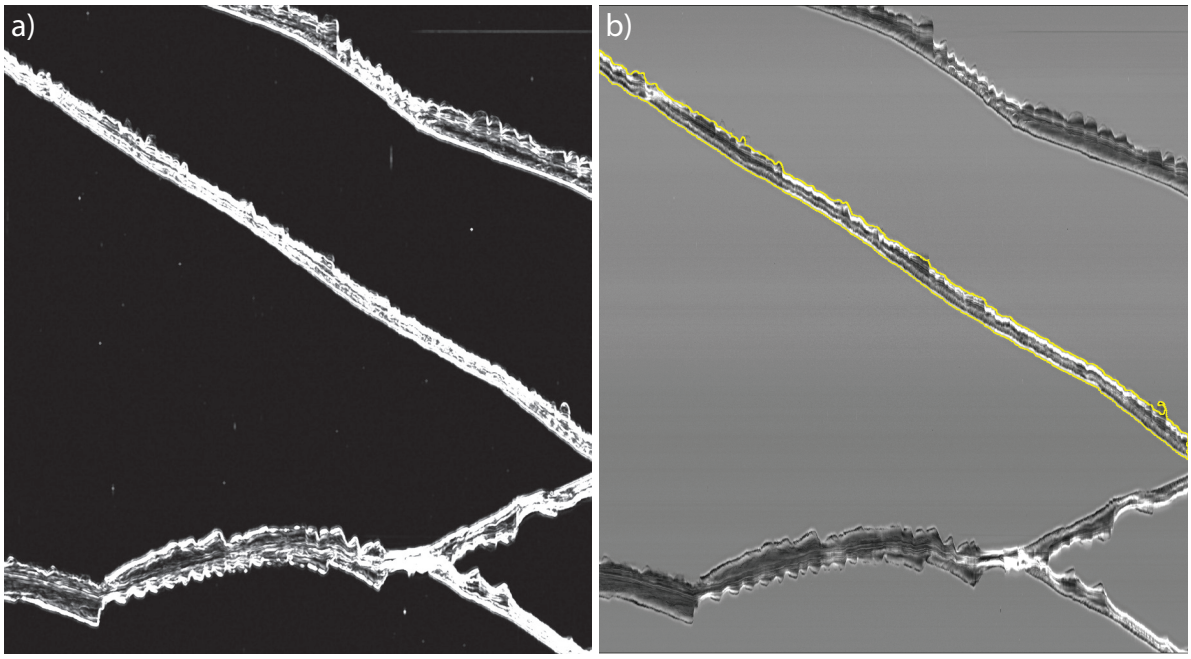

Figure B.7.: a) From the kymograph in Figure B.6 a time interval in which one cell is running is selected (here the cell starting at the upper left corner) and a variance filter is applied. b) The segmentation results in the outlines of the cell (yellow line).

pixel, thus it is possible to miss some cell protrusions when only analysing the middle of the microlanes. For example, cell protrusions could form more at the side, which could lead to measuring a shorter length than the actual one of the cell. To diminish those effects, we decreased the width of the microlanes from 20 to 15 μm compared to the ring-shaped microlanes. For this width the position of the cell front usually varies only slightly over the width of the microlane. At the back of the cell there are sometimes very thin extensions that can be in rare, extreme cases more than 100 μm long. These extensions can be easily missed by the middle line. Thus, we expect larger error ranges for the determination of the rear position. However, it is not clear whether those long extensions are still properly connected to the cell body. Consequently, they might have only small influences on the migration behaviour. To avoid those problems cells with extreme extensions were excluded from the analysis.

All in all, this is a quite simple method to analyse phase-contrast images. The contour analysis in the kymographs turned out to work quite well which is usually not that easy for the normal images of the cells. Recent advantages in the field of machine learning give rise to new possibilities for segmentation of low contrast images that could improve the results here [221]. However, for the analysis of the mean front velocity for example this accuracy should be definitely sufficient.

List of abbreviations

1D	one-dimensional
2D	two-dimensional
3D	three-dimensional
CUSUM	cumulative sum
DMSO	dimethyl sulfoxide
DNA	deoxyribonucleic acid
ECM	extra-cellular matrix
EMT	epithelial-mesenchymal transition
MET	mesenchymal-epithelial transition
miR-200c	micro RNA 200c
miRNA	micro RNA
mRNA	messenger RNA
MSD	mean squared displacement
PBS	phosphate-buffered saline
PDMS	polydimethylsiloxane
PEG	polyethylene glycol
PLL	polylysine
PRW	persistent random walk
RFP	red fluorescent protein
RNA	ribonucleic acid

Bibliography

[1] Schreiber, Christoph ; Segerer, Felix J. ; Wagner, Ernst ; Roidl, Andreas ; Rädler, Joachim O.: Ring-Shaped Microlanes and Chemical Barriers as a Platform for Probing Single-Cell Migration. In: *Scientific Reports* 6 (2016), 26858. http://dx.doi.org/10.1038/srep26858. – DOI 10.1038/srep26858

[2] Brückner, David B. ; Fink, Alexandra ; Schreiber, Christoph ; Röttgermann, Peter J. F. ; Rädler, Joachim O. ; Broedersz, Chase P.: Stochastic nonlinear dynamics of confined cell migration in two-state systems. In: *Nature Physics* 15 (2019), Nr. 6, 595-601. http://dx.doi.org/10.1038/s41567-019-0445-4. – DOI 10.1038/s41567–019–0445–4

[3] Schuster, Simon L. ; Segerer, Felix J. ; Gegenfurtner, Florian A. ; Kick, Kerstin ; Schreiber, Christoph ; Albert, Max ; Vollmar, Angelika M. ; Rädler, Joachim O. ; Zahler, Stefan: Contractility as a global regulator of cellular morphology, velocity, and directionality in low-adhesive fibrillary microenvironments. In: *Biomaterials* 102 (2016), 137-147. http://dx.doi.org/10.1016/j.biomaterials.2016.06.021. – DOI 10.1016/j.biomaterials.2016.06.021

[4] Ljepoja, Bojan ; Schreiber, Christoph ; Gegenfurtner, Florian A. ; García-Roman, Jonathan ; Köhler, Bianca ; Zahler, Stefan ; Rädler, Joachim O. ; Wagner, Ernst ; Roidl, Andreas: Inducible microRNA-200c decreases motility of breast cancer cells and reduces filamin A. In: *PLOS ONE* 14 (2019), Nr. 11, e0224314. http://dx.doi.org/10.1371/journal.pone.0224314. – DOI 10.1371/journal.pone.0224314

[5] Fink, Alexandra ; Brückner, David B. ; Schreiber, Christoph ; Röttgermann, Peter J. F. ; Broedersz, Chase P. ; Rädler, Joachim O.: Area and Geometry Dependence of Cell Migration in Asymmetric Two-State Micropatterns. In: *Biophysical Journal* (2019). http://dx.doi.org/https://doi.org/10.1016/j.bpj.2019.11.3389. – DOI https://doi.org/10.1016/j.bpj.2019.11.3389. – ISSN 0006–3495

[6] Zhou, Fang ; Schaffer, Sophia A. ; Schreiber, Christoph ; Segerer, Felix J. ; Goychuk, Andriy ; Frey, Erwin ; Rädler, Joachim O.: Quasi-periodic migration of single cells on short microlanes. In: *bioRxiv* (2019), 809939. http://dx.doi.org/10.1101/809939. – DOI 10.1101/809939

[7] Friedl, Peter ; Wolf, Katarina: Tumour-cell invasion and migration: diversity and escape mechanisms. In: *Nat Rev Cancer* 3 (2003), Nr. 5, 362-374. http://dx.doi.org/10.1038/nrc1075

[8] Friedl, Peter ; Gilmour, Darren: Collective cell migration in morphogenesis,

regeneration and cancer. In: *Nat Rev Mol Cell Biol* 10 (2009), Nr. 7, 445-457. http://dx.doi.org/10.1038/nrm2720

[9] Singer, Adam J. ; Clark, Richard A.: Cutaneous Wound Healing. In: *New England Journal of Medicine* 341 (1999), Nr. 10, 738-746. http://dx.doi.org/10.1056/nejm199909023411006. – DOI 10.1056/nejm199909023411006

[10] Luster, A. D. ; Alon, R. ; Andrian, U. H.: Immune cell migration in inflammation: present and future therapeutic targets. In: *Nat Immunol* 6 (2005), Nr. 12, 1182-90. http://dx.doi.org/10.1038/ni1275. – DOI 10.1038/ni1275

[11] Hanahan, Douglas ; Weinberg, Robert A.: The hallmarks of cancer. In: *cell* 100 (2000), Nr. 1, S. 57–70

[12] Mellado, Mario ; Martínez-Muñoz, Laura ; Cascio, Graciela ; Lucas, Pilar ; Pablos, José L. ; Rodríguez-Frade, José M.: T Cell Migration in Rheumatoid Arthritis. In: *Frontiers in Immunology* 6 (2015), Nr. 384. http://dx.doi.org/10.3389/fimmu.2015.00384. – DOI 10.3389/fimmu.2015.00384

[13] Lauffenburger, Douglas A. ; Horwitz, Alan F.: Cell migration: a physically integrated molecular process. In: *Cell* 84 (1996), Nr. 3, S. 359–369

[14] Ridley, Anne J. ; Schwartz, Martin A. ; Burridge, Keith ; Firtel, Richard A. ; Ginsberg, Mark H. ; Borisy, Gary ; Parsons, J. T. ; Horwitz, Alan R.: Cell Migration: Integrating Signals from Front to Back. In: *Science* 302 (2003), Nr. 5651, 1704-1709. http://dx.doi.org/10.1126/science.1092053. – DOI 10.1126/science.1092053

[15] Gail, Mitchell H. ; Boone, Charles W.: The Locomotion of Mouse Fibroblasts in Tissue Culture. In: *Biophysical Journal* 10 (1970), Nr. 10, 980-993. http://dx.doi.org/10.1016/S0006-3495(70)86347-0. – DOI 10.1016/S0006–3495(70)86347–0

[16] Li, Liang ; NÃ¸rrelykke, Simon F. ; Cox, Edward C.: Persistent Cell Motion in the Absence of External Signals: A Search Strategy for Eukaryotic Cells. In: *PLoS ONE* 3 (2008), Nr. 5, e2093. http://dx.doi.org/10.1371/journal.pone.0002093. – DOI 10.1371/journal.pone.0002093

[17] Xia, Younan ; Whitesides, George M.: SOFT LITHOGRAPHY. In: *Annual Review of Materials Science* 28 (1998), Nr. 1, 153-184. http://dx.doi.org/10.1146/annurev.matsci.28.1.153. – DOI 10.1146/annurev.matsci.28.1.153

[18] Lautenschläger, Franziska ; Piel, Matthieu: Microfabricated devices for cell biology: all for one and one for all. In: *Current Opinion in Cell Biology* 25 (2013), Nr. 1, 116-124. http://dx.doi.org/10.1016/j.ceb.2012.10.017. – DOI 10.1016/j.ceb.2012.10.017

[19] Piel, Matthieu ; Théry, Manuel: *Micropatterning in Cell Biology Part A: Methods in Cell Biology*. Bd. 119. Elsevier, 2014. – ISBN 0124167462

[20] Maiuri, Paolo ; Terriac, Emmanuel ; Paul-Gilloteaux, Perrine ; Vignaud, Timothée ; McNally, Krista ; Onuffer, James ; Thorn, Kurt ; Nguyen,

Phuong A. ; Georgoulia, Nefeli ; Soong, Daniel ; Jayo, Asier ; Beil, Nina ; Beneke, Jürgen ; Hong Lim, Joleen C. ; Pei-Ying Sim, Chloe ; Chu, Yeh-Shiu ; Jiménez-Dalmaroni, Andrea ; Joanny, Jean-François ; Thiery, Jean-Paul ; Erfle, Holger ; Parsons, Maddy ; Mitchison, Timothy J. ; Lim, Wendell A. ; Lennon-Duménil, Ana-Maria ; Piel, Matthieu ; Théry, Manuel: The first World Cell Race. In: *Current Biology* 22 (2012), Nr. 17, R673-R675. http://dx.doi.org/10.1016/j.cub.2012.07.052. – DOI 10.1016/j.cub.2012.07.052

[21] DiMilla, P. A. ; Barbee, K. ; Lauffenburger, D. A.: Mathematical model for the effects of adhesion and mechanics on cell migration speed. In: *Biophysical Journal* 60 (1991), Nr. 1, 15-37. http://dx.doi.org/10.1016/S0006-3495(91)82027-6. – DOI 10.1016/S0006–3495(91)82027–6

[22] DiMilla, PA ; Stone, JA ; Quinn, JA ; Albelda, SM ; Lauffenburger, DA: Maximal migration of human smooth muscle cells on fibronectin and type IV collagen occurs at an intermediate attachment strength. In: *The Journal of Cell Biology* 122 (1993), Nr. 3, 729-737. http://dx.doi.org/10.1083/jcb.122.3.729. – DOI 10.1083/jcb.122.3.729

[23] Maheshwari, G. ; Brown, G. ; Lauffenburger, D.A. ; Wells, A. ; Griffith, L.G.: Cell adhesion and motility depend on nanoscale RGD clustering. In: *Journal of Cell Science* 113 (2000), Nr. 10, 1677-1686. http://jcs.biologists.org/content/113/10/1677.abstract

[24] Palecek, Sean P. ; Loftus, Joseph C. ; Ginsberg, Mark H. ; Lauffenburger, Douglas A. ; Horwitz, Alan F.: Integrin-ligand binding properties govern cell migration speed through cell-substratum adhesiveness. In: *Nature* 385 (1997), 537. http://dx.doi.org/10.1038/385537a0. – DOI 10.1038/385537a0

[25] Smith, Jason T. ; Elkin, James T. ; Reichert, W. M.: Directed cell migration on fibronectin gradients: Effect of gradient slope. In: *Experimental Cell Research* 312 (2006), Nr. 13, 2424-2432. http://dx.doi.org/10.1016/j.yexcr.2006.04.005. – DOI 10.1016/j.yexcr.2006.04.005

[26] Zorn, Matthias L. ; Marel, Anna-Kristina ; Segerer, Felix J. ; Rädler, Joachim O.: Phenomenological approaches to collective behavior in epithelial cell migration. In: *Biochimica et Biophysica Acta (BBA) - Molecular Cell Research* (2015), Nr. 0. http://dx.doi.org/10.1016/j.bbamcr.2015.05.021. – DOI 10.1016/j.bbamcr.2015.05.021

[27] Friedl, Peter ; Wolf, Katarina: Plasticity of cell migration: a multiscale tuning model. In: *The Journal of Cell Biology* (2009). http://dx.doi.org/10.1083/jcb.200909003. – DOI 10.1083/jcb.200909003

[28] Liu, Yan-Jun ; Le Berre, Maël ; Lautenschlaeger, Franziska ; Maiuri, Paolo ; Callan-Jones, Andrew ; Heuzé, Mélina ; Takaki, Tohru ; Voituriez, Raphaël ; Piel, Matthieu: Confinement and Low Adhesion Induce Fast Amoeboid Migration of Slow Mesenchymal Cells. In: *Cell* 160 (2015), Nr. 4, 659-672. http://dx.doi.org/10.1016/j.cell.2015.01.007. – DOI 10.1016/j.cell.2015.01.007

[29] Krause, Matthias ; Gautreau, Alexis: Steering cell migration: lamellipodium

dynamics and the regulation of directional persistence. In: *Nature Reviews Molecular Cell Biology* 15 (2014), 577. http://dx.doi.org/10.1038/nrm3861. – DOI 10.1038/nrm3861

[30] Petrie, Ryan J. ; Doyle, Andrew D. ; Yamada, Kenneth M.: Random versus directionally persistent cell migration. In: *Nat Rev Mol Cell Biol* 10 (2009), Nr. 8, 538-549. http://dx.doi.org/10.1038/nrm2729

[31] Svitkina, Tatyana M. ; Verkhovsky, Alexander B. ; McQuade, Kyle M. ; Borisy, Gary G.: Analysis of the Actin-Myosin II System in Fish Epidermal Keratocytes: Mechanism of Cell Body Translocation. In: *The Journal of Cell Biology* 139 (1997), Nr. 2, 397-415. http://dx.doi.org/10.1083/jcb.139.2.397. – DOI 10.1083/jcb.139.2.397

[32] Geiger, Benjamin ; Spatz, Joachim P. ; Bershadsky, Alexander D.: Environmental sensing through focal adhesions. In: *Nat Rev Mol Cell Biol* 10 (2009), Nr. 1, 21-33. http://dx.doi.org/10.1038/nrm2593

[33] Huttenlocher, Anna ; Sandborg, Rebecca R. ; Horwitz, Alan F.: Adhesion in cell migration. In: *Current Opinion in Cell Biology* 7 (1995), Nr. 5, 697-706. http://dx.doi.org/10.1016/0955-0674(95)80112-X. – DOI 10.1016/0955–0674(95)80112–X

[34] Giannone, Grégory ; Dubin-Thaler, Benjamin J. ; Rossier, Olivier ; Cai, Yunfei ; Chaga, Oleg ; Jiang, Guoying ; Beaver, William ; Döbereiner, Hans-Günther ; Freund, Yoav ; Borisy, Gary ; Sheetz, Michael P.: Lamellipodial Actin Mechanically Links Myosin Activity with Adhesion-Site Formation. In: *Cell* 128 (2007), Nr. 3, 561-575. http://dx.doi.org/10.1016/j.cell.2006.12.039. – DOI 10.1016/j.cell.2006.12.039

[35] Ridley, Anne J.: Life at the Leading Edge. In: *Cell* 145 (2011), Nr. 7, 1012-1022. http://dx.doi.org/10.1016/j.cell.2011.06.010. – DOI 10.1016/j.cell.2011.06.010

[36] Sadok, Amine ; Marshall, Chris J.: Rho GTPases. In: *Small GTPases* 5 (2014), Nr. 4, e983878. http://dx.doi.org/10.4161/sgtp.29710. – DOI 10.4161/sgtp.29710

[37] Garcia-Mata, Rafael ; Boulter, Etienne ; Burridge, Keith: The 'invisible hand': regulation of RHO GTPases by RHOGDIs. In: *Nat Rev Mol Cell Biol* 12 (2011), Nr. 8, 493-504. http://dx.doi.org/10.1038/nrm3153

[38] Lawson, Campbell D. ; Burridge, Keith: The on-off relationship of Rho and Rac during integrin-mediated adhesion and cell migration. In: *Small GTPases* 5 (2014), Nr. 1, e27958. http://dx.doi.org/10.4161/sgtp.27958. – DOI 10.4161/sgtp.27958

[39] Machacek, Matthias ; Hodgson, Louis ; Welch, Christopher ; Elliott, Hunter ; Pertz, Olivier ; Nalbant, Perihan ; Abell, Amy ; Johnson, Gary L. ; Hahn, Klaus M. ; Danuser, Gaudenz: Coordination of Rho GTPase activities during cell protrusion. In: *Nature* 461 (2009), Nr. 7260, 99-103. http://dx.doi.org/10.1038/nature08242. – DOI 10.1038/nature08242

[40] Peskin, Charles S. ; Odell, Garrett M. ; Oster, George F.: Cellular motions and thermal fluctuations: the Brownian ratchet. In: *Biophysical journal* 65 (1993), Nr. 1, 316-324. http://dx.doi.org/10.1016/S0006-3495(93)81035-X. – DOI 10.1016/S0006–3495(93)81035–X

[41] Mogilner, A. ; Oster, G.: Cell motility driven by actin polymerization. In: *Biophysical Journal* 71 (1996), Nr. 6, 3030-3045. http://dx.doi.org/10.1016/S0006-3495(96)79496-1. – DOI 10.1016/S0006–3495(96)79496–1

[42] Schaus, Thomas E. ; Borisy, Gary G.: Performance of a Population of Independent Filaments in Lamellipodial Protrusion. In: *Biophysical Journal* 95 (2008), Nr. 3, 1393-1411. http://dx.doi.org/10.1529/biophysj.107.125005. – DOI 10.1529/biophysj.107.125005

[43] Marcy, Yann ; Prost, Jacques ; Carlier, Marie-France ; Sykes, Cécile: Forces generated during actin-based propulsion: A direct measurement by micromanipulation. In: *Proceedings of the National Academy of Sciences of the United States of America* 101 (2004), Nr. 16, 5992-5997. http://dx.doi.org/10.1073/pnas.0307704101. – DOI 10.1073/pnas.0307704101

[44] Kruse, K. ; Joanny, J. F. ; JÃ¼licher, F. ; Prost, J.: Contractility and retrograde flow in lamellipodium motion. In: *Physical Biology* 3 (2006), Nr. 2, 130-137. http://dx.doi.org/10.1088/1478-3975/3/2/005. – DOI 10.1088/1478–3975/3/2/005

[45] Dolati, Setareh ; Kage, Frieda ; Mueller, Jan ; MÃ¼sken, Mathias ; Kirchner, Marieluise ; Dittmar, Gunnar ; Sixt, Michael ; Rottner, Klemens ; Falcke, Martin: On the relation between filament density, force generation, and protrusion rate in mesenchymal cell motility. In: *Molecular Biology of the Cell* 29 (2018), Nr. 22, 2674-2686. http://dx.doi.org/10.1091/mbc.E18-02-0082. – DOI 10.1091/mbc.E18–02–0082

[46] Parekh, Sapun H. ; Chaudhuri, Ovijit ; Theriot, Julie A. ; Fletcher, Daniel A.: Loading history determines the velocity of actin-network growth. In: *Nature Cell Biology* 7 (2005), Nr. 12, 1219-1223. http://dx.doi.org/10.1038/ncb1336. – DOI 10.1038/ncb1336

[47] Schreiber, Christian H. ; Stewart, Murray ; Duke, Thomas: Simulation of cell motility that reproduces the force–velocity relationship. In: *Proceedings of the National Academy of Sciences* 107 (2010), Nr. 20, 9141-9146. http://dx.doi.org/10.1073/pnas.1002538107. – DOI 10.1073/pnas.1002538107

[48] Danuser, Gaudenz ; Allard, Jun ; Mogilner, Alex: Mathematical Modeling of Eukaryotic Cell Migration: Insights Beyond Experiments. In: *Annual review of cell and developmental biology* 29 (2013), 501-528. http://dx.doi.org/10.1146/annurev-cellbio-101512-122308. – DOI 10.1146/annurev–cellbio–101512–122308

[49] Craig, E. M. ; Dey, S. ; Mogilner, A.: The emergence of sarcomeric, graded-polarity and spindle-like patterns in bundles of short cytoskeletal polymers and two opposite molecular motors. In: *Journal of Physics: Condensed*

Matter 23 (2011), Nr. 37, 374102. http://dx.doi.org/10.1088/0953-8984/23/37/374102. – DOI 10.1088/0953–8984/23/37/374102

[50] Friedrich, Benjamin M. ; Fischer-Friedrich, Elisabeth ; Gov, Nir S. ; Safran, Samuel A.: Sarcomeric Pattern Formation by Actin Cluster Coalescence. In: *PLOS Computational Biology* 8 (2012), Nr. 6, e1002544. http://dx.doi.org/10.1371/journal.pcbi.1002544. – DOI 10.1371/journal.pcbi.1002544

[51] Li, Ying ; Bhimalapuram, Prabhakar ; Dinner, Aaron R.: Model for how retrograde actin flow regulates adhesion traction stresses. In: *Journal of Physics: Condensed Matter* 22 (2010), Nr. 19, 194113. http://dx.doi.org/10.1088/0953-8984/22/19/194113. – DOI 10.1088/0953–8984/22/19/194113

[52] Howard, J.: *Mechanics of Motor Proteins and the Cytoskeleton*. Sinauer, 2005 https://books.google.de/books?id=cwoCPwAACAAJ. – ISBN 9780878933334

[53] Gardel, Margaret L. ; Sabass, Benedikt ; Ji, Lin ; Danuser, Gaudenz ; Schwarz, Ulrich S. ; Waterman, Clare M.: Traction stress in focal adhesions correlates biphasically with actin retrograde flow speed. In: *The Journal of Cell Biology* 183 (2008), Nr. 6, 999-1005. http://dx.doi.org/10.1083/jcb.200810060. – DOI 10.1083/jcb.200810060

[54] Maiuri, Paolo ; Rupprecht, Jean-François ; Wieser, Stefan ; Ruprecht, Verena ; Bénichou, Olivier ; Carpi, Nicolas ; Coppey, Mathieu ; De Beco, Simon ; Gov, Nir ; Heisenberg, Carl-Philipp ; Lage Crespo, Carolina ; Lautenschlaeger, Franziska ; Le Berre, Maël ; Lennon-Dumenil, Ana-Maria ; Raab, Matthew ; Thiam, Hawa-Racine ; Piel, Matthieu ; Sixt, Michael ; Voituriez, Raphaël: Actin Flows Mediate a Universal Coupling between Cell Speed and Cell Persistence. In: *Cell* 161 (2015), Nr. 2, 374-386. http://dx.doi.org/10.1016/j.cell.2015.01.056. – DOI 10.1016/j.cell.2015.01.056

[55] Thueroff, Florian ; Goychuk, Andriy ; Reiter, Matthias ; Frey, Erwin: Bridging the gap between single cell migration and collective dynamics. In: *bioRxiv* (2019), 548677. http://dx.doi.org/10.1101/548677. – DOI 10.1101/548677

[56] Graner, François ; Glazier, James A.: Simulation of biological cell sorting using a two-dimensional extended Potts model. In: *Physical Review Letters* 69 (1992), Nr. 13, 2013-2016. http://dx.doi.org/10.1103/PhysRevLett.69.2013. – DOI 10.1103/PhysRevLett.69.2013

[57] Barnhart, Erin L. ; Lee, Kun-Chun ; Keren, Kinneret ; Mogilner, Alex ; Theriot, Julie A.: An Adhesion-Dependent Switch between Mechanisms That Determine Motile Cell Shape. In: *PLoS Biol* 9 (2011), Nr. 5, e1001059. http://dx.doi.org/10.1371/journal.pbio.1001059. – DOI 10.1371/journal.pbio.1001059

[58] Begemann, I. ; Saha, T. ; Lamparter, L. ; Rathmann, I. ; Grill, D. ; Golbach, L. ; Rasch, C. ; Keller, U. ; Trappmann, B. ; Matis, M. ; Gerke, V. ; Klingauf, J. ; Galic, M.: Mechanochemical self-organization determines search pattern in migratory cells. In: *Nature Physics* 15 (2019), Nr. 8, 848-857.

http://dx.doi.org/10.1038/s41567-019-0505-9. – DOI 10.1038/s41567–019–0505–9

[59] Camley, Brian A. ; Zhao, Yanxiang ; Li, Bo ; Levine, Herbert ; Rappel, Wouter-Jan: Periodic Migration in a Physical Model of Cells on Micropatterns. In: *Physical Review Letters* 111 (2013), Nr. 15, 158102. http://link.aps.org/doi/10.1103/PhysRevLett.111.158102

[60] Banerjee, Shiladitya ; Sknepnek, Rastko ; Marchetti, M. C.: Optimal shapes and stresses of adherent cells on patterned substrates. In: *Soft Matter* 10 (2014), Nr. 14, 2424-2430. http://dx.doi.org/10.1039/C3SM52647J. – DOI 10.1039/C3SM52647J

[61] Herant, Marc ; Dembo, Micah: Form and Function in Cell Motility: From Fibroblasts to Keratocytes. In: *Biophysical Journal* 98 (2010), Nr. 8, 1408-1417. http://dx.doi.org/10.1016/j.bpj.2009.12.4303. – DOI 10.1016/j.bpj.2009.12.4303

[62] Mogilner, Alex: Mathematics of cell motility: have we got its number? In: *Journal of Mathematical Biology* 58 (2009), Nr. 1-2, 105-134. http://dx.doi.org/10.1007/s00285-008-0182-2. – DOI 10.1007/s00285–008–0182–2

[63] Holmes, William R. ; Edelstein-Keshet, Leah: A Comparison of Computational Models for Eukaryotic Cell Shape and Motility. In: *PLOS Computational Biology* 8 (2012), Nr. 12, e1002793. http://dx.doi.org/10.1371/journal.pcbi.1002793. – DOI 10.1371/journal.pcbi.1002793

[64] Ryan, Gillian L. ; Watanabe, Naoki ; Vavylonis, Dimitrios: A review of models of fluctuating protrusion and retraction patterns at the leading edge of motile cells. In: *Cytoskeleton* 69 (2012), Nr. 4, 195-206. http://dx.doi.org/10.1002/cm.21017. – DOI 10.1002/cm.21017

[65] Albert, Philipp J. ; Schwarz, Ulrich S.: Modeling cell shape and dynamics on micropatterns. In: *Cell Adhesion & Migration* 10 (2016), Nr. 4, 1-13. http://dx.doi.org/10.1080/19336918.2016.1148864. – DOI 10.1080/19336918.2016.1148864

[66] Mrksich, Milan ; Whitesides, George M.: Patterning self-assembled monolayers using microcontact printing: A new technology for biosensors? In: *Trends in Biotechnology* 13 (1995), Nr. 6, 228-235. http://dx.doi.org/10.1016/S0167-7799(00)88950-7. – DOI 10.1016/S0167–7799(00)88950–7

[67] Zhao, Xiao-Mei ; Xia, Younan ; Whitesides, George M.: Soft lithographic methods for nano-fabrication. In: *Journal of Materials Chemistry* 7 (1997), Nr. 7, 1069-1074. http://dx.doi.org/10.1039/A700145B. – DOI 10.1039/A700145B

[68] Kane, Ravi S. ; Takayama, Shuichi ; Ostuni, Emanuele ; Ingber, Donald E. ; Whitesides, George M.: Patterning proteins and cells using soft lithography. In: *Biomaterials* 20 (1999), Nr. 23-24, 2363-2376. http://dx.doi.org/10.1016/S0142-9612(99)00165-9. – DOI 10.1016/S0142–9612(99)00165–9

[69] Roberts, Carmichael ; Chen, Christopher S. ; Mrksich, Milan ; Martichonok, Valerie ; Ingber, Donald E. ; Whitesides, George M.: Using Mixed Self-Assembled Monolayers Presenting RGD and (EG)3OH Groups To Characterize Long-Term Attachment of Bovine Capillary Endothelial Cells to Surfaces. In: *Journal of the American Chemical Society* 120 (1998), Nr. 26, 6548-6555. http://dx.doi.org/10.1021/ja972467o. – DOI 10.1021/ja972467o

[70] Bernard, Andre ; Renault, Jean P. ; Michel, Bruno ; Bosshard, Hans R. ; Delamarche, Emmanuel: Microcontact printing of proteins. In: *Advanced Materials* 12 (2000), Nr. 14, S. 1067–1070

[71] Kaufmann, Tobias ; Ravoo, Bart J.: Stamps, inks and substrates: polymers in microcontact printing. In: *Polymer Chemistry* 1 (2010), Nr. 4, 371-387. http://dx.doi.org/10.1039/B9PY00281B. – DOI 10.1039/B9PY00281B

[72] Théry, Manuel ; Piel, Matthieu: Adhesive Micropatterns for Cells: A Microcontact Printing Protocol. In: *Cold Spring Harbor Protocols* 2009 (2009), Nr. 7, pdb.prot5255. http://dx.doi.org/10.1101/pdb.prot5255. – DOI 10.1101/pdb.prot5255

[73] In: Picone, Remigio ; Baum, Buzz ; McKendry, Rachel: *Chapter 5 - Plasma Microcontact Patterning (PμFCP): A Technique for the Precise Control of Surface Patterning at Small-Scale*. Bd. 119. Academic Press, 2014. – ISBN 0091–679X, 73-90

[74] Segerer, Felix J. ; Röttgermann, Peter Johan F. ; Schuster, Simon ; Piera Alberola, Alicia ; Zahler, Stefan ; Rädler, Joachim O.: Versatile method to generate multiple types of micropatterns. In: *Biointerphases* 11 (2016), Nr. 1, 011005. http://dx.doi.org/10.1116/1.4940703. – DOI 10.1116/1.4940703

[75] Azioune, Ammar ; Storch, Marko ; Bornens, Michel ; Thery, Manuel ; Piel, Matthieu: Simple and rapid process for single cell micro-patterning. In: *Lab on a Chip* 9 (2009), Nr. 11, 1640-1642. http://dx.doi.org/10.1039/B821581M. – DOI 10.1039/B821581M

[76] Slater, John H. ; Miller, Jordan S. ; Yu, Shann S. ; West, Jennifer L.: Fabrication of Multifaceted Micropatterned Surfaces with Laser Scanning Lithography. In: *Advanced Functional Materials* 21 (2011), Nr. 15, 2876-2888. http://dx.doi.org/10.1002/adfm.201100297. – DOI 10.1002/adfm.201100297

[77] Bélisle, Jonathan M. ; Correia, James P. ; Wiseman, Paul W. ; Kennedy, Timothy E. ; Costantino, Santiago: Patterning protein concentration using laser-assisted adsorption by photobleaching, LAPAP. In: *Lab on a Chip* 8 (2008), Nr. 12, 2164-2167. http://dx.doi.org/10.1039/B813897D. – DOI 10.1039/B813897D

[78] Strale, Pierre-Olivier ; Azioune, Ammar ; Bugnicourt, Ghislain ; Lecomte, Yohan ; Chahid, Makhlad ; Studer, Vincent: Multiprotein Printing by Light-Induced Molecular Adsorption. In: *Advanced Materials* 28 (2016),

Nr. 10, 2024-2029. http://dx.doi.org/10.1002/adma.201504154. – DOI 10.1002/adma.201504154

[79] Delaittre, Guillaume ; Greiner, Alexandra M. ; Pauloehrl, Thomas ; Bastmeyer, Martin ; Barner-Kowollik, Christopher: Chemical approaches to synthetic polymer surface biofunctionalization for targeted cell adhesion using small binding motifs. In: *Soft Matter* 8 (2012), Nr. 28, 7323-7347. http://dx.doi.org/10.1039/C2SM07407A. – DOI 10.1039/C2SM07407A

[80] Baneyx, Gretchen ; Baugh, Loren ; Vogel, Viola: Fibronectin extension and unfolding within cell matrix fibrils controlled by cytoskeletal tension. In: *Proceedings of the National Academy of Sciences* 99 (2002), Nr. 8, 5139-5143. http://dx.doi.org/10.1073/pnas.072650799. – DOI 10.1073/pnas.072650799

[81] Smith, Michael L. ; Gourdon, Delphine ; Little, William C. ; Kubow, Kristopher E. ; Eguiluz, R. A. ; Luna-Morris, Sheila ; Vogel, Viola: Force-Induced Unfolding of Fibronectin in the Extracellular Matrix of Living Cells. In: *PLOS Biology* 5 (2007), Nr. 10, e268. http://dx.doi.org/10.1371/journal.pbio.0050268. – DOI 10.1371/journal.pbio.0050268

[82] Desai, Ravi A. ; Khan, Mohammed K. ; Gopal, Smitha B. ; Chen, Christopher S.: Subcellular spatial segregation of integrin subtypes by patterned multicomponent surfaces. In: *Integrative Biology* 3 (2011), Nr. 5, 560-567. http://dx.doi.org/10.1039/C0IB00129E. – DOI 10.1039/C0IB00129E

[83] Piner, Richard D. ; Zhu, Jin ; Xu, Feng ; Hong, Seunghun ; Mirkin, Chad A.: "Dip-Pen" Nanolithography. In: *Science* 283 (1999), Nr. 5402, 661-663. http://dx.doi.org/10.1126/science.283.5402.661. – DOI 10.1126/science.283.5402.661

[84] Rodriguez, Natalia M. ; Desai, Ravi A. ; Trappmann, Britta ; Baker, Brendon M. ; Chen, Christopher S.: Micropatterned Multicolor Dynamically Adhesive Substrates to Control Cell Adhesion and Multicellular Organization. In: *Langmuir* 30 (2014), Nr. 5, 1327-1335. http://dx.doi.org/10.1021/la404037s. – DOI 10.1021/la404037s

[85] Röttgermann, Peter J. F. ; Dawson, Kenneth A. ; Rädler, Joachim O.: Time-Resolved Study of Nanoparticle Induced Apoptosis Using Microfabricated Single Cell Arrays. In: *Microarrays* 5 (2016), Nr. 2, 8. https://www.mdpi.com/2076-3905/5/2/8

[86] Chatzopoulou, Elisavet I. ; Roskopf, Claudia C. ; Sekhavati, Farzad ; Braciak, Todd A. ; Fenn, Nadja C. ; Hopfner, Karl-Peter ; Oduncu, Fuat S. ; Fey, Georg H. ; Rädler, Joachim O.: Chip-based platform for dynamic analysis of NK cell cytolysis mediated by a triplebody. In: *Analyst* 141 (2016), Nr. 7, 2284-2295. http://dx.doi.org/10.1039/C5AN02585K. – DOI 10.1039/C5AN02585K

[87] Murschhauser, Alexandra ; Röttgermann, Peter J. F. ; Woschée, Daniel ; Ober, Martina F. ; Yan, Yan ; Dawson, Kenneth A. ; Rädler, Joachim O.: A high-throughput microscopy method for single-cell analysis of event-time correlations in nanoparticle-induced cell death. In: *Communications Biology* 2

(2019), Nr. 1, 35. http://dx.doi.org/10.1038/s42003-019-0282-0. – DOI 10.1038/s42003–019–0282–0

[88] Chen, Christopher S. ; Mrksich, Milan ; Huang, Sui ; Whitesides, George M. ; Ingber, Donald E.: Geometric Control of Cell Life and Death. In: *Science* 276 (1997), Nr. 5317, 1425-1428. http://dx.doi.org/10.1126/science.276.5317.1425. – DOI 10.1126/science.276.5317.1425

[89] Fröhlich, Fabian ; Reiser, Anita ; Fink, Laura ; Woschée, Daniel ; Ligon, Thomas ; Theis, Fabian J. ; Rädler, Joachim O. ; Hasenauer, Jan: Multi-experiment nonlinear mixed effect modeling of single-cell translation kinetics after transfection. In: *npj Systems Biology and Applications* 4 (2018), Nr. 1, 42. http://dx.doi.org/10.1038/s41540-018-0079-7. – DOI 10.1038/s41540–018–0079–7

[90] Théry, Manuel ; Racine, Victor ; Piel, Matthieu ; Pépin, Anne ; Dimitrov, Ariane ; Chen, Yong ; Sibarita, Jean-Baptiste ; Bornens, Michel: Anisotropy of cell adhesive microenvironment governs cell internal organization and orientation of polarity. In: *Proceedings of the National Academy of Sciences* 103 (2006), Nr. 52, 19771-19776. http://dx.doi.org/10.1073/pnas.0609267103. – DOI 10.1073/pnas.0609267103

[91] Tee, Yee H. ; Shemesh, Tom ; Thiagarajan, Visalatchi ; Hariadi, Rizal F. ; Anderson, Karen L. ; Page, Christopher ; Volkmann, Niels ; Hanein, Dorit ; Sivaramakrishnan, Sivaraj ; Kozlov, Michael M. ; Bershadsky, Alexander D.: Cellular chirality arising from the self-organization of the actin cytoskeleton. In: *Nat Cell Biol* 17 (2015), Nr. 4, 445-457. http://dx.doi.org/10.1038/ncb3137. – DOI 10.1038/ncb3137

[92] Bernitt, Erik ; Koh, Cheng G. ; Gov, Nir ; Döbereiner, Hans-Günther: Dynamics of Actin Waves on Patterned Substrates: A Quantitative Analysis of Circular Dorsal Ruffles. In: *PLoS ONE* 10 (2015), Nr. 1, e0115857. http://dx.doi.org/10.1371/journal.pone.0115857. – DOI 10.1371/journal.pone.0115857

[93] Brock, Amy ; Chang, Eric ; Ho, Chia-Chi ; LeDuc, Philip ; Jiang, Xingyu ; Whitesides, George M. ; Ingber, Donald E.: Geometric Determinants of Directional Cell Motility Revealed Using Microcontact Printing. In: *Langmuir* 19 (2003), Nr. 5, 1611-1617. http://dx.doi.org/10.1021/la026394k. – DOI 10.1021/la026394k

[94] Doyle, Andrew D. ; Wang, Francis W. ; Matsumoto, Kazue ; Yamada, Kenneth M.: One-dimensional topography underlies three-dimensional fibrillar cell migration. In: *The Journal of Cell Biology* 184 (2009), Nr. 4, 481-490. http://dx.doi.org/10.1083/jcb.200810041. – DOI 10.1083/jcb.200810041

[95] Desai, Ravi A. ; Gopal, Smitha B. ; Chen, Sophia ; Chen, Christopher S.: Contact inhibition of locomotion probabilities drive solitary versus collective cell migration. In: *Journal of The Royal Society Interface* 10 (2013), Nr. 88, 20130717. http://dx.doi.org/10.1098/rsif.2013.0717. – DOI 10.1098/rsif.2013.0717

[96] Kandere-Grzybowska, Kristiana ; Campbell, Christopher J. ; Mahmud,

Goher ; Komarova, Yulia ; Soh, Siowling ; Grzybowski, Bartosz A.: Cell motility on micropatterned treadmills and tracks. In: *Soft Matter* 3 (2007), Nr. 6, 672-679. http://dx.doi.org/10.1039/B617308J. – DOI 10.1039/B617308J

[97] Pouthas, FranÃ§ois ; Girard, Philippe ; Lecaudey, Virginie ; Ly, Thi Bach N. ; Gilmour, Darren ; Boulin, Christian ; Pepperkok, Rainer ; Reynaud, Emmanuel G.: In migrating cells, the Golgi complex and the position of the centrosome depend on geometrical constraints of the substratum. In: *Journal of Cell Science* 121 (2008), Nr. 14, 2406-2414. http://dx.doi.org/10.1242/jcs.026849. – DOI 10.1242/jcs.026849

[98] Chang, Stephanie S. ; Guo, Wei-hui ; Kim, Youngeun ; Wang, Yu-li: Guidance of Cell Migration by Substrate Dimension. In: *Biophysical Journal* 104 (2013), Nr. 2, 313-321. http://dx.doi.org/10.1016/j.bpj.2012.12.001. – DOI 10.1016/j.bpj.2012.12.001

[99] Caballero, David ; Voituriez, Raphaël ; Riveline, Daniel: Protrusion Fluctuations Direct Cell Motion. In: *Biophysical Journal* 107 (2014), Nr. 1, 34-42. http://dx.doi.org/10.1016/j.bpj.2014.05.002. – DOI 10.1016/j.bpj.2014.05.002

[100] Caballero, David ; Comelles, Jordi ; Piel, Matthieu ; Voituriez, Raphaël ; Riveline, Daniel: Ratchetaxis: Long-Range Directed Cell Migration by Local Cues. In: *Trends in Cell Biology* 25 (2015), Nr. 12, 815-827. http://dx.doi.org/10.1016/j.tcb.2015.10.009. – DOI 10.1016/j.tcb.2015.10.009

[101] Ko, Young-Gwang ; Co, Carlos C. ; Ho, Chia-Chi: Directing cell migration in continuous microchannels by topographical amplification of natural directional persistence. In: *Biomaterials* 34 (2013), Nr. 2, 353-360. http://dx.doi.org/10.1016/j.biomaterials.2012.09.071. – DOI 10.1016/j.biomaterials.2012.09.071

[102] Mahmud, Goher ; Campbell, Christopher J. ; Bishop, Kyle J. M. ; Komarova, Yulia A. ; Chaga, Oleg ; Soh, Siowling ; Huda, Sabil ; Kandere-Grzybowska, Kristiana ; Grzybowski, Bartosz A.: Directing cell motions on micropatterned ratchets. In: *Nature Phys.* 5 (2009), Nr. 8, 606-612. http://dx.doi.org/10.1038/nphys1306. – DOI 10.1038/nphys1306

[103] Marel, Anna-Kristina ; Zorn, Matthias ; Klingner, Christoph ; Wedlich-Söldner, Roland ; Frey, Erwin ; Rädler, Joachim O.: Flow and Diffusion in Channel-Guided Cell Migration. In: *Biophysical Journal* 107 (2014), Nr. 5, 1054-1064. http://dx.doi.org/10.1016/j.bpj.2014.07.017. – DOI 10.1016/j.bpj.2014.07.017

[104] Wan, Leo Q. ; Ronaldson, Kacey ; Park, Miri ; Taylor, Grace ; Zhang, Yue ; Gimble, Jeffrey M. ; Vunjak-Novakovic, Gordana: Micropatterned mammalian cells exhibit phenotype-specific left-right asymmetry. In: *Proceedings of the National Academy of Sciences* 108 (2011), Nr. 30, 12295-12300. http://dx.doi.org/10.1073/pnas.1103834108. – DOI 10.1073/pnas.1103834108

[105] Vedula, Sri Ram K. ; Leong, Man C. ; Lai, Tan L. ; Hersen, Pascal ; Kabla, Alexandre J. ; Lim, Chwee T. ; Ladoux, BenoÃ®t: Emerging modes of collective

cell migration induced by geometrical constraints. In: *Proceedings of the National Academy of Sciences* 109 (2012), Nr. 32, 12974-12979. http://dx.doi.org/10.1073/pnas.1119313109. – DOI 10.1073/pnas.1119313109

[106] Piel, Matthieu ; Théry, Manuel: *Micropatterning in Cell Biology Part C: Methods in Cell Biology*. Bd. 121. Elsevier, 2014. – ISBN 012800281

[107] Paul, Colin D. ; Hung, Wei-Chien ; Wirtz, Denis ; Konstantopoulos, Konstantinos: Engineered Models of Confined Cell Migration. In: *Annual Review of Biomedical Engineering* 18 (2016), Nr. 1

[108] Brown, Robert: XXVII. A brief account of microscopical observations made in the months of June, July and August 1827, on the particles contained in the pollen of plants; and on the general existence of active molecules in organic and inorganic bodies. In: *The Philosophical Magazine* 4 (1828), Nr. 21, S. 161–173

[109] Einstein, A.: Über die von der molekularkinetischen Theorie der Wärme geforderte Bewegung von in ruhenden Flüssigkeiten suspendierten Teilchen. In: *Annalen der Physik* 322 (1905), Nr. 8, 549-560. http://dx.doi.org/10.1002/andp.19053220806. – DOI 10.1002/andp.19053220806

[110] Einstein, A.: Zur Theorie der Brownschen Bewegung. In: *Annalen der Physik* 324 (1906), Nr. 2, 371-381. http://dx.doi.org/10.1002/andp.19063240208. – DOI 10.1002/andp.19063240208

[111] Przibram, Karl: Über die ungeordnete Bewegung niederer Tiere. II. In: *Archiv für Entwicklungsmechanik der Organismen* 43 (1917), Nr. 1-2, S. 20–27

[112] Fürth, Reinhold: Die brownsche bewegung bei berücksichtigung einer persistenz der bewegungsrichtung. mit anwendungen auf die bewegung lebender infusorien. In: *Zeitschrift für Physik* 2 (1920), Nr. 3, S. 244–256

[113] Uhlenbeck, G. E. ; Ornstein, L. S.: On the Theory of the Brownian Motion. In: *Physical Review* 36 (1930), Nr. 5, 823-841. http://link.aps.org/doi/10.1103/PhysRev.36.823

[114] DUNN, G. A. ; BROWN, A. F.: A Unified Approach to Analysing Cell Motility. In: *Journal of Cell Science* 1987 (1987), Nr. Supplement 8, 81-102. http://jcs.biologists.org/content/1987/Supplement_8/81

[115] Campos, Daniel ; Méndez, VicenÃ§ ; Llopis, Isaac: Persistent random motion: Uncovering cell migration dynamics. In: *Journal of Theoretical Biology* 267 (2010), Nr. 4, 526-534. http://dx.doi.org/10.1016/j.jtbi.2010.09.022. – DOI 10.1016/j.jtbi.2010.09.022

[116] Gorelik, Roman ; Gautreau, Alexis: Quantitative and unbiased analysis of directional persistence in cell migration. In: *Nat. Protocols* 9 (2014), Nr. 8, 1931-1943. http://dx.doi.org/10.1038/nprot.2014.131. – DOI 10.1038/nprot.2014.131

[117] Czirók, András ; Schlett, Katalin ; Madarász, Emília ; Vicsek, Tamás: Exponential Distribution of Locomotion Activity in Cell Cultures. In: *Physical*

Review Letters 81 (1998), Nr. 14, 3038-3041. http://link.aps.org/doi/10.1103/PhysRevLett.81.3038

[118] Takagi, Hiroaki ; Sato, Masayuki J. ; Yanagida, Toshio ; Ueda, Masahiro: Functional Analysis of Spontaneous Cell Movement under Different Physiological Conditions. In: *PLoS ONE* 3 (2008), Nr. 7, e2648. http://dx.doi.org/10.1371/journal.pone.0002648. – DOI 10.1371/journal.pone.0002648

[119] Huda, Sabil ; Weigelin, Bettina ; Wolf, Katarina ; Tretiakov, Konstantin V. ; Polev, Konstantin ; Wilk, Gary ; Iwasa, Masatomo ; Emami, Fateme S. ; Narojczyk, Jakub W. ; Banaszak, Michal ; Soh, Siowling ; Pilans, Didzis ; Vahid, Amir ; Makurath, Monika ; Friedl, Peter ; Borisy, Gary G. ; Kandere-Grzybowska, Kristiana ; Grzybowski, Bartosz A.: Lévy-like movement patterns of metastatic cancer cells revealed in microfabricated systems and implicated in vivo. In: *Nature Communications* 9 (2018), Nr. 1, 4539. http://dx.doi.org/10.1038/s41467-018-06563-w. – DOI 10.1038/s41467–018–06563–w

[120] Dieterich, Peter ; Klages, Rainer ; Preuss, Roland ; Schwab, Albrecht: Anomalous dynamics of cell migration. In: *Proceedings of the National Academy of Sciences* 105 (2008), Nr. 2, 459-463. http://dx.doi.org/10.1073/pnas.0707603105. – DOI 10.1073/pnas.0707603105

[121] Berg, Howard C.: *Random walks in biology*. Princeton University Press, 1993. – ISBN 0691000646

[122] Berg, Howard C.: *E. coli in Motion*. Springer Science & Business Media, 2008. – ISBN 0387216383

[123] Potdar, Alka A. ; Jeon, Junhwan ; Weaver, Alissa M. ; Quaranta, Vito ; Cummings, Peter T.: Human Mammary Epithelial Cells Exhibit a Bimodal Correlated Random Walk Pattern. In: *PLoS ONE* 5 (2010), Nr. 3, e9636. http://dx.doi.org/10.1371/journal.pone.0009636. – DOI 10.1371/journal.pone.0009636

[124] Gruver, J. S. ; Potdar, Alka A. ; Jeon, Junhwan ; Sai, Jiqing ; Anderson, Bridget ; Webb, Donna ; Richmond, Ann ; Quaranta, Vito ; Cummings, Peter T. ; Chung, Chang Y.: Bimodal Analysis Reveals a General Scaling Law Governing Nondirected and Chemotactic Cell Motility. In: *Biophysical Journal* 99 (2010), Nr. 2, 367-376. http://dx.doi.org/10.1016/j.bpj.2010.03.073. – DOI 10.1016/j.bpj.2010.03.073

[125] Selmeczi, D. ; Li, L. ; Pedersen, L. I. I. ; Nrrelykke, S. F. ; Hagedorn, P. H. ; Mosler, S. ; Larsen, N. B. ; Cox, E. C. ; Flyvbjerg, H.: Cell motility as random motion: A review. In: *Eur Phys J Spec Top* 157 (2008), Nr. 1, 1-15. http://dx.doi.org/10.1140/epjst/e2008-00626-x. – DOI 10.1140/epjst/e2008–00626–x

[126] Bénichou, O. ; Loverdo, C. ; Moreau, M. ; Voituriez, R.: Intermittent search strategies. In: *Reviews of Modern Physics* 83 (2011), Nr. 1, 81-129. http://link.aps.org/doi/10.1103/RevModPhys.83.81

[127] Edwards, Andrew M. ; Phillips, Richard A. ; Watkins, Nicholas W. ; Freeman, Mervyn P. ; Murphy, Eugene J. ; Afanasyev, Vsevolod ; Buldyrev, Sergey V. ; Luz, M. G. E. ; Raposo, E. P. ; Stanley, H. E. ; Viswanathan, Gandhimohan M.: Revisiting LÃ©vy flight search patterns of wandering albatrosses, bumblebees and deer. In: *Nature* 449 (2007), 1044. http://dx.doi.org/10.1038/nature06199. – DOI 10.1038/nature06199

[128] Selmeczi, David ; Mosler, Stephan ; Hagedorn, Peter H. ; Larsen, Niels B. ; Flyvbjerg, Henrik: Cell Motility as Persistent Random Motion: Theories from Experiments. In: *Biophysical Journal* 89 (2005), Nr. 2, 912-931. http://dx.doi.org/10.1529/biophysj.105.061150. – DOI 10.1529/biophysj.105.061150

[129] Bi, Dapeng ; Lopez, Jorge H. ; Schwarz, J. M. ; Manning, M. L.: Energy barriers and cell migration in densely packed tissues. In: *Soft Matter* 10 (2014), Nr. 12, 1885-1890. http://dx.doi.org/10.1039/C3SM52893F. – DOI 10.1039/C3SM52893F

[130] Camley, Brian A. ; Rappel, Wouter-Jan: Velocity alignment leads to high persistence in confined cells. In: *Physical Review E* 89 (2014), Nr. 6, 062705. http://link.aps.org/doi/10.1103/PhysRevE.89.062705

[131] Comelles, Jordi ; Caballero, David ; Voituriez, Raphaël ; Hortigüela, Verónica ; Wollrab, Viktoria ; Godeau, Amélie L. ; Samitier, Josep ; Martínez, Elena ; Riveline, Daniel: Cells as Active Particles in Asymmetric Potentials: Motility under External Gradients. In: *Biophysical Journal* 107 (2014), Nr. 7, 1513-1522. http://dx.doi.org/10.1016/j.bpj.2014.08.001. – DOI 10.1016/j.bpj.2014.08.001

[132] Le Berre, M. ; Liu, Yan-Jun ; Hu, J. ; Maiuri, Paolo ; Bénichou, O. ; Voituriez, R. ; Chen, Y. ; Piel, M.: Geometric Friction Directs Cell Migration. In: *Physical Review Letters* 111 (2013), Nr. 19, 198101. http://link.aps.org/doi/10.1103/PhysRevLett.111.198101

[133] Phillips, Rob ; Kondev, Jane ; Theriot, Julie ; Orme, Nigel ; Garcia, Hernan: *Physical biology of the cell*. Garland Science New York, 2009. – ISBN 0815341636

[134] Mutlu, Merve ; Raza, Umar ; Saatci, Özge ; Eyüpoğlu, Erol ; Yurdusev, Emre ; Şahin, Özgür: miR-200c: a versatile watchdog in cancer progression, EMT, and drug resistance. In: *Journal of Molecular Medicine* 94 (2016), Nr. 6, 629-644. http://dx.doi.org/10.1007/s00109-016-1420-5. – DOI 10.1007/s00109–016–1420–5

[135] Huang, Yong ; Shen, Xing J. ; Zou, Quan ; Wang, Sheng P. ; Tang, Shun M. ; Zhang, Guo Z.: Biological functions of microRNAs: a review. In: *Journal of Physiology and Biochemistry* 67 (2011), Nr. 1, 129-139. http://dx.doi.org/10.1007/s13105-010-0050-6. – DOI 10.1007/s13105–010–0050–6

[136] Ameres, Stefan L. ; Zamore, Phillip D.: Diversifying microRNA sequence and function. In: *Nature Reviews Molecular Cell Biology* 14 (2013), 475. http://dx.doi.org/10.1038/nrm3611. – DOI 10.1038/nrm3611

[137] Kumar, Suresh ; Nag, Alo ; C. Mandal, Chandi: A Comprehensive Review on miR-200c, A Promising Cancer Biomarker with Therapeutic Potential. In: *Current Drug Targets* 16 (2015), Nr. 12, 1381-1403. https://www.ingentaconnect.com/content/ben/cdt/2015/00000016/00000012/art00014

[138] Kopp, Florian ; Oak, Prajakta S. ; Wagner, Ernst ; Roidl, Andreas: miR-200c Sensitizes Breast Cancer Cells to Doxorubicin Treatment by Decreasing TrkB and Bmi1 Expression. In: *PLOS ONE* 7 (2012), Nr. 11, e50469. http://dx.doi.org/10.1371/journal.pone.0050469. – DOI 10.1371/journal.pone.0050469

[139] Thiery, Jean P.: Epithelial-mesenchymal transitions in tumour progression. In: *Nat Rev Cancer* 2 (2002), Nr. 6, 442-454. http://dx.doi.org/10.1038/nrc822

[140] Yilmaz, Mahmut ; Christofori, Gerhard: EMT, the cytoskeleton, and cancer cell invasion. In: *Cancer and Metastasis Reviews* 28 (2009), Nr. 1-2, 15-33. http://dx.doi.org/10.1007/s10555-008-9169-0. – DOI 10.1007/s10555–008–9169–0

[141] Jurmeister, Sarah ; Baumann, Marek ; Balwierz, Aleksandra ; Keklikoglou, Ioanna ; Ward, Aoife ; Uhlmann, Stefan ; Zhang, Jitao D. ; Wiemann, Stefan ; Sahin, Özgür: MicroRNA-200c represses migration and invasion of breast cancer cells by targeting actin-regulatory proteins FHOD1 and PPM1F. In: *Molecular and cellular biology* 32 (2012), Nr. 3, S. 633–651

[142] Belaud, Vanessa ; Petithory, Tatiana ; Ponche, Arnaud ; Mauclair, Cyril ; Donnet, Christophe ; Pieuchot, Laurent ; Benayoun, Stephane ; Anselme, Karine: Influence of multiscale and curved structures on the migration of stem cells. In: *Biointerphases* 13 (2018), Nr. 6, 06D408. http://dx.doi.org/10.1116/1.5042747. – DOI 10.1116/1.5042747

[143] Chihiro, Okutani ; Akira, Wagatsuma ; Kunihiko, Mabuchi ; Takayuki, Hoshino: Cell descent caused by boundary curvature of a high topographical structure for a device that changes cell density. In: *Japanese Journal of Applied Physics* 56 (2017), Nr. 6S1, 06GM03. http://stacks.iop.org/1347-4065/56/i=6S1/a=06GM03

[144] Codling, Edward A. ; Plank, Michael J. ; Benhamou, Simon: Random walk models in biology. In: *Journal of The Royal Society Interface* 5 (2008), Nr. 25, 813-834. http://dx.doi.org/10.1098/rsif.2008.0014. – DOI 10.1098/rsif.2008.0014

[145] Kass-Hout, T. A. ; Xu, Z. ; McMurray, P. ; Park, S. ; Buckeridge, D. L. ; Brownstein, J. S. ; Finelli, L. ; Groseclose, S. L.: Application of change point analysis to daily influenza-like illness emergency department visits. In: *J Am Med Inform Assoc* 19 (2012), Nr. 6, 1075-81. http://dx.doi.org/10.1136/amiajnl-2011-000793. – DOI 10.1136/amiajnl–2011–000793

[146] Bisai, D ; Chatterjee, S ; Khan, A ; Barman, N K.: Statistical Analysis of Trend and Change Point in Surface Air Temperature Time Series for Midnapore Weather Observatory, West Bengal, India. In: *Hydrol Current Res* 5 (2014),

169. http://dx.doi.org/10.4172/2157-7587.1000169. – DOI 10.4172/2157–7587.1000169

[147] Ross, Sheldon M. ; Kelly, John J. ; Sullivan, Roger J. ; Perry, William J. ; Mercer, Donald ; Davis, Ruth M. ; Washburn, Thomas D. ; Sager, Earl V. ; Boyce, Joseph B. ; Bristow, Vincent L.: *Stochastic processes*. Bd. 2. Wiley New York, 1996

[148] Röttgermann, P. J. ; Hertrich, S. ; Berts, I. ; Albert, M. ; Segerer, F. J. ; Moulin, J. F. ; Nickel, B. ; Radler, J. O.: Cell motility on polyethylene glycol block copolymers correlates to fibronectin surface adsorption. In: *Macromol Biosci* 14 (2014), Nr. 12, 1755-63. http://dx.doi.org/10.1002/mabi.201400246. – DOI 10.1002/mabi.201400246

[149] Small, J. V. ; Stradal, Theresia ; Vignal, Emmanuel ; Rottner, Klemens: The lamellipodium: where motility begins. In: *Trends in Cell Biology* 12 (2002), Nr. 3, 112-120. http://dx.doi.org/10.1016/S0962-8924(01)02237-1. – DOI 10.1016/S0962–8924(01)02237–1

[150] Lehnert, Dirk ; Wehrle-Haller, Bernhard ; David, Christian ; Weiland, Ulrich ; Ballestrem, Christoph ; Imhof, Beat A. ; Bastmeyer, Martin: Cell behaviour on micropatterned substrata: limits of extracellular matrix geometry for spreading and adhesion. In: *Journal of Cell Science* 117 (2004), Nr. 1, 41-52. http://dx.doi.org/10.1242/jcs.00836. – DOI 10.1242/jcs.00836

[151] Breinig, Marco ; Klein, Felix A. ; Huber, Wolfgang ; Boutros, Michael: A chemical-genetic interaction map of small molecules using high-throughput imaging in cancer cells. In: *Molecular Systems Biology* 11 (2015), Nr. 12, 846-846. http://dx.doi.org/10.15252/msb.20156400. – DOI 10.15252/msb.20156400

[152] Kopp, Florian ; Hermawan, Adam ; Oak, Prajakta ; Herrmann, Annika ; Wagner, Ernst ; Roidl, Andreas: Salinomycin treatment reduces metastatic tumor burden by hampering cancer cell migration. In: *Molecular Cancer* 13 (2014), Nr. 1, 16. http://www.molecular-cancer.com/content/13/1/16

[153] Hayashi, Yoshihiro ; Osanai, Makoto ; Lee, Gang-Hong: Fascin-1 expression correlates with repression of E-cadherin expression in hepatocellular carcinoma cells and augments their invasiveness in combination with matrix metalloproteinases. In: *Cancer Science* 102 (2011), Nr. 6, 1228-1235. http://dx.doi.org/10.1111/j.1349-7006.2011.01910.x. – DOI 10.1111/j.1349–7006.2011.01910.x

[154] Thompson, E. W. ; Paik, S. ; Brunner, N. ; Sommers, C. L. ; Zugmaier, G. ; Clarke, R. ; Shima, T. B. ; Torri, J. ; Donahue, S. ; Lippman, M. E. ; al. et: Association of increased basement membrane invasiveness with absence of estrogen receptor and expression of vimentin in human breast cancer cell lines. In: *J Cell Physiol* 150 (1992), Nr. 3, S. 534–44. http://dx.doi.org/10.1002/jcp.1041500314. – DOI 10.1002/jcp.1041500314

[155] Wang, Fan ; He, Lei ; Dai, Wei-Qi ; Xu, Ya-Ping ; Wu, Dong ; Lin, Chun-Lei ; Wu, Shu-Mei ; Cheng, Ping ; Zhang, Yan ; Shen, Miao ; Wang, Chen-Feng ; Lu, Jie ; Zhou, Ying-Qun ; Xu, Xuan-Fu ; Xu, Ling ; Guo, Chuan-

Yong: Salinomycin Inhibits Proliferation and Induces Apoptosis of Human Hepatocellular Carcinoma Cells In Vitro and In Vivo. In: *PLoS ONE* 7 (2012), Nr. 12, e50638. http://dx.doi.org/10.1371/journal.pone.0050638. – DOI 10.1371/journal.pone.0050638

[156] Boehmerle, W. ; Endres, M.: Salinomycin induces calpain and cytochrome c-mediated neuronal cell death. In: *Cell Death Dis* 2 (2011), e168. http://dx.doi.org/10.1038/cddis.2011.46

[157] Ljepoja, Bojan ; García-Roman, Jonathan ; Sommer, Ann-Katrin ; Fröhlich, Thomas ; Arnold, Georg J. ; Wagner, Ernst ; Roidl, Andreas: A proteomic analysis of an in vitro knock-out of miR-200c. In: *Scientific Reports* 8 (2018), Nr. 1, 6927. http://dx.doi.org/10.1038/s41598-018-25240-y. – DOI 10.1038/s41598–018–25240–y

[158] Chao, Yvonne L. ; Shepard, Christopher R. ; Wells, Alan: Breast carcinoma cells re-express E-cadherin during mesenchymal to epithelial reverting transition. In: *Molecular Cancer* 9 (2010), Nr. 1, 179. http://dx.doi.org/10.1186/1476-4598-9-179. – DOI 10.1186/1476–4598–9–179

[159] Lombaerts, M. ; Wezel, T. van ; Philippo, K. ; Dierssen, J. W. F. ; Zimmerman, R. M. E. ; Oosting, J. ; Eijk, R. van ; Eilers, P. H. ; Water, B. van d. ; Cornelisse, C. J. ; Cleton-Jansen, A. M.: E-cadherin transcriptional downregulation by promoter methylation but not mutation is related to epithelial-to-mesenchymal transition in breast cancer cell lines. In: *British Journal of Cancer* 94 (2006), Nr. 5, 661-671. http://dx.doi.org/10.1038/sj.bjc.6602996. – DOI 10.1038/sj.bjc.6602996

[160] Sinh, Nguyen D. ; Endo, Kaori ; Miyazawa, Keiji ; Saitoh, Masao: Ets1 and ESE1 reciprocally regulate expression of ZEB1/ZEB2, dependent on ERK1/2 activity, in breast cancer cells. In: *Cancer Science* 108 (2017), Nr. 5, 952-960. http://dx.doi.org/10.1111/cas.13214. – DOI 10.1111/cas.13214

[161] Stossel, Thomas P. ; Condeelis, John ; Cooley, Lynn ; Hartwig, John H. ; Noegel, Angelika ; Schleicher, Michael ; Shapiro, Sandor S.: Filamins as integrators of cell mechanics and signalling. In: *Nature Reviews Molecular Cell Biology* 2 (2001), Nr. 2, 138-145. http://dx.doi.org/10.1038/35052082. – DOI 10.1038/35052082

[162] Nakamura, Fumihiko ; Stossel, Thomas P. ; Hartwig, John H.: The filamins. In: *Cell Adhesion & Migration* 5 (2011), Nr. 2, 160-169. http://dx.doi.org/10.4161/cam.5.2.14401. – DOI 10.4161/cam.5.2.14401

[163] Baldassarre, Massimiliano ; Razinia, Ziba ; Burande, Clara F. ; Lamsoul, Isabelle ; Lutz, Pierre G. ; Calderwood, David A.: Filamins Regulate Cell Spreading and Initiation of Cell Migration. In: *PLOS ONE* 4 (2009), Nr. 11, e7830. http://dx.doi.org/10.1371/journal.pone.0007830. – DOI 10.1371/journal.pone.0007830

[164] Alon, Uri: *An introduction to systems biology: design principles of biological circuits*. Chapman and Hall/CRC, 2006. – ISBN 142001143X

[165] Geiger, Benjamin ; Bershadsky, Alexander ; Pankov, Roumen ; Yamada, Kenneth M.: Transmembrane crosstalk between the extracellular matrix and the cytoskeleton. In: *Nat Rev Mol Cell Biol* 2 (2001), Nr. 11, 793-805. http://dx.doi.org/10.1038/35099066

[166] Arnold, Marco ; Hirschfeld-Warneken, Vera C. ; Lohmüller, Theobald ; Heil, Patrick ; Blümmel, Jacques ; Cavalcanti-Adam, Elisabetta A. ; López-García, Mónica ; Walther, Paul ; Kessler, Horst ; Geiger, Benjamin ; Spatz, Joachim P.: Induction of Cell Polarization and Migration by a Gradient of Nanoscale Variations in Adhesive Ligand Spacing. In: *Nano Letters* 8 (2008), Nr. 7, 2063-2069. http://dx.doi.org/10.1021/nl801483w. – DOI 10.1021/nl801483w

[167] Cavalcanti-Adam, Elisabetta A. ; Volberg, Tova ; Micoulet, Alexandre ; Kessler, Horst ; Geiger, Benjamin ; Spatz, Joachim P.: Cell Spreading and Focal Adhesion Dynamics Are Regulated by Spacing of Integrin Ligands. In: *Biophysical Journal* 92 (2007), Nr. 8, 2964-2974. http://dx.doi.org/10.1529/biophysj.106.089730. – DOI 10.1529/biophysj.106.089730

[168] Smith, Jason T. ; Tomfohr, John K. ; Wells, Matthew C. ; Beebe, Thomas P. ; Kepler, Thomas B. ; Reichert, W. M.: Measurement of Cell Migration on Surface-Bound Fibronectin Gradients. In: *Langmuir* 20 (2004), Nr. 19, 8279-8286. http://dx.doi.org/10.1021/la0489763. – DOI 10.1021/la0489763

[169] Schwarz, Jan ; Bierbaum, Veronika ; Vaahtomeri, Kari ; Hauschild, Robert ; Brown, Markus ; Vries, Ingrid de ; Leithner, Alexander ; Reversat, Anne ; Merrin, Jack ; Tarrant, Teresa ; Bollenbach, Tobias ; Sixt, Michael: Dendritic Cells Interpret Haptotactic Chemokine Gradients in a Manner Governed by Signal-to-Noise Ratio and Dependent on GRK6. In: *Current Biology* 27 (2017), Nr. 9, 1314-1325. http://dx.doi.org/10.1016/j.cub.2017.04.004. – DOI 10.1016/j.cub.2017.04.004

[170] Engvall, Eva ; Ruoslahti, Erkki: Binding of soluble form of fibroblast surface protein, fibronectin, to collagen. In: *International Journal of Cancer* 20 (1977), Nr. 1, 1-5. http://dx.doi.org/10.1002/ijc.2910200102. – DOI 10.1002/ijc.2910200102

[171] Anderson, N. L. ; Anderson, Norman G.: The Human Plasma Proteome. In: *Molecular & Cellular Proteomics* 1 (2002), Nr. 11, 845. http://dx.doi.org/10.1074/mcp.R200007-MCP200. – DOI 10.1074/mcp.R200007–MCP200

[172] Kirfel, G. ; Rigort, A. ; Borm, B. ; Herzog, V.: Cell migration: mechanisms of rear detachment and the formation of migration tracks. In: *Eur J Cell Biol* 83 (2004), Nr. 11-12, 717-24. http://dx.doi.org/10.1078/0171-9335-00421. – DOI 10.1078/0171–9335–00421

[173] Hay, Elizabeth D.: Extracellular matrix. In: *The Journal of cell biology* 91 (1981), Nr. 3, S. 205s–223s

[174] Hennig, Katharina ; Wang, Irene ; Moreau, Philippe ; Valon, Leo ; De Beco, Simon ; Coppey, Mathieu ; Miroshnikova, Yekaterina ; Albiges Rizo,

Corinne ; Favard, Cyril ; Voituriez, Raphael ; Balland, martial: Stick-slip dynamics of cell adhesion triggers spontaneous symmetry breaking and directional migration. In: *bioRxiv* (2018), 354696. http://dx.doi.org/10.1101/354696. – DOI 10.1101/354696

[175] Han, Sangyoon J. ; Rodriguez, Marita L. ; Al-Rekabi, Zeinab ; Sniadecki, Nathan J.: Spatial and temporal coordination of traction forces in one-dimensional cell migration. In: *Cell Adhesion & Migration* 10 (2016), Nr. 5, 529-539. http://dx.doi.org/10.1080/19336918.2016.1221563. – DOI 10.1080/19336918.2016.1221563

[176] Lamalice, Laurent ; Le Boeuf, Fabrice ; Huot, Jacques: Endothelial Cell Migration During Angiogenesis. In: *Circulation Research* 100 (2007), Nr. 6, 782-794. http://dx.doi.org/10.1161/01.RES.0000259593.07661.1e. – DOI 10.1161/01.RES.0000259593.07661.1e

[177] McCarthy, J B. ; Palm, S L. ; Furcht, L T.: Migration by haptotaxis of a Schwann cell tumor line to the basement membrane glycoprotein laminin. In: *The Journal of Cell Biology* 97 (1983), Nr. 3, 772-777. http://dx.doi.org/10.1083/jcb.97.3.772. – DOI 10.1083/jcb.97.3.772

[178] Xia, Younan ; Qin, Dong ; Whitesides, George M.: Microcontact printing with a cylindrical rolling stamp: A practical step toward automatic manufacturing of patterns with submicrometer-sized features. In: *Advanced Materials* 8 (1996), Nr. 12, 1015-1017. http://dx.doi.org/10.1002/adma.19960081217. – DOI 10.1002/adma.19960081217

[179] Yamada, Mayumi ; Suzuki, Yusuke ; Nagasaki, Shinji C. ; Okuno, Hiroyuki ; Imayoshi, Itaru: Light Control of the Tet Gene Expression System in Mammalian Cells. In: *Cell Reports* 25 (2018), Nr. 2, 487-500.e6. http://dx.doi.org/10.1016/j.celrep.2018.09.026. – DOI 10.1016/j.celrep.2018.09.026

[180] Friedl, Peter ; Wolf, Katarina: Proteolytic interstitial cell migration: a five-step process. In: *Cancer and Metastasis Reviews* 28 (2009), Nr. 1-2, 129-135. http://dx.doi.org/10.1007/s10555-008-9174-3. – DOI 10.1007/s10555–008–9174–3

[181] Friedl, Peter ; Wolf, Katarina: Tube Travel: The Role of Proteases in Individual and Collective Cancer Cell Invasion. In: *Cancer Research* 68 (2008), Nr. 18, 7247-7249. http://dx.doi.org/10.1158/0008-5472.can-08-0784. – DOI 10.1158/0008–5472.can–08–0784

[182] In: Eccles, Suzanne A. ; Box, Carol ; Court, William: *Cell migration/invasion assays and their application in cancer drug discovery*. Bd. 11. Elsevier, 2005. – ISBN 1387–2656, 391-421

[183] Kramer, Nina ; Walzl, Angelika ; Unger, Christine ; Rosner, Margit ; Krupitza, Georg ; Hengstschläger, Markus ; Dolznig, Helmut: In vitro cell migration and invasion assays. In: *Mutation Research/Reviews in Mutation Research* 752 (2013), Nr. 1, 10-24. http://dx.doi.org/10.1016/j.mrrev.2012.08.001. – DOI 10.1016/j.mrrev.2012.08.001

[184] Lautscham, Lena A. ; Kämmerer, Christoph ; Lange, Janina R. ; Kolb, Thorsten ; Mark, Christoph ; Schilling, Achim ; Strissel, Pamela L. ; Strick, Reiner ; Gluth, Caroline ; Rowat, Amy C. ; Metzner, Claus ; Fabry, Ben: Migration in Confined 3D Environments Is Determined by a Combination of Adhesiveness, Nuclear Volume, Contractility, and Cell Stiffness. In: *Biophysical Journal* 109 (2015), Nr. 5, 900-913. http://dx.doi.org/10.1016/j.bpj.2015.07.025. – DOI 10.1016/j.bpj.2015.07.025

[185] Davidson, Patricia M. ; Denais, Celine ; Bakshi, Maya C. ; Lammerding, Jan: Nuclear Deformability Constitutes a Rate-Limiting Step During Cell Migration in 3-D Environments. In: *Cellular and Molecular Bioengineering* 7 (2014), Nr. 3, 293-306. http://dx.doi.org/10.1007/s12195-014-0342-y. – DOI 10.1007/s12195–014–0342–y

[186] Renkawitz, Jörg ; Kopf, Aglaja ; Stopp, Julian ; Vries, Ingrid de ; Driscoll, Meghan K. ; Merrin, Jack ; Hauschild, Robert ; Welf, Erik S. ; Danuser, Gaudenz ; Fiolka, Reto ; Sixt, Michael: Nuclear positioning facilitates amoeboid migration along the path of least resistance. In: *Nature* 568 (2019), Nr. 7753, 546-550. http://dx.doi.org/10.1038/s41586-019-1087-5. – DOI 10.1038/s41586–019–1087–5

[187] Lo, Chun-Min ; Wang, Hong-Bei ; Dembo, Micah ; Wang, Yu-li: Cell Movement Is Guided by the Rigidity of the Substrate. In: *Biophysical Journal* 79 (2000), Nr. 1, 144-152. http://dx.doi.org/10.1016/S0006-3495(00)76279-5. – DOI 10.1016/S0006–3495(00)76279–5

[188] Novikova, Elizaveta A. ; Raab, Matthew ; Discher, Dennis E. ; Storm, Cornelis: Persistence-Driven Durotaxis: Generic, Directed Motility in Rigidity Gradients. In: *Physical Review Letters* 118 (2017), Nr. 7, 078103. https://link.aps.org/doi/10.1103/PhysRevLett.118.078103

[189] Boekhorst, Veronika t. ; Preziosi, Luigi ; Friedl, Peter: Plasticity of Cell Migration In Vivo and In Silico. In: *Annual Review of Cell and Developmental Biology* 32 (2016), Nr. 1, 491-526. http://dx.doi.org/10.1146/annurev-cellbio-111315-125201. – DOI 10.1146/annurev–cellbio–111315–125201

[190] In: Vignaud, Timothée ; Ennomani, Hajer ; Théry, Manuel: *Chapter 6 - Polyacrylamide Hydrogel Micropatterning*. Bd. Volume 120. Academic Press, 2014. – ISBN 0091–679X, 93-116

[191] Ahmed, Wylie W. ; Wolfram, Tobias ; Goldyn, Alexandra M. ; Bruellhoff, Kristina ; Rioja, Borja A. ; Möller, Martin ; Spatz, Joachim P. ; Saif, Taher A. ; Groll, Jürgen ; Kemkemer, Ralf: Myoblast morphology and organization on biochemically micro-patterned hydrogel coatings under cyclic mechanical strain. In: *Biomaterials* 31 (2010), Nr. 2, 250-258. http://dx.doi.org/10.1016/j.biomaterials.2009.09.047. – DOI 10.1016/j.biomaterials.2009.09.047

[192] Yu, Haiyang ; Xiong, Sijing ; Tay, Chor Y. ; Leong, Wen S. ; Tan, Lay P.: A novel and simple microcontact printing technique for tacky, soft substrates and/or

complex surfaces in soft tissue engineering. In: *Acta Biomaterialia* 8 (2012), Nr. 3, 1267-1272. http://dx.doi.org/10.1016/j.actbio.2011.09.006. – DOI 10.1016/j.actbio.2011.09.006

[193] Tang, Xin ; Yakut Ali, M. ; Saif, M. Taher A.: A novel technique for micro-patterning proteins and cells on polyacrylamide gels. In: *Soft Matter* 8 (2012), Nr. 27, 7197-7206. http://dx.doi.org/10.1039/C2SM25533B. – DOI 10.1039/C2SM25533B

[194] In: Plotnikov, Sergey V. ; Sabass, Benedikt ; Schwarz, Ulrich S. ; Waterman, Clare M.: *Chapter 20 - High-Resolution Traction Force Microscopy*. Bd. 123. Academic Press, 2014. – ISBN 0091–679X, 367-394

[195] Balaban, Nathalie Q. ; Schwarz, Ulrich S. ; Riveline, Daniel ; Goichberg, Polina ; Tzur, Gila ; Sabanay, Ilana ; Mahalu, Diana ; Safran, Sam ; Bershadsky, Alexander ; Addadi, Lia ; Geiger, Benjamin: Force and focal adhesion assembly: a close relationship studied using elastic micropatterned substrates. In: *Nature Cell Biology* 3 (2001), Nr. 5, 466-472. http://dx.doi.org/10.1038/35074532. – DOI 10.1038/35074532

[196] Schwarz, Ulrich S. ; Soiné, Jérôme R. D.: Traction force microscopy on soft elastic substrates: A guide to recent computational advances. In: *Biochimica et Biophysica Acta (BBA) - Molecular Cell Research* 1853 (2015), Nr. 11, Part B, 3095-3104. http://dx.doi.org/10.1016/j.bbamcr.2015.05.028. – DOI 10.1016/j.bbamcr.2015.05.028

[197] Ofer, Noa ; Mogilner, Alexander ; Keren, Kinneret: Actin disassembly clock determines shape and speed of lamellipodial fragments. In: *Proceedings of the National Academy of Sciences* 108 (2011), Nr. 51, 20394-20399. http://dx.doi.org/10.1073/pnas.1105333108. – DOI 10.1073/pnas.1105333108

[198] Zhang, Jian ; Guo, Wei-Hui ; Wang, Yu-Li: Microtubules stabilize cell polarity by localizing rear signals. In: *Proceedings of the National Academy of Sciences* 111 (2014), Nr. 46, 16383-16388. http://dx.doi.org/10.1073/pnas.1410533111. – DOI 10.1073/pnas.1410533111

[199] Etienne-Manneville, Sandrine: Microtubules in Cell Migration. In: *Annual Review of Cell and Developmental Biology* 29 (2013), Nr. 1, 471-499. http://dx.doi.org/10.1146/annurev-cellbio-101011-155711. – DOI 10.1146/annurev–cellbio–101011–155711

[200] Hell, Stefan W. ; Wichmann, Jan: Breaking the diffraction resolution limit by stimulated emission: stimulated-emission-depletion fluorescence microscopy. In: *Optics Letters* 19 (1994), Nr. 11, 780-782. http://dx.doi.org/10.1364/OL.19.000780. – DOI 10.1364/OL.19.000780

[201] Betzig, Eric ; Patterson, George H. ; Sougrat, Rachid ; Lindwasser, O. W. ; Olenych, Scott ; Bonifacino, Juan S. ; Davidson, Michael W. ; Lippincott-Schwartz, Jennifer ; Hess, Harald F.: Imaging Intracellular Fluorescent Proteins at Nanometer Resolution. In: *Science* 313 (2006),

Nr. 5793, 1642. http://dx.doi.org/10.1126/science.1127344. – DOI 10.1126/science.1127344

[202] Rust, Michael J. ; Bates, Mark ; Zhuang, Xiaowei: Sub-diffraction-limit imaging by stochastic optical reconstruction microscopy (STORM). In: *Nature Methods* 3 (2006), Nr. 10, 793-796. http://dx.doi.org/10.1038/nmeth929. – DOI 10.1038/nmeth929

[203] Hess, Samuel T. ; Girirajan, Thanu P. K. ; Mason, Michael D.: Ultra-High Resolution Imaging by Fluorescence Photoactivation Localization Microscopy. In: *Biophysical Journal* 91 (2006), Nr. 11, 4258-4272. http://dx.doi.org/10.1529/biophysj.106.091116. – DOI 10.1529/biophysj.106.091116

[204] Kanchanawong, Pakorn ; Shtengel, Gleb ; Pasapera, Ana M. ; Ramko, Ericka B. ; Davidson, Michael W. ; Hess, Harald F. ; Waterman, Clare M.: Nanoscale architecture of integrin-based cell adhesions. In: *Nature* 468 (2010), Nr. 7323, 580-584. http://dx.doi.org/10.1038/nature09621. – DOI 10.1038/nature09621

[205] Jinek, Martin ; Chylinski, Krzysztof ; Fonfara, Ines ; Hauer, Michael ; Doudna, Jennifer A. ; Charpentier, Emmanuelle: A Programmable Dual-RNA–Guided DNA Endonuclease in Adaptive Bacterial Immunity. In: *Science* 337 (2012), Nr. 6096, 816-821. http://dx.doi.org/10.1126/science.1225829. – DOI 10.1126/science.1225829

[206] Fenno, Lief ; Yizhar, Ofer ; Deisseroth, Karl: The Development and Application of Optogenetics. In: *Annual Review of Neuroscience* 34 (2011), Nr. 1, 389-412. http://dx.doi.org/10.1146/annurev-neuro-061010-113817. – DOI 10.1146/annurev–neuro–061010–113817

[207] Wu, Yi I. ; Frey, Daniel ; Lungu, Oana I. ; Jaehrig, Angelika ; Schlichting, Ilme ; Kuhlman, Brian ; Hahn, Klaus M.: A genetically encoded photoactivatable Rac controls the motility of living cells. In: *Nature* 461 (2009), Nr. 7260, 104-108. http://dx.doi.org/10.1038/nature08241. – DOI 10.1038/nature08241

[208] Levskaya, Anselm ; Weiner, Orion D. ; Lim, Wendell A. ; Voigt, Christopher A.: Spatiotemporal control of cell signalling using a light-switchable protein interaction. In: *Nature* 461 (2009), Nr. 7266, 997-1001. http://dx.doi.org/10.1038/nature08446. – DOI 10.1038/nature08446

[209] Valon, Léo ; Marín-Llauradó, Ariadna ; Wyatt, Thomas ; Charras, Guillaume ; Trepat, Xavier: Optogenetic control of cellular forces and mechanotransduction. In: *Nature Communications* 8 (2017), 14396. http://dx.doi.org/10.1038/ncomms14396. – DOI 10.1038/ncomms14396

[210] Mayor, Roberto ; Carmona-Fontaine, Carlos: Keeping in touch with contact inhibition of locomotion. In: *Trends in Cell Biology* 20 (2010), Nr. 6, 319-328. http://dx.doi.org/10.1016/j.tcb.2010.03.005. – DOI 10.1016/j.tcb.2010.03.005

[211] Scarpa, Elena ; Roycroft, Alice ; Theveneau, Eric ; Terriac, Emmanuel ; Piel, Matthieu ; Mayor, Roberto: A novel method to study contact inhibition of locomotion using micropatterned substrates. In: *Biology Open* 2 (2013), Nr. 9, 901-906. http://dx.doi.org/10.1242/bio.20135504. – DOI 10.1242/bio.20135504

[212] Batson, J. ; Astin, J. W. ; Nobes, C. D.: Regulation of contact inhibition of locomotion by Eph–ephrin signalling. In: *Journal of Microscopy* 251 (2013), Nr. 3, 232-241. http://dx.doi.org/10.1111/jmi.12024. – DOI 10.1111/jmi.12024

[213] Hynes, Richard O.: Integrins: Bidirectional, Allosteric Signaling Machines. In: *Cell* 110 (2002), Nr. 6, 673-687. http://dx.doi.org/10.1016/S0092-8674(02)00971-6. – DOI 10.1016/S0092–8674(02)00971–6

[214] Philipsborn, Anne C. ; Lang, Susanne ; Bernard, Andre ; Loeschinger, Jurgen ; David, Christian ; Lehnert, Dirk ; Bastmeyer, Martin ; Bonhoeffer, Friedrich: Microcontact printing of axon guidance molecules for generation of graded patterns. In: *Nat. Protocols* 1 (2006), Nr. 3, 1322-1328. http://dx.doi.org/10.1038/nprot.2006.251. – DOI 10.1038/nprot.2006.251

[215] Elwing, Hans: Protein absorption and ellipsometry in biomaterial research. In: *Biomaterials* 19 (1998), Nr. 4, 397-406. http://dx.doi.org/10.1016/S0142-9612(97)00112-9. – DOI 10.1016/S0142–9612(97)00112–9

[216] Stenberg, Esa ; Persson, Björn ; Roos, Håkan ; Urbaniczky, Csaba: Quantitative determination of surface concentration of protein with surface plasmon resonance using radiolabeled proteins. In: *Journal of Colloid and Interface Science* 143 (1991), Nr. 2, 513-526. http://dx.doi.org/10.1016/0021-9797(91)90284-F. – DOI 10.1016/0021–9797(91)90284–F

[217] Hough, Paul V.: *Method and means for recognizing complex patterns.* 1962

[218] Illingworth, J. ; Kittler, J.: A survey of the hough transform. In: *Computer Vision, Graphics, and Image Processing* 44 (1988), Nr. 1, 87-116. http://dx.doi.org/10.1016/S0734-189X(88)80033-1. – DOI 10.1016/S0734–189X(88)80033–1

[219] Crocker, John C. ; Grier, David G.: Methods of Digital Video Microscopy for Colloidal Studies. In: *Journal of Colloid and Interface Science* 179 (1996), Nr. 1, 298-310. http://dx.doi.org/10.1006/jcis.1996.0217. – DOI 10.1006/jcis.1996.0217

[220] *http://site.physics.georgetown.edu/matlab/index.html*

[221] Ronneberger, Olaf ; Fischer, Philipp ; Brox, Thomas: U-Net: Convolutional Networks for Biomedical Image Segmentation. In: Navab, Nassir (Hrsg.) ; Hornegger, Joachim (Hrsg.) ; Wells, William M. (Hrsg.) ; Frangi, Alejandro F. (Hrsg.): *Medical Image Computing and Computer-Assisted Intervention*, Springer International Publishing, 2015. – ISBN 978–3–319–24574–4, S. 234–241

Danksagung

An dieser Stelle ein herzliches Dankeschön an alle, die in irgendeiner Form an der Entstehung dieser Arbeit beteiligt waren:

Joachim Rädler für die Möglichkeit diese Arbeit schreiben zu können. Danke für die vielen guten Ideen und Anregungen und auch für die Freiheit selbst das Thema der Arbeit mitgestalten zu können.

Allen meinen Kooperationspartnern für die gute Zusammenarbeit. Bojan und Andi für viele Diskussionen nicht nur über micro RNA und Zellmigration. David und Chase für die spannenden Einblicke in die Theorie der Zellbewegung auf Dumbbells.

Dem ganzen Lehrstuhl Rädler für die tolle Atmosphäre und ganz besonders der Arbeitsgruppe Rädler. An alle die im Laufe der Zeit dazu gekommen und gegangen sind, es hat Spaß gemacht mit euch zu arbeiten und natürlich auch die zahlreichen Winterschulen und sonstigen Festivitäten!

Danke besonders auch an das Büro mit Matthias, Tobi, Judith, Anita, Sophia, Bene, Sonja, Miriam, Alexandra, Max, Ina und Kilian für viele gute fachliche Diskussionen und Hilfe, aber selbstverständlich auch für die Kickerpartien, Eisbachbesuche, Bärtierchenforschung, Pilatesstunden und vieles mehr, das die Doktorarbeit zu einer unvergesslichen Zeit gemacht hat!

Der ganzen restlichen Zellmannschaft mit Felix, meinem Masterarbeitsbetreuer von dem ich viel gelernt habe und auch danach für das gute Teamwork beim Donut Projekt. Alex für die gute Zusammenarbeit und auch so immer für ein offenes Ohr. An Fang, Ricarda und auch an die ehemaligen Elli, Peter, Jürgen, David, Rafal, und Farzad.

Insbesondere auch an Gerlinde und auch an Charlott und Susi, dass ihr euch um alles kümmert und den Laden am laufen haltet.

Meinen Studenten Verena, Mike und Max, die meine Beträungsqualitäten erdulden mussten.

Ganz besonders auch allen fleißigen Korrekturlesern!

Und auch an meine Freunde und Familie für die Unterstützung abseits der Uni.